Optical and Electrical Studies on Crystalline Tin Sulphide

by

M. Merdan, BSc

Thesis submitted to the
University of Nottingham
for the degree of
Doctor of Philosophy

August 1977

BEST COPY AVAILABLE.

TEXT IN ORIGINAL IS

CLOSE TO THE EDGE OF

THE PAGE

TO MY PARENTS

ABSTRACT

A Fourier transform far infrared spectrometer has been constructed to perform reflectivity and transmission measurements on small semiconductor samples in the temperature range 10-300 $^{\circ}$K. Far infrared and Raman spectra selection rules have been obtained by the Correlation method from the factor group analysis of the SnS subset. Crystals of n- and p- type SnS have been prepared, and the preparation methods are critically reviewed with reference to the T-p-x diagram. The electrical properties (Hall effect, carrier concentration, Hall mobility and barrier height) are measured for these specimens in the temperature range 40-300°K. Methods of obtaining electrical contacts to SnS are exhaustively studied. Broadband photoconductivity and photovoltaic measurements are reported on n- and p-type specimens in the spectral range 0.5-2.1 eV at temperatures from 300°K to 10°K. Band structure and impurity energies are suggested to account for the observed results. The band edge shift with temperature is also measured. Far infrared reflectivity and transmission measurements are made between 300°K and 10°K in order to determine the lattice vibration frequencies. Kramers-Krönig analysis and computer fitting routines are used to obtain this information from the reflectivity data. The interlayer forces are compared with those obtained in the isomorphic materials GeS and GeSe. Similar spectroscopic and analytic techniques have also been used to examine the room temperature optical properties of ZnS+Fe (Marmatite).

CONTENTS

Abstract

C H A P T E R   O N E

INTRODUCTION

1.1   Extent of this thesis

The thesis describes investigations into the electrical
and optical properties of crystalline SnS from room
temperature down to 10 °K. In an appendix we also present
the room temperature infrared transmission and reflection
data of marmatite.

We begin with a general review of the far infrared pro-
perties of layered semiconductors, giving (for the first
time) a group theoretical analysis of SnS subset by means
of the correlation method [Fataley   et al., 1972],
thereby deducing the lattice vibrational modes.

The methods of preparing single crystals of SnS are dis-
cussed in detail, with reference to the T - p - x diagram
in Chapter Two. We also discuss the preparation of n-
and p-type crystalline SnS in a form suitable for elect-
rical and optical investigation.

In Chapter Three, the electrical properties (Hall effect,
carrier concentration, Hall mobility and barrier height
measurements) are outlined together with a discussion of
various contact procedures which have been used to form
ohmic and non-ohmic contacts for the electrical and opto-
electrical measurements.

In Chapter Four, we report for the first time broad-band
(0.5-2.1 eV) photoconductivity and photovoltaic measure-
ments for various temperatures from 300 °K down to 10 °K and

we suggest a band edge structure to SnS which provides an explanation of our photoconductivity data. This explanation is given in the absence of any band edge structure literature for SnS. Appendix A to this chapter describes the apparatus used to perform photoconductivity and photovoltaic effects in the temperature range 10 - 300 °K. The band edge shift with temperature is also measured.

Chapter Five covers the description of apparatus used for far infrared spectroscopy together with the modifications made on the electronic units. The sample cell design is discussed and the optical, electronic and mechanical problems encountered during the far infrared reflection and transmission experiments are reviewed.

Far infrared reflectivity and transmission data on n- and p-type crystalline SnS at various temperatures from 300 °K down to 10 °K are reported in Chapter Six. Lattice vibrational modes of SnS were obtained by means of Kramers-Krönig analysis and least squares-fit computer programs applied to our far infrared reflectivity spectrum. Interlayer forces were discussed in comparison with those in the isomorphic materials GeS and GeSe for which data has been obtained by Wiley *et al.* 1976, and Chandrasekhar and Zwick 1976, respectively. Appendix B of this chapter is given in order to explain the physical meaning of the least squares-fit computer program. In Appendix C the room temperature optical properties of ZnS+Fe (marmatite) are investigated. The optical constants were obtained by means of similar Kramers-Krönig analysis and least squares-fit computer program.

1.2   Layered Compounds

These compounds form a class of molecular crystals in which the molecular unit (the individual layer) is an infinitely extended sheet in two dimensions. These compounds are characterised by highly anisotropic bonding forces and structurally identical layers; the forces between the layers are known to be weak by comparison with the forces within the layer. These materials display a wide range of behaviour varying from almost two-dimensional to almost three-dimensional with a similar variation in the isotropy of their properties.

Recently, there has been an intensive interest in both the electrical and optical properties of layered crystals in order to determine their fundamental physical properties. [Wilson and Yoffe, 1969 and Van der Valk and Haas, 1977, and references in these.] These compounds show a broad variation of electrical properties, ranging from electrical insulators such as HfS_2 through semiconductors such as SnS and MoS_2 subsets, to metals such as $NbSe_2$, which is a superconductor below 7 °K. [Wieting and Verble, 1971.]

1.2.1   General properties of MX_2 type layered crystals.

In order to understand the properties of the MX type layered materials, we first present a short review of MX_2 systems. The MX_2 layer materials form a structurally and chemically well defined family. Electrically, however, they cover a wide spectrum of properties as mentioned earlier, from an insulator like HfS_2, through semiconductors like MoS_2, SnS_2, $SnSe_2$ and semi-metals like NbS_2 and VSe_2. [Wilson and Yoffe, 1969.]

The MX_2 layer crystal structure consists of layers of the M atoms sandwiched between two layers of the X atoms, as seen, for example, in Figure 1.1. The bonding within the layer is generally thought to be mainly covalent. However, the bonding between neighbouring double layers is most likely to be of the van der Waals type, although Smith et al., 1977 and Lucovsky et al.,1976, suggest that long range coulomb forces are also found to some extent in these materials, such as SnS_2 and $SnSe_2$. They also remark that the coulomb interaction is more important in the sulphide than the selenide, due to the larger electronegativity difference between Sn and S. There is no proof in the literature on the bonding force in these materials, that it is indeed of a van der Waals type.

The cleavage properties of the stoichiometric materials are quite remarkable. The crystals are not friable and may be pulled apart on sellotape. Obviously the extremely aniso-tropic character of the layer compounds, built in at the atomic level, dominates all the mechanical, electrical and optical properties of such materials.

The frequencies of the transverse optical mode parallel and perpendicular to the layers differ by a factor of nearly two. [Clasen et al. 1975, Grisel et al. 1976, Lucovsky et al. 1976a, 1976b.] Recently, Van der Valk and Haas (1977) have published a paper in which they review the anisotropic be-haviour of lattice vibrations of layered compounds.

The expansion coefficient is about a factor of 10 in a direction perpendicular to the layers rather than parallel

Fig:1-1: Basic form of layer compounds

X
M   a)General Form
X
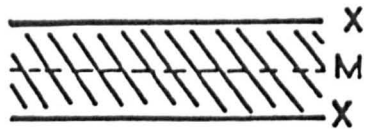
van der Waals gap
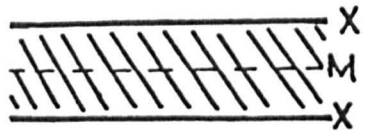
X
M   Sandwich of
X   'Anion' and 'Cation' sheets.

b)Coordination units for MX$_2$ layer structures.

X
M
X
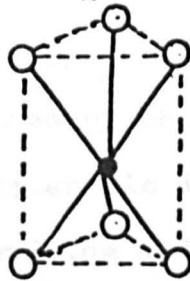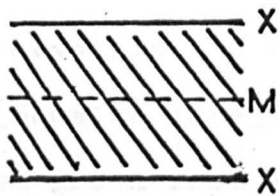
AbA
trigonal prism
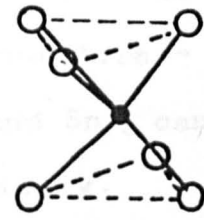
AbC
octahedron

c)Further types of sandwich (11$\bar{2}$0 sections).

X   X   X
M   M   M
X   X   X
                              M
                              X

octa.   trig. pr.
CdI$_2$, CdCl$_2$ MoS$_2$,NbS$_2$ Gas, Gase.
types.   types.

X   Set of sites
M
X   M only 2/3 occupied
M   X   leading to honey-
X   comp array.
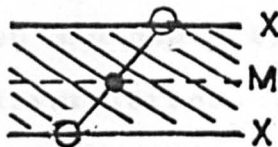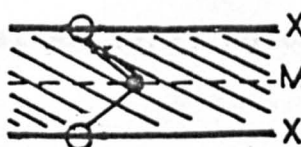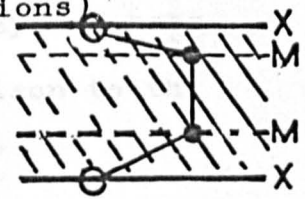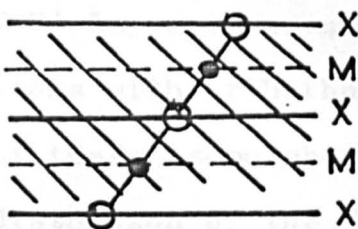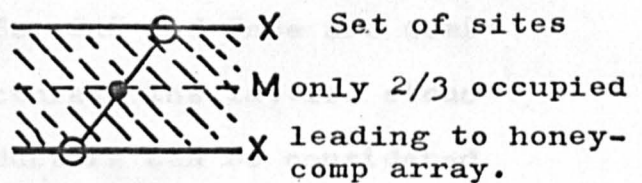
Bi$_2$Te$_3$.   BiI$_3$, CrCl$_3$.

NiAs
(BB.)
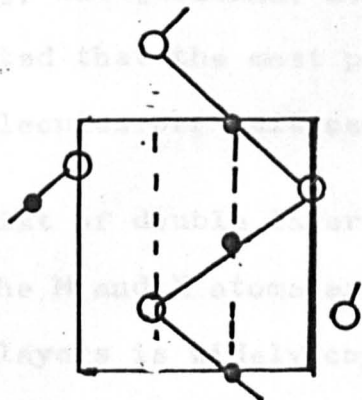
CdI$_2$
(c6)
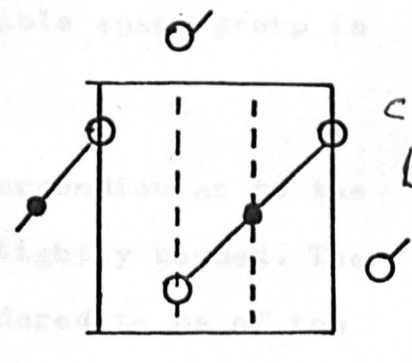
Relation of the MX$_2$ layer structure to MX structures.

to them [Brixner, 1963]. Conversely, the velocity of sound in this latter direction is twice that parallel to $\vec{c}$. [Guseinov and Rasulov, 1966.] The thermal conductivity is also up by almost a factor of 10 parallel to the layers. The electrical conductivity perpendicular to the planes is down by a factor of at least 100 on that in the planes for MoS_2 etc. MoS_2 and CdI_2 show an excitonic absorption.

Only MoS_2 occurs naturally in appreciable quantities. The other crystals are best obtained by chemical vapour transport [Schafer 1964]. Layer materials like CdI_2 and SnS_2 can also be grown from solution and the melt respectively.

A recurrent theme in all the studies of these materials has been the effects of the much weaker interlayer forces [Zallen and Slade 1974, Zallen 1974] in comparison to the intralayer forces.

1.2.2 MX type layered crystals: General Properties

We principally consider the IV-VI group of MX crystals. The IV-VI layer compounds GeS, GeSe, SnS and SnSe are semiconductors with orthorhombic structure. The lattice structure of these isomorphous semiconductors can be considered as a distortion of the NaCl structure. For GeS, GeSe [Dutto and Jeffrey, 1965], SnS [Hofmann, 1935] and SnSe [Okazaki, 1956] it is reported that the most probable space group is D_{2h}^{16}, with four molecules per unit cell.

The crystals consist of double layers perpendicular to the c axis in which the M and X atoms are tightly bonded. The bonding of these layers is widely considered to be of the

van der Waals type. However, it may be possible that long range forces of a Coulomb type are also involved. This has been suggested for MX systems such as GaSe by Fischer and Brebner (1962) and for MX_2 crystals such as $SnSe_2$ and SnS_2 by Lucovsky et al., 1976 and Smith et al., 1977. The evidence for this suggestion is the large local effective charge deduced from infrared measurements.

Every M atom is surrounded by six X atoms and every X atom by six M atoms, so that the bond lengths can be grouped into a set of three almost orthogonal (shorter) M-X bonds and a set of three (longer) M-X bonds.

One can, therefore, expect that this type of bonding will result in lattice dynamical, electrical and optical aniso-tropy. It has been reported that crystals like SnS display anisotropic electrical and optical properties. For example, the Hall mobility parallel to the c axis is appro-ximately five times less than that perpendicular to the $\vec{c}$ axis[Albers et al. 1960, Haas and Corbay 1961, and Albers et al. 1962] and the effective mass parallel to the c-axis $m_{\parallel}^* \approx m_0$, whereas in a plane perpendicular to the c-axis $m_{\perp}^* \approx 0.2m_0$ [Haas and Corbay 1961, and Albers et al. 1962]. Vlachos et al.(1976) reported that GeSe has an indirect gap of 1.22 eV $\vec{E}\|\vec{a}$ and 1.18 eV of $\vec{E}\|\vec{b}$ at room temperature. Wiley et al. (1975) also remark that GeS has a highly aniso-tropic absorption edge, being directly allowed for $\vec{E}\|\vec{a}$ and $\vec{E}\|\vec{c}$ directions, and forbidden for $\vec{E}\|\vec{b}$.

Despite the recent investigations on the IV-VI ortho-rhombic GeS-like semiconductors, many of their physical

constants are still not yet clearly determined.

1.3 Far Infrared Properties of Semiconductors

1.3.1 Introduction

The examination of semiconductors in the far infrared can be of interest for several reasons:

Firstly, the optical data can be easily related to the semiconductor transport properties because at these long wavelengths a simple non-quantum mechanical theory holds [Perkowitz and Thorland, 1974].

Secondly, over a wide range of carrier concentration in most semiconductors, the lower branch of the coupled plasmon-phonon mode falls almost wholly in the far infrared and its frequency can be observed at the reflectivity minimum.

Thirdly, the fundamental lattice vibrations - phonon frequencies - can be observed in the far infrared reflectivity and transmission experiments, thereby allowing us to obtain the lattice contribution to dielectric constants by means of Kramers-Krönig analysis and oscillator fits. In addition, the information about the 'interlayer-intralayer' forces in semiconductors can be obtained by performing both the far infrared (reflectivity) and Raman (back scattering) experiments.

The reflection coefficient for a semi-infinite medium in the case of normal incidence is given by

$$R = [(n-1)^2+k^2]/[(n+1)^2+k^2]$$

(1.1)

where n and k are the real and imaginary parts of the complex index of refraction and

$$n^2 = \varepsilon(\omega)$$

where ε is the complex dielectric function and ω is the optical frequency. The dielectric function can be written as the sum of a lattice term and a free carrier term:

$$\varepsilon(\omega) = \varepsilon_{lat}(\omega) + \varepsilon_{fc}(\omega).$$

The lattice contribution is given by Born and Huang (1954)

$$\varepsilon_{lat}(\omega) = \varepsilon_\infty + \frac{(\varepsilon_0 - \varepsilon_\infty)\omega_T^2}{(\omega_T^2 - \omega^2) + i\Gamma\omega}$$

where ε_0 and ε_∞ are the low and high frequency dielectric constants. And we may write

$$\varepsilon(\omega) = \varepsilon_1(\omega) - i\varepsilon_2(\omega)$$

so

$$\varepsilon_1(\omega) = n^2 - k^2 = \varepsilon_\infty + \frac{(\varepsilon_0 - \varepsilon_\infty)2(\omega_T^2 - \omega^2)\omega_T^2}{(\omega_T^2 - \omega^2)^2 + \omega^2\Gamma^2}$$

and

$$\varepsilon_2(\omega) = 2nk = \frac{(\varepsilon_0 - \varepsilon_\infty)\omega_T^2\omega\Gamma}{(\omega^2 - \omega^2)^2 + \omega^2\Gamma^2}.$$

The lattice dielectric function exhibits a resonance at the transverse optical frequency ω_T with a damping constant given by Γ.

The free-carrier term is given by Lyden, (1964)

$$\varepsilon_{fc} = \omega_p^2\varepsilon_\infty\left[-\left\langle\frac{\mathcal{J}_k^2}{1+\omega^2\mathcal{J}_k^2}\right\rangle + \frac{i}{\omega}\left\langle\frac{\mathcal{J}_k}{1+\omega^2\mathcal{J}_k^2}\right\rangle\right]$$

where the plasma frequency ω_p is defined by

$$\omega^2_p = \frac{4\pi Ne^2}{m^*\varepsilon_\infty}$$

where N is the free electron concentration, e is the electronic charge, m^* is the electronic effective mass and $\mathcal{J}_k$ is the energy-dependent electron scattering time. The angular brackets indicate averaging over the electron-distribution function.

In recent years a number of papers have been published on the vibrational spectra of SnS subset. For example, GeS [Wiley et al. 1975, 1976, Eymord and Otto 1976, Mihalovič et al. 1976, Gregore and Stetter 1975, Gregore et al. 1976]; SnS [Nikolič et al. 1974, Chamberlain et al. 1976, Nikolič et al. 1977]; GeSe [Siapkas et al. 1976, Chandrasekhar and Zwick 1976]. All these workers have deduced the optical constants of the respective IV-VI orthorhombic compounds by using Kramers-Krönig analysis and oscillator-fit computer programs.

1.3.2 Infrared and Raman Spectroscopy - Selection Rules:

With the recent increase in interest in infrared and Raman spectra of crystals, it has become important to determine which vibrational modes are optically active and to know the character of these modes. Hornig (1948), Winston and Halford (1949) and Bhagavantam and Venkatarayudu (1951) pioneered the development of methods for obtaining selection rules which determine this character.

In this section, it is intended to apply space-group selection rules to the analysis of the infrared lattice

spectrum of the SnS subset together with a brief review of 'correlation method' [Fataley et al., 1970] used. This technique has not previously been applied to this material and we present this treatment for the first time.

We concentrate on the use of the correlation tables in obtaining the vibrational selection rules for solids, but we do not review the detailed theory of the method. This has been discussed in several recent papers and books [Winston and Halford, 1949; Bhagavantam and Venkatarayudu, 1951; Slater 1963-67]. The procedure consists in writing down the character table and irreducible representations of the isomorphous point group corresponding to the space groups of the crystal.

The first step in the correlation method is to find out the crystal structure of the sample under investigation. Crystallographic information may be obtained from the international crystallography tables, for example, see Wyckoff 1963-4 and Henry and Lonsdale 1965.

The Bravais space cell is used in the correlation method to obtain the irreducible representation for the lattice vibrations. The crystallographic unit cell may be identical with the Bravais cell, or it may be larger by a simple multiple. This can be ascertained from the capital letter in the X-ray symbol for the crystal structure. For all crystal structures designated by a symbol containing P (for primitive) such as for orthorhombic SnS (Pnma), the crystallographic unit cell and Bravais unit cell are identical. Crystal structures designated by other capital letters A,B,

C, F, I, R have crystallographic unit cells that contain 2, 2, 2, 4, 2, 3 or 1, [Fataley et al. 1972, p.4] respectively.

Now, we will proceed to use the correlation method for defining the selection rules of the optical modes of the SnS subset. For SnS, the space group is designated D_{2h}^{16} or Pnma or 62 SnS, with four molecules per Bravais unit cell [Hofmann, 1935]. There are therefore four equivalent Sn atoms and four equivalent S atoms in the Bravais unit cell. We now need to know the possible 'site symmetry' or point groups for the space group D_{2h}^{16}. The possible site symmetries for this space group D_{2h}^{16} are given $2C_i(4)$; $C_s(4)$; $C_1(8)$ [Fataley et al. 1972, Appendix 1, p.173 or Fataley et al. 1971]. Here, the most useful information is the number contained in parenthesis, since it represents the number of equivalent atoms which have that particular site symmetry; for example, $C_s(4)$ indicates that there are four equivalent atoms occupying sites of symmetry C_s.

Some of the site symmetries have numerical coefficients, such as $2C_i(4)$. The coefficient two shows the presence of two different and distinct kinds of C_i site in this unit cell. Each can accommodate four equivalent atoms.

Now, consider the case of SnS. First, four equivalent Sn atoms can be accommodated in the possible site symmetry. There are two possible site symmetries, C_i and C_s; both of which can accommodate four equivalent atoms. One or the other will be correct, but additional information is needed to make the choice. For this we turn again to the crystallographic tables, which state [Wyckoff, 1964] that the Sn atoms

lie on the C_s site.

If we look [Wyckoff, 1964] for SnS

$$V_h^{16}(\text{Pbnm}) \quad (4c) \pm (uv\tfrac{1}{4}; \ \tfrac{1}{2}-u, \ v+\tfrac{1}{2},\tfrac{1}{4})$$

is seen.

We can write the following alphabetical ordering from the above data.

Table 1

Site	Alphabetical order	Wyckoff notation or alphabetical ordering of site position	Atom
$2C_i(4)$	$C_i(4)$	a	
	$C_i(4)$	b	
$C_s(4)$	$C_s(4)$	c	Sn and S
$C_1(8)$	$C_1(8)$	d	($\mp$c)

Now we have enough information to form the correlation between site symmetries and factor group analysis.

Table 2

The correlation for the lattice vibrations of the Sn atoms in SnS crystals
between the Site Group C_S and the Factor Group D_{2h}.

f^γ	t^γ	C_S site species, γ	Correlation $\sigma(zx)$	D_{2h} factor group species α	C_α	$\dfrac{a_\gamma}{a_\alpha = a_{A'} + a_{A''}}$
8	$2(T_{x,y})$	A'		A_g	1	2
				B_{2g}	1	2
				B_{1u}	1	2
				B_{3u}	1	2
4	$1(T_z)$	A''		B_{1g}	1	1
				B_{3g}	1	1
				A_u	1	1
				B_{2u}	1	1

Note: Table 2 was formed using the following information:

t^γ is the number of translations in a site species γ;

f^γ — the degrees of vibrational freedom present in each site species γ for an equivalent set of atoms, ions or molecules. This can be calculated $f^\gamma = t^\gamma \cdot n$, where n is the number of atoms in an equivalent set.

a_γ represents the degrees of freedom contributed by each site species γ to a factor group species α. The value of a_γ can be calculated as follows:

$$f^\gamma = a_\gamma \sum_\alpha {}^\gamma c_\alpha,$$

where C_α is the degeneracy of the species α of the factor group. The usual values of C_α are summarised in Table 3.

<u>Table 3</u>

Species	Value of C_α
A	1
B	1
E	2
F	3
G	4
H	5

The total irreducible representation of each equivalent set of atoms in the Γeg set is constructed in the following manner:

$$\Gamma\text{eg set} = \sum_\alpha a_\alpha \cdot \alpha$$

where a_α is the number of lattice vibrations of the equivalent set of atoms in the species α of the factor group. The total irreducible representation of the crystal, Γcrys., can be constructed as follows: Γcrys = Γeg set 1 + Γeg set 2 + ...

This irreducible representation of Γcrys contains the acoustical vibrations, so:

$$\Gamma\text{cryst.vib} = \Gamma\text{cryst} - \Gamma\text{acoustic}.$$

Now for Sn atoms in D_{2h},

$$\Gamma\text{eg.set 1}_{(Sn)} = 2 \cdot A_g + 2 \cdot B_{2g} + 2 \cdot B_{1u} + 2 \cdot B_{3u} + B_{1g} + B_{3g} + A_u + B_{2u}.$$

If we repeat this procedure for S atoms we will get the same results as for Sn atoms. Because S atoms are also accommodated in C_s site symmetry, and the number of S atoms is equal to Sn atoms in SnS, then

$$\Gamma\text{eg.set 2}_{(S)} = 2 \cdot A_g + 2 \cdot B_{2g} + 2 \cdot B_{1u} + 2 \cdot B_{3u} + B_{1g} + B_{3g} + A_u + B_{2u}.$$

Thus,

$$\Gamma\text{sns crystal} = \Gamma\text{eg.set 1} + \text{set 2} =$$
$$= 4 \cdot A_g + 4 \cdot B_{2g} + 4 \cdot B_{1u} + 4 \cdot B_{3u} + 2 \cdot B_{1g} + 2 \cdot B_{3g} + 2 \cdot A_u + 2 \cdot B_{2u}$$

is obtained.

But

$$\Gamma\text{cryst.vib} = \Gamma\text{crys} - \Gamma\text{acoustic}$$

and the acoustical modes are readily identifiable in factor groups, since they have the same character as the translation. Table 4 shows this identification. (See next page.)

Table 4 gives the following selection rules for the order of Raman and infrared active modes in SnS:

Raman spectrum: 12 fundamental lattice vibrations allowed, four A_g, four B_{2g}, two B_{1g} and three B_{3g}.

Table 4

D_{2h} Factor Group Species, Translations, Acoustical Modes, Number of Lattice Vibrations

and Infrared and Raman Activity of SnS Crystal

D_{2h} factor group species	Translation species	Acoustical mode species	ΓSnS crystal coefficients	ΓSnS.vib coefficients	Infrared activity	Raman polarization tensor species	Raman activity
A_g			4	4		$\alpha_{xx}, \alpha_{yy}, \alpha_{zz}$	✓
B_{2g}			4	4		α_{xz}	✓
B_{1u}	T_z	1	4	3	✓		
B_{3u}	T_x	1	4	3	✓		
B_{1g}			2	2		α_{xy}	✓
B_{3g}			2	2		α_{yz}	✓
A_u			2	2			
B_{2u}	T_y	1	2	1	✓		

Infrared spectrum: 7 fundamental lattice vibrations

allowed; three B_{1u}, three B_{3u} and

one B_{2u}.

Two vibrations, A_u, will be inactive in both the infrared and the Raman spectra.

If we look at the above result obtained for SnS subset, it is seen to be the same as that obtained by Zeyher et al. [unpublished, 1976] who used a different notation and a different method to obtain the mode assignments and selection rules.

Kress et al. (1976) reported that the optic active modes split into Raman and infrared active vibrations due to a centre of inversion between the layers. This splitting vanishes if the interlayer forces are neglected, since the diperiodic group [Wood, 1974] DG32 has no inversion centre. Recent measurements [Wiley et al. 1976, Chandrasekhar and Zwick 1976] have shown that many of the infrared active modes are nearly degenerate with the Raman active modes. This kind of splitting has also been observed by Verble and Wieting (1970), Wieting and Verble (1971), Zallen et al.(1971). These researchers have carried out infrared and Raman experiments for the layered compounds MoS_2, As_2S_3 and As_2Se_3 and have reached the same conclusion as Kress et al. (1976).

The above 'correlation method' for selection rule analysis is seen to be very simple and unambiguous.

1.4   Review of SnS

1.4.1   Crystal structure and bond structure: SnS crystallises

in orthorhombic $\left(D_{2h}^{16}\right)$ structure [Hofmann, 1935] with lat-tice parameters a = 3.98 A°, b = 4.33 A°, c = 11.18 A°. There are four molecules in the unit cell. This structure, which is pseudo-tetragonal [Albers et al. 1960], may be thought of as a rather strongly distorted sodium chloride structure. Every Sn atom is surrounded by six S atoms, three at a short distance (2.68 A°) with the interatomic directions almost perpendicular to each other (88°10', 88°10' and 95°8'), and three atoms at a somewhat longer distance (3.88 A°) with the interatomic directions at angles 118°, 118° and 75° respectively. The interatomic distances of the second group form an angle of 78° with the inter-atomic directions of the first group of S atoms [Lambros et al. 1974].

Several papers [Albers et al. 1960, 1961; Albers and Schol 1961; Nikolić et al. 1974, 1976; Chamberlain et al. 1976] have reported the growing of small crystals of SnS from the melt. Albers and Schol (1961) have given the T - p - x phase diagram of the Sn-S system (this will be discussed in Chapter 2).

The crystal consists of double layers perpendicular to the c-axis in which the Sn and S atoms are tightly bound. The bonding between these layers is much weaker, having a (001) cleavage plane. This structure represents an intermediate state between a true layer structure and a three-dimensional crystal. The crystal structure of SnS is shown in Figs.1.2 and1.3 . Unfortunately there is no literature on the band structure of SnS. However, we tentatively suggest a band structure in Chapter 4 in order to explain our photo-
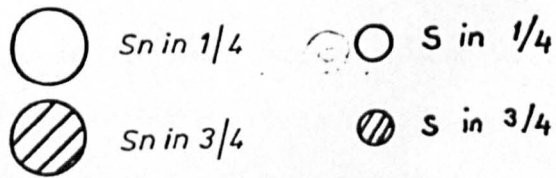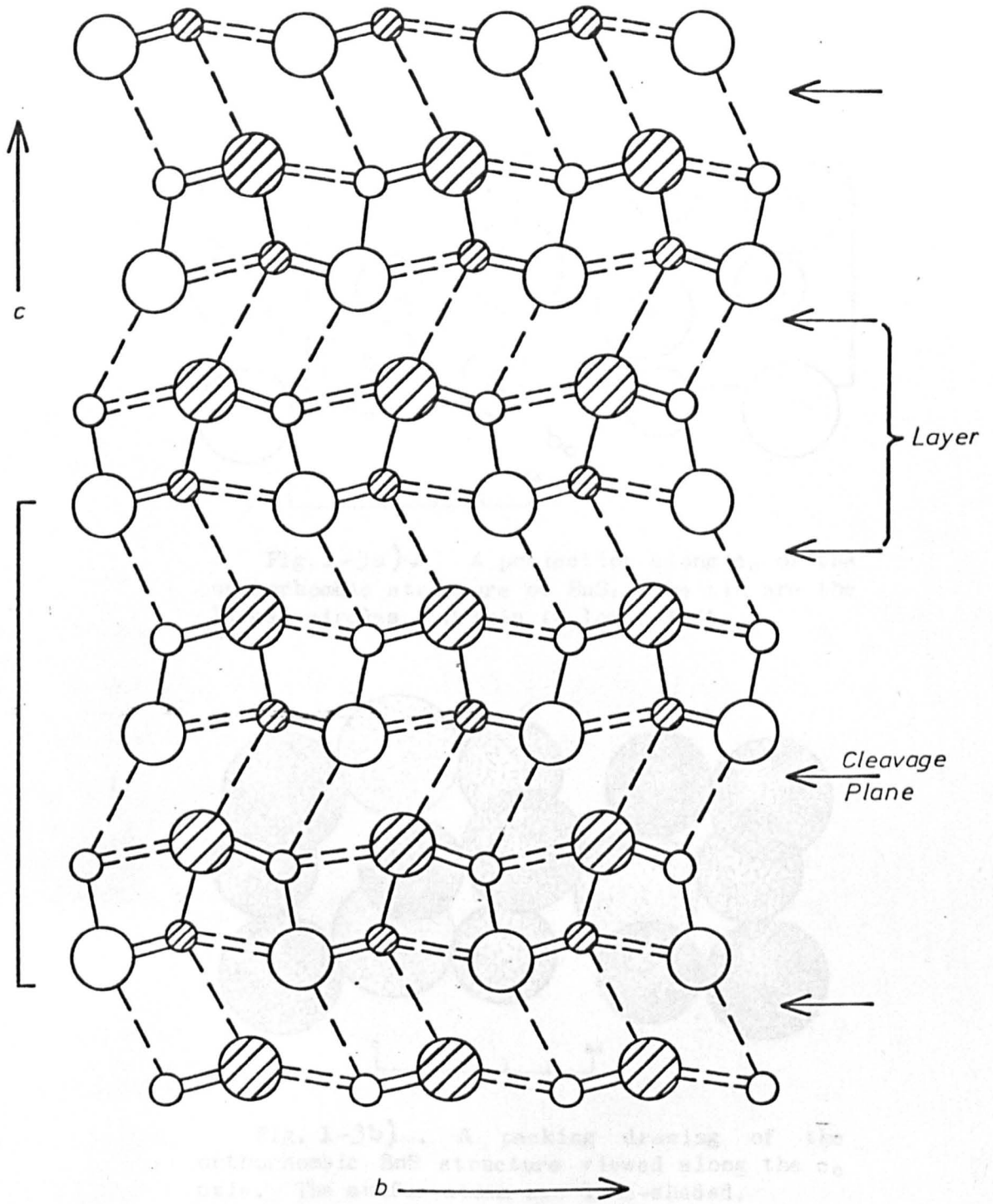
Fig: 1-2)Crystal structure of SnS after Hofmann
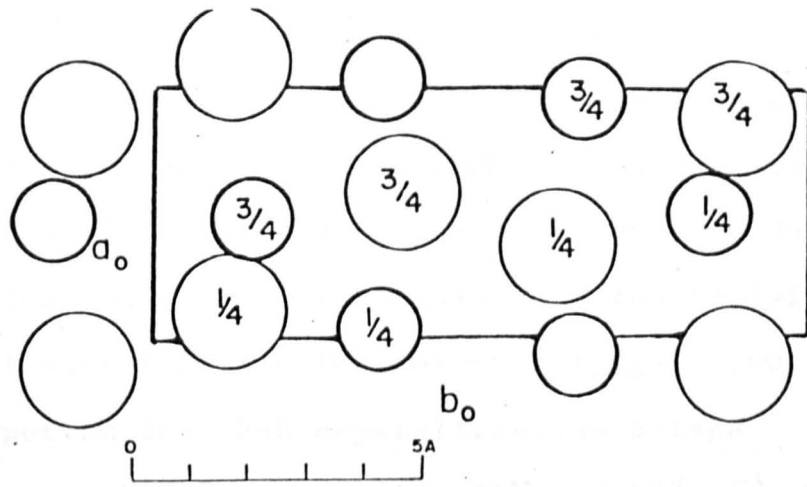
Fig. 1-3a). A projection along c_o of the orthorhombic structure of SnS. The tin are the larger circles. Origin in lower left.
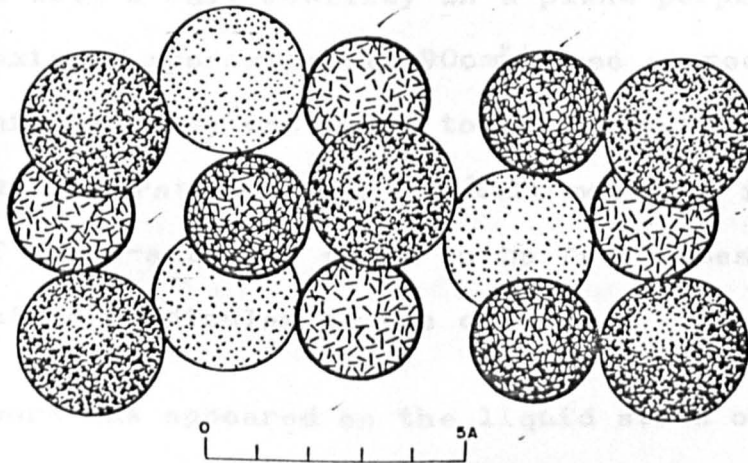
Fig. 1-3b). A packing drawing of the orthorhombic SnS structure viewed along the c_o axis. The sulfur atoms are line-shaded.

(After Wyckoff R.W.G. Vol.I-1960)

conductivity data.

1.4.2 Electrical Properties

Anderson et al. (1943, 1945a, 1945b) have studied the electrical conduction and the thermoelectric power [Anderson et al. 1947] of SnS pellets. They found p-type conductivity and a band gap approximately 1.2 eV at room temperature. Braithwaite (1951) found photoconductivity in SnS powder with a long wavelength threshold of 1.1μu ($\approx$ 1.13 eV) again at room temperature. Later, Albers et al. (1960, 1961, 1962) reported that SnS crystallises as p-type material with a carrier concentration 10^{17} and 10^{18} cm^{-3} with Hall mobility μ_H of 65cm^2/v·sec at room temperature. They also performed Hall effect and mobility experiments on oriented samples with a Hall mobility in a plane perpendicular to the c-axis of approximately 90cm^2/v·sec at room temperature. This mobility was found to be proportional to $T^{-2.2}$ at higher temperatures, and the Hall mobility in the direction of the c-axis was found to be five times smaller than that perpendicular to the c-axis.

Some published work has appeared on the liquid state of SnS by Boutin and Bourgon (1961) who concluded that SnS was a semiconductor in the liquid state, having a band gap of 1.9 eV. The conductivity was 24 ohm^{-1} cm^{-1} at 895°C and 31.2 ohm^{-1} cm^{-1} at 930°C, as obtained by a·c and d·c conductivity measurements. Recent work on the liquid state of SnS has been published by Handfield et al. (1966) who concluded that in the liquid state it forms a similar structure to that of the solid.

1.4.3 Optical Spectra

Gobrecht and Barschat (1957) studied the infrared trans-
mission, photoconductivity and reflective spectra of
layers of SnS, and estimated a band gap of 1.25 eV at
room temperature. Albers et al. (1960) deduced the band-
gap to be 1.02 ± 0.04 eV at room temperature from the
infrared transmission measurements on cleavage plates per-
pendicular to the c-axis and obtained an effective mass
of the holes of $m^* = 0.4 m_o$. A later paper by Albers et
al. (1961) reports that the indirect bandgap was 1.08 eV
at 300°K and 1.115 eV at 77°K as obtained by absorption
measurements. The effective charge of the atoms $e^* = 0.7$ eV
and the effective mass of the holes in the three principal
crystal directions ($m_a^* = m_b^* = 0.2 m_o$, $m_c^* \approx m_o$) were deter-
mined from reflection measurements in the infrared. They
remark that the number of equivalent maxima of the valence
band is at least four. Haas and Corbay (1961) investigated
infrared reflection spectra of SnS in the wavelength region
2 to 25μm ($5000 - 400$ cm^{-1}) and reported that the observed
dispersion was a combined effect of lattice vibrations and
free holes. They calculated that the index of refraction
$n_o = 3.6 \pm 0.1$, the dielectric constant $\varepsilon = 19.5 \pm 2$, the
effective charge on the atom $e^* = 0.7 e_o$, and the hole
effective mass $m_\perp^* = 0.2 m_o$, $m_c^* \approx m_o$. These values were in
agreement with the previous work of Albers. Recently,
Takahashi et al. (1972) have studied the optical proper-
ties of single crystals of SnSe and SnS at 300°K and 77°K
by measuring the absorption spectra along the three prin-
cipal axes in the energy range 0.1 to 1.3 eV. They found

the absorption bands were around 0.33 eV and 0.88 eV for $\vec{E}\parallel\vec{a}$, around 0.83 eV for $\vec{E}\parallel\vec{b}$, and around 0.33 eV and 0.88 eV for $\vec{E}\parallel\vec{c}$. They attributed these absorption bands to free carrier absorption. More recently Lambros et al. (1974) performed optical absorption experiments on crystalline SnS in the wavelength range 2.2 - 0.8 μm ($\approx$0.56-1.55 eV) at temperatures between 100 - 300°K. They found indirect band-gaps of 1.142 and 1.095 eV for $\vec{E}\parallel\vec{a}$ $\vec{E}\parallel\vec{b}$ at room temperature. They also mentioned that the phonon assisted transitions with energies 0.033 or 0.038 eV and 0.082 or 0.113 eV, with reference to the two main axes $\bar{a}$ and $\bar{b}$. Nikolić et al. (1974) performed far infrared reflectivity experiments over the wavelength range 0.5 to 200 μm. They derived the optical constant of SnS from a Kramers-Krönig analysis and calculated the transverse optical and longitudinal optical frequencies at room temperature. In this connection we reported (Chamberlain et al. 1976) far infrared reflectivity and transmission data using both polarised and partially polarised light in the three main directions, in the temperature range 10 - 300°K. The most recent work appearing on Raman scattering of single crystals of SnS at room temperature [Nikolić et al. 1977) obtains values for the Raman active modes in this material.

CHAPTER TWO

DESCRIPTION OF SPECIMEN PREPARATION

2.1 Introduction

Single-crystalline samples of the majority of the
IV-VI compounds can be prepared by melting suitable
amounts of the components in evacuated quartz ampoules.
In the preparation of SnS, GeS, PbS etc., where the
reacting elements have a high vapour pressure, it is
necessary to increase the furnace temperature very
slowly, and to allow considerable time for reaction.
This may take at least a day to bring the temperature
to the melting point of the compound in order to avoid
explosions, which are usually due to the vapour of free
unreacted sulphur. Obviously, clean conditions and a
dust free atmosphere are essential in this work. Another
advisable precaution is to ensure that the reacting metal
is cut into small pieces in order to make a good mixture.
Soft metals such as In, Pb and Sn may be cut with a sharp
knife, and it is advisable to etch the metals to be used
after cutting. Suitable etchants for metals are to be
found in various metallurgical handbooks (Smithells, 1955,
Lyman, 1948).

Preparations of SnS specimen have been reported previously by a few workers (Albers et al, 1960; Haas and Corbay, 1961; Rau, 1966; Takahashi et al, 1972; Vujatović and Nikolić, 1976). The techniques of Albers' group involve a double distillation and introduction of compensating impurities, finally producing p-type specimens of $\sim 5 \times 10^{16}$ cm^{-3} (300 °K) for use in optical work. We have used techniques developed by Vujatović and Nikolić which result in higher mobility samples but with impurity concentration marginally greater than those achieved by Albers for his optical specimens, although the samples used for their electrical measurements are virtually identical with our own (10^{17}-10^{19} cm^{-3}). Our sample growing technique will be discussed in next section. We now review for completeness the method of Albers et al.

The technique of the Albers' group was to prepare SnS in a quartz ampoule from components taken in the stoichiometric ratio. The ampoule was heated to 900 °C, while one part of the tube was kept at 400 °C in order to avoid explosions. The whole tube was heated up slowly to 900 °C. A molten zone was passed through the sample at a rate of about 1 cm per hour in order to obtain single crystals. The resultant SnS contains various impurities (Fe, Pb, Al, Sb, Ni, Mn, Cu) with a total concentration of the order of 10^{18} to 10^{19} cm^{-3}. The impurity content is then chemically reduced (Albers et al, 1961) by means of a double distillation at 960 °C. Spectro-chemical analysis of this purified SnS showed that

the concentration of all detectable elements was below the limits of detectability with the exception of Pb, which was still present at a concentration of 7.10^{16} at/cm^3.

2.2 Growth Technique

The single crystal samples of SnS were produced from the pure elements by means of the Bridgman technique as described previously by Vujatovic and Nikolic, (1976). The stoichiometric amount of the constituent elements (manufactured by Koch-Light, 99.9999 o/o grade) were weighed out. The total weight was always taken to be less than five gr in order to avoid explosions due to over pressure of sulphur at 900 ^{o}C (approximately 100 atmosphere, Albers et al. 1960). Sulphur was powder like and Sn was cut into small pieces with a clean sharp knife, and then the components were put together in a 12 mm diameter, thick wall ($\sim$ 1.5 - 3 mm) quartz ampoule as seen in Figure 2.1. The lower part of the ampoule had a conical shape and was about 35mm long. The ampoules were then evacuated by means of a rotary-diffusion pump system. When the pressure reached 10^{-5} torr or better, the ampoule was sealed off.

Single crystals of SnS were grown in two stages as follows: in the first stage, the ampoule, containing the constituent elements, was placed in a cold furnace and heated up at a rate of about 25 ^{o}C/hr until the temperature reached 1000 ^{o}C. This is well above the melting points of both elements but it is essential to work at this

temperature in order to increase the efficiency of
the reaction. Normally, this temperature was kept for
2-3 hours before cooling down gradually to room temp-
erature. In the second stage, those ampoules with
polycrystalline SnS were placed in a second quartz tube
in order to prevent oxidation in case of possible
breaking of the first ampoule during the solidification
process. The second ampoule was evacuated and sealed
off as before when the pressure was 10^{-5} torr or better.
The resultant double-walled quartz ampoules were placed
in an initially cold vertical furnace whose final
temperature profile is shown in Figure 2.2.

The furnace was heated up at a rate of 25 $^\circ$C/hr.
until this profile was achieved, and the sample temperature
was 1000 $^\circ$C. This temperature was kept constant for
several hours. Then the ampoule was lowered down into
the cooler zone at an initial rate of 2 cm/day until
the melt solidifies (approximately 870 $^\circ$C); the rate was
then increased to 24 cm/day until the sample was cooled
down to room temperature. The process typically took one week.

2.3 Results and Conclusions

In order to grow single crystals under controlled
conditions it is necessary to have a knowledge of the
phase diagram (T-p-x) of the system involved.

The T-p-x diagram of the Sn-S system was investigated
by Albers and Schol (1961). The T-x relation of this
diagram is given in Figure 2.3. There are two large
regions of liquid immiscibility. One of these occurs
on the Sn-rich side (10-48 at o/o S) and extends to

Fig.2-1) Quartz ampoule to

grow SnS.

Fig.2-2)Temperature profile of the furnace used for

growing the single crystals.
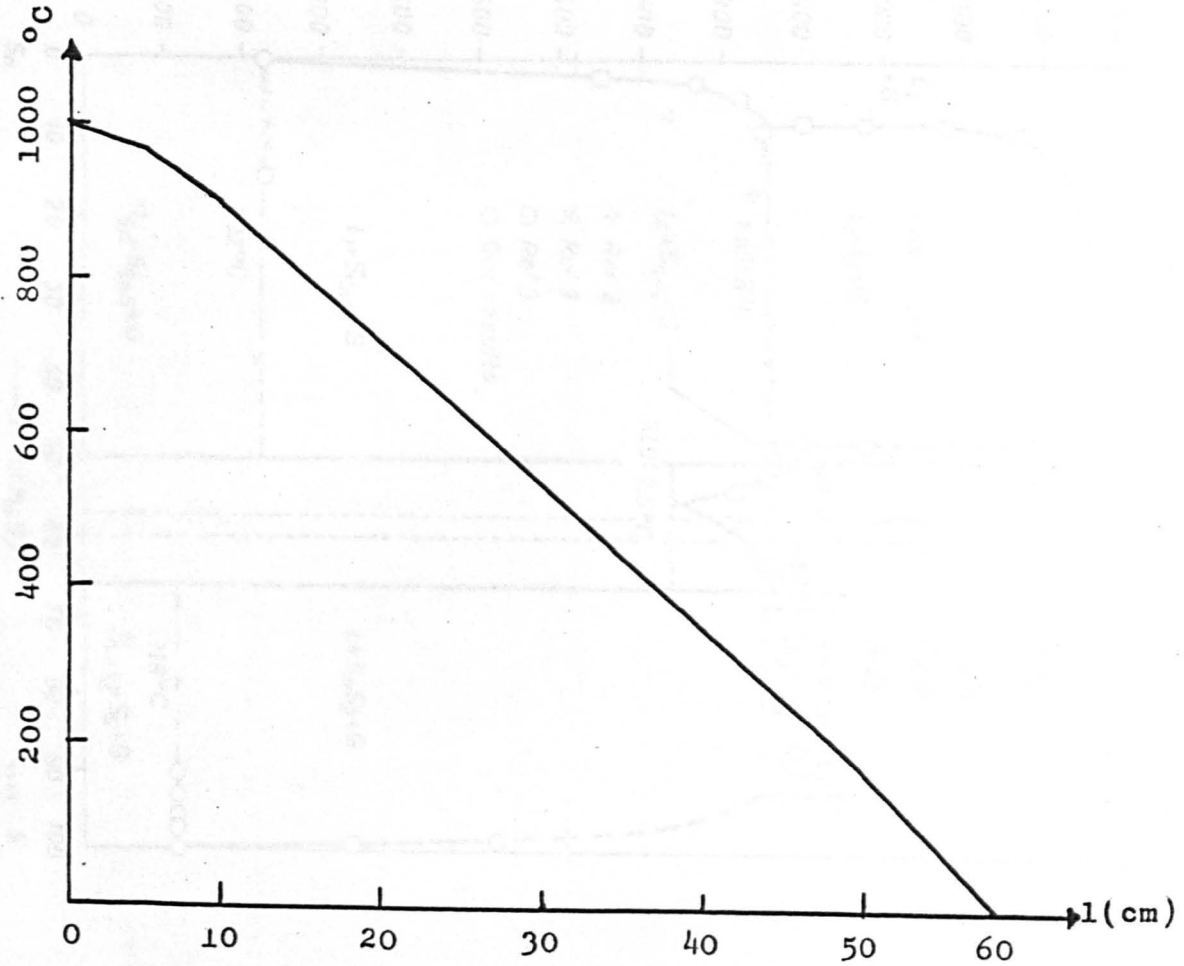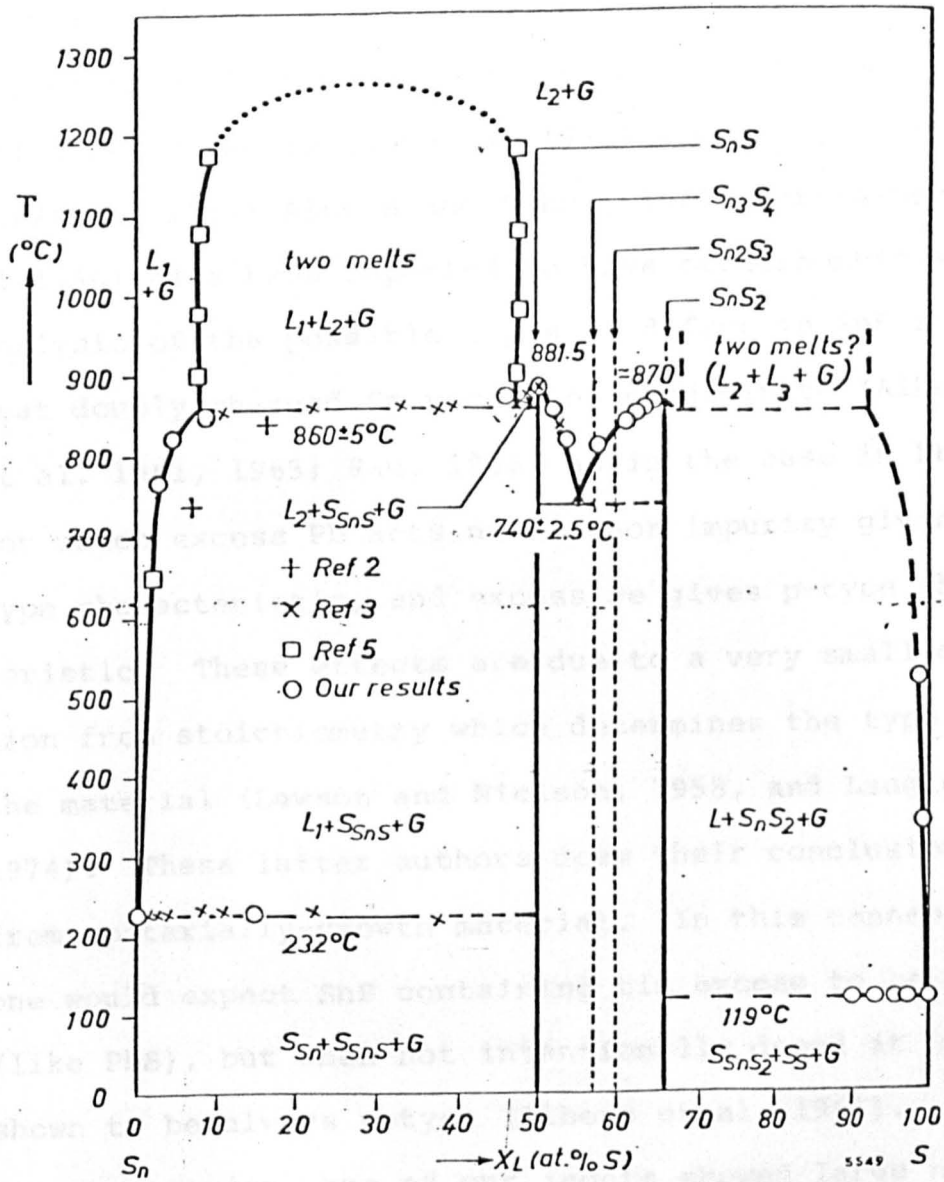
Fig.2-3) T-X$_L$ Projection of the system Sn-S
(After Albers and Schol, 1961)

An electron-diffraction investigation of SnS films (Badachhape and Goswani, 1964) deposited on substrates kept at 300-350 °C has shown that SnS crystallises in the cubic NaCl-type lattice with a=5.16 °A. However, solid SnS crystals (Hofmann, 1935) and Sn_2S_3 (Mootz and Kunzmann, 1962; Albers and Schol, 1961; Karakhanova et al 1966) have been reported to have orthorhombic structure. Analysis of the possible types of defect in SnS shows that doubly charged Sn vacancies predominate (Albers et al. 1961, 1963; Rau, 1966) as in the case in PbSe, for which excess Pb acts as a donor impurity giving n-type characteristic, and excess Se gives p-type characteristic. These effects are due to a very small deviation from stoichiometry which determines the type of the material (Lawson and Nielson, 1958, and Laugier, 1974). These latter authors drew their conclusions from epitaxially-growth material. In this connection, one would expect SnS containing tin excess to be n-type (like PbS), but when not intentionally doped it has been shown to be always p-type (Albers et al. 1961). However, on one occasion, one of our ingots showed large n-type regions as measured by a thermopile method. Unfortunately, the process was unrepeatable; the n-type character was probably due to Sn excess in a similar fashion to PbSe as discussed earlier.

Our ampoules had a conical tip, so that initially only a small volume of the melt is supercooled. The object of using this design is to ensure that only a few nuclei (ideally only one) will be formed initially. Although we had no control of the orientation of the

the quadruple point at 860 $^{\circ}$C, where solid SnS co-exists with a liquid phase having a composition close to SnS and an Sn excess. Another occurs on the S-rich side (68-95 at. o/o S), where solid SnS$_2$ co-exists with a liquid phase having a composition close to SnS$_2$ but with liquid sulphur excess.

SnS and SnS$_2$ are both found in the Sn-S system: their melting points are 881.5$\pm$2.5 $^{\circ}$C and 870$\pm$2.5 $^{\circ}$C, respectively. SnS and SnS$_2$ form a eutectic at 55 at. o/o S with a melting point of 740$\pm$2.5 $^{\circ}$C. It is concluded that in the Sn-S system, Sn$_2$S$_3$ and Sn$_3$S$_4$ compounds may also exist. (Gerassimov et al. 1937; Rok and Boeyens, 1957; and Albers and Schol, 1961). Sn$_2$S$_3$ and Sn$_3$S$_4$ are formed by a peritectic reaction at 745 $^{\circ}$C and 710 $^{\circ}$C respectively. A subsequent re-investigation of Sn-S system by Karakhanova et al (1966) was made in the 40-62 at o/o S range in order to study in more detail the problem of the existence of the Sn$_2$S$_3$ and Sn$_3$S$_4$ phases. In this work it is reported that the melting point of SnS is 875$\pm$5 $^{\circ}$C which is in agreement with earlier investigations within the limits of experimental error. SnS exhibits a polymorphic transition (Karakhanova, 1966) in the region of temperature 585-600 $^{\circ}$C. The most recent investigations are by Abrikosov et al. (1969), who also report this effect in the heating and cooling curves of the alloys in the 40-56 at o/o S range. Measurements of the specific heat of SnS were made by Orr and Christensen (1958), who also reported this polymorphic transition at 602 $^{\circ}$C.

first single crystal seed, the resultant ingot was

always 20-25° off one of the main orientation directions

($\vec{a}$ or $\vec{b}$ axis). Because of the cracking of the ampoules

during the solidification of the IV-VI group crystals

of the SnS subset, we always used double-walled evacuated

ampoules. Similar effects have been reported by Yabumoto

(1958); Asanabe and Okazaki (1960); and Asanabe (1959)

for GeS, GeSe and SnSe respectively. We noted that twin-

ning (mostly simple twinning) occurs frequently as

reported earlier by Hofmann (1935) and Albers et al (1960).

However, it must be remarked that twinning can be minimised

by using narrow ampoules, less than 10 mm inner diameter.

Thus the crystal can be grown as one solid phase at one

orientation. X-ray Laue diagrams of SnS crystals yielded

pin point spots with no trace of spreading; these pin

points also observed by Vujatović (1976). All crystals

obtained show a perfect cleavage on the (040) face.

Each time approximately 5 gr SnS crystals were obtained

for the subsequent electrical and optical measurements which

will be reported in later chapters. We must remark that

it is relatively difficult to achieve a high degree,

and a large area of homogenity of SnS. Several ecthants

were used in order to improve sample surfaces including

that which is given by Nikolić et al 1974. (100 ml ethanol

+ 12 ml HCl + 6 ml HNO_3 at 60 $^{\circ}$C for 15 min.). Only

limited success, however, was obtained with this etch.

CHAPTER THREE

ELECTRICAL MEASUREMENTS ON CRYSTALLINE TIN SULPHIDE

3.1   Introduction

In this chapter techniques for the provision of electrical contacts to homogenous samples of n- and p- type tin sulphide are established. The characteristics of these contacts are examined, and measurements of barrier heights are reported for a number of contact materials. In addition, some Hall-effect and conductivity measurements which were undertaken to characterise the samples prior to optical studies are discussed.

A number of procedures for making electrical contacts to tin sulphide will now be discussed.

3.2   Contact Technique

Soldered, silver paste (painted), alloyed and welded contacts onto crystalline n- and p- type SnS specimens were made by using ordinary (lead-tin) solder, silver paint, indium pellets, tin and lead pellets. All samples were freshly cleaved from the ingot unless otherwise stated. The various methods are now considered in turn.

3.2.1 Welded Contacts

38 S.W.G. platinium wires were used to form welded contacts onto SnS by using a condensor discharge. In many cases platinium wire diffused into the specimens or the material was physically damaged by the discharge. The contacts produced by this technique were weak mechanically, and it was concluded that welded contacts should be avoided if possible.

3.2.2 Soldered Contact

The second method involved attaching leads to SnS using ordinary commercial solder (lead-tin) and an acid flux. The contacts made by this method were not particularly reliable or reproducible and varied from sample to sample, in some cases showing blocking behaviour and in other cases non-blocking behaviour.

3.2.3 Silver Paint

Silver paint contacts were made in order to measure D.C. conductivity of SnS. Those contacts were mechanically quite strong between 77 ^{O}K and 700 ^{O}K. However, they were noisy and showed blocking behaviour. Because of this they could not be used for D.C. conductivity measurements.

3.2.4 Alloyed Contacts

With this method, metal-SnS contacts were made with a variety of metals and their voltage-current characteristics were examined (Nikolić et al., 1976).

Two similar methods were used to make the alloying contacts. The apparatus used in the first technique is shown in Fig. 3.1. The heater is wound out of Kanthal wire and has a resistance of 100 ohm. The heater is powered by a variac, and the sample is placed on a thin quartz plate over the heater. The sample temperature is monitored with a chromel-alumel thermocouple placed below the quartz plate. A silica tube arrangement is placed over the whole sample/heater assembly.

Prismatical samples with dimensions of about 15 x 4 x 0.3 mm were cut from the cleaved thin plate. Indium pellets with diameter of 0.8 mm were divided into two pieces. The In pieces were etched with diluted HNO_3, rinsed with acetone and then washed with plenty of distilled water. The hemispherical In pellets were placed on the SnS and pressed slightly against SnS with match sticks. The specimens were then placed on the quartz plate. Before starting to heat, pure Argon gas was flushed through the jar in order to remove away remaining air in the container. The heater was then turned on, and the temperature increased at a rate of about 50 $^{\circ}$C per minute. When the temperature reached 150 $^{\circ}$C, HCl vapour was introduced by bubbling pure Argon gas

Heater

Sample

Outlet

Argon

H Cl

Variac
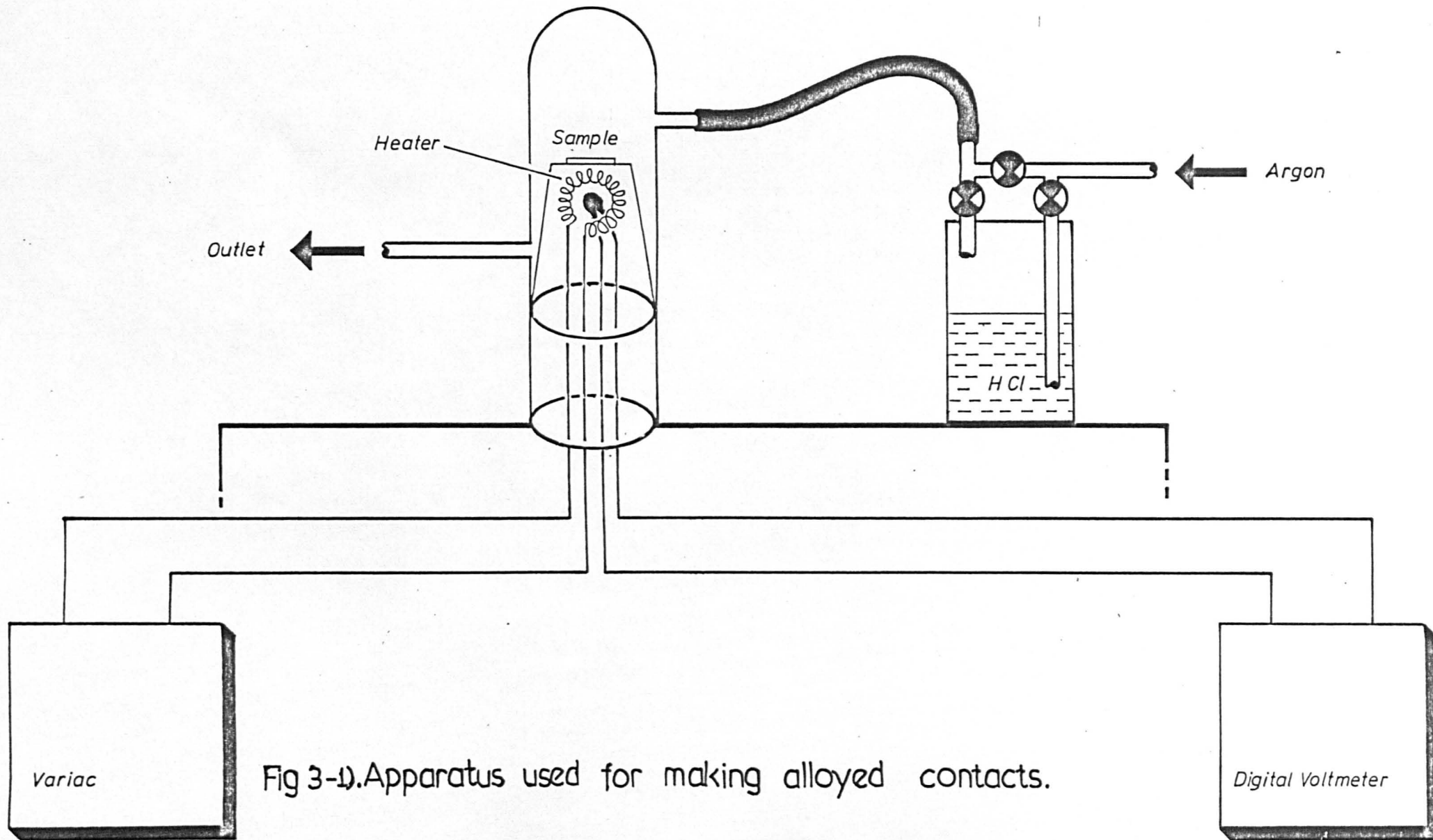
Fig 3-1). Apparatus used for making alloyed contacts.

Digital Voltmeter

through HCl acid. When the temperature reached 350 °C it was held constant for about a minute before cooling the specimens.

In the second method, the sample is alloyed in a vacuum in the bell jar of an evaporator. With this method, In, Sn, and Pb contacts were made to SnS. Small (0.8 mm diameter) pellets of the contact materials were prepared and etched as previously described in diluted HNO_3 followed by an identical rinsing procedure. The pressed contacts were placed on the semiconductor and the Bell jar was evacuated 10^{-5} torr or better before heating. Alternatively the pumping was stopped at 10^{-5} torr and pure argon gas introduced into the bell jar before heating as in the previous technique. The temperature was increased at a rate of about 10 °C per minute up to 350 °C and then (in the case of In contacts) held constant for approximately 20 minutes. For Sn and Pb contacts, however, the temperature is raised to 500 °C, because of the higher melting points of these materials.

With these methods, contacts could be made that were stable and reproducible. Both ohmic and non-ohmic contacts were made as seen in Figs. 3.2 - 3.5.

3.3 Barrier Height Measurements

Barrier height measurements were made at the range of temperature 30 - 150 °C for In-SnS-In and In-SnS-Ag systems. The specimens were prepared as
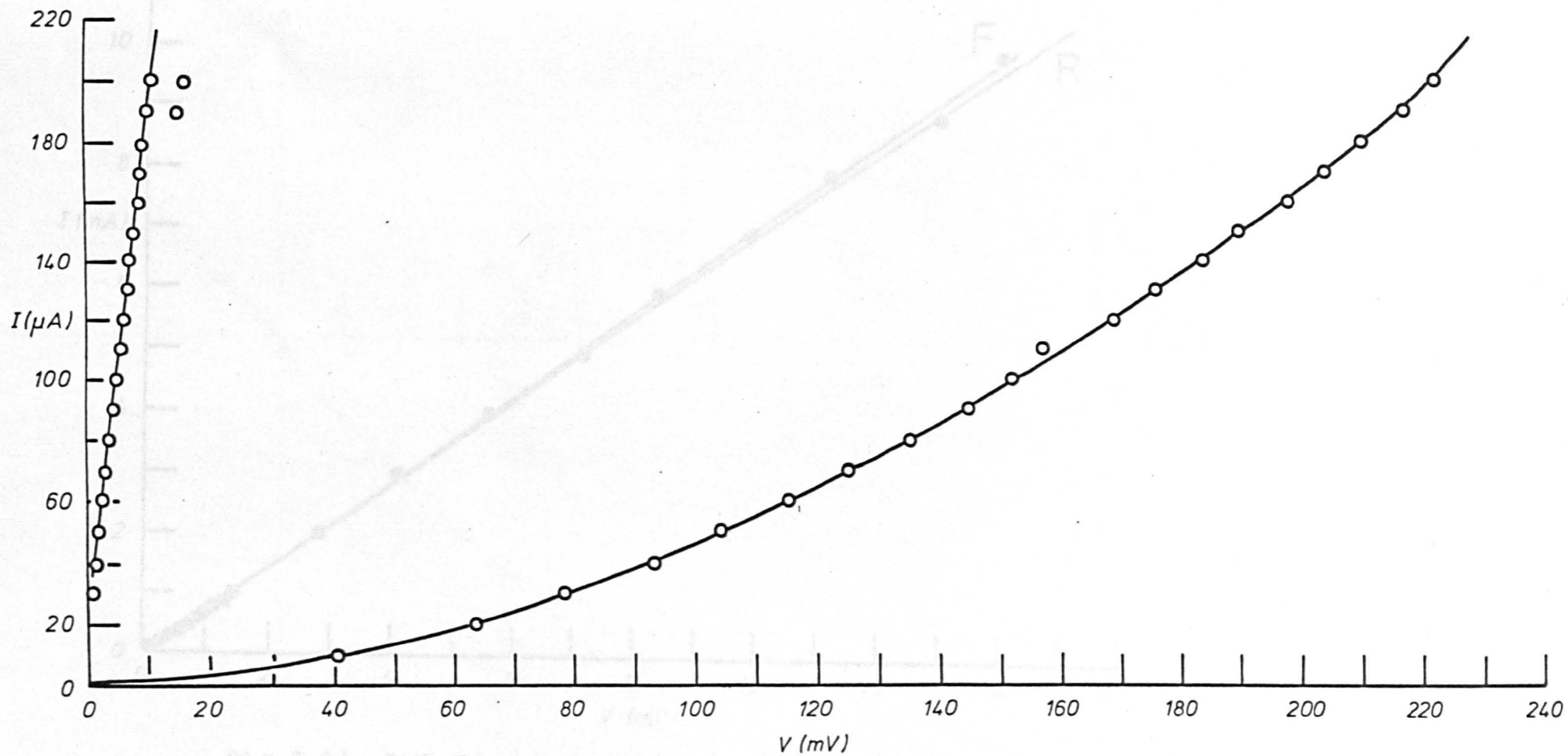
Fig.3-2):I-V Characteristics of alloyed In contacts onto n-type SnS.
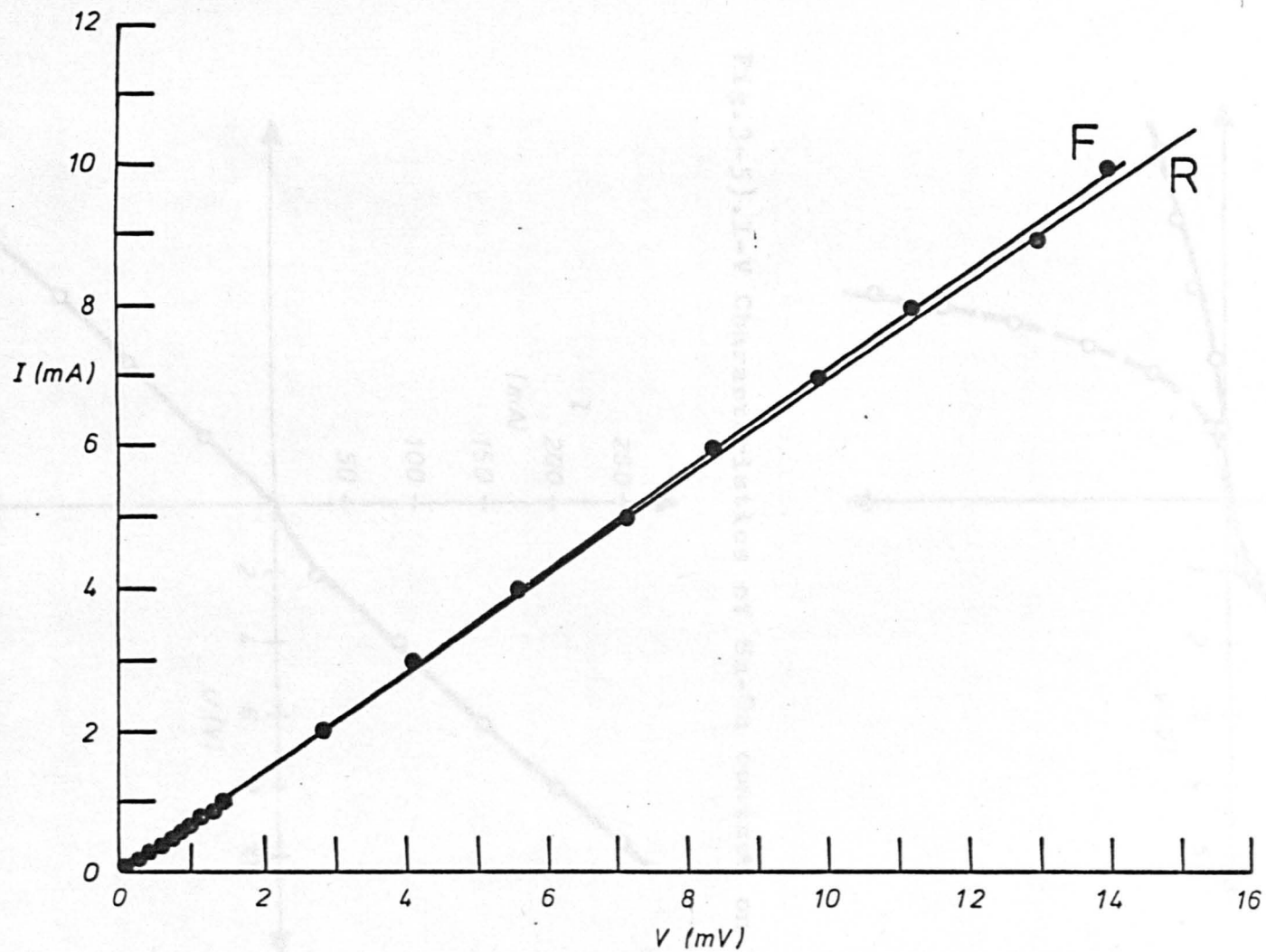
Fig.3-3). I-V Characteristics of alloyed In contacts onto p-type SnS.

Fig.3-4).I-V Characteristics of In-In contacts on SnS.
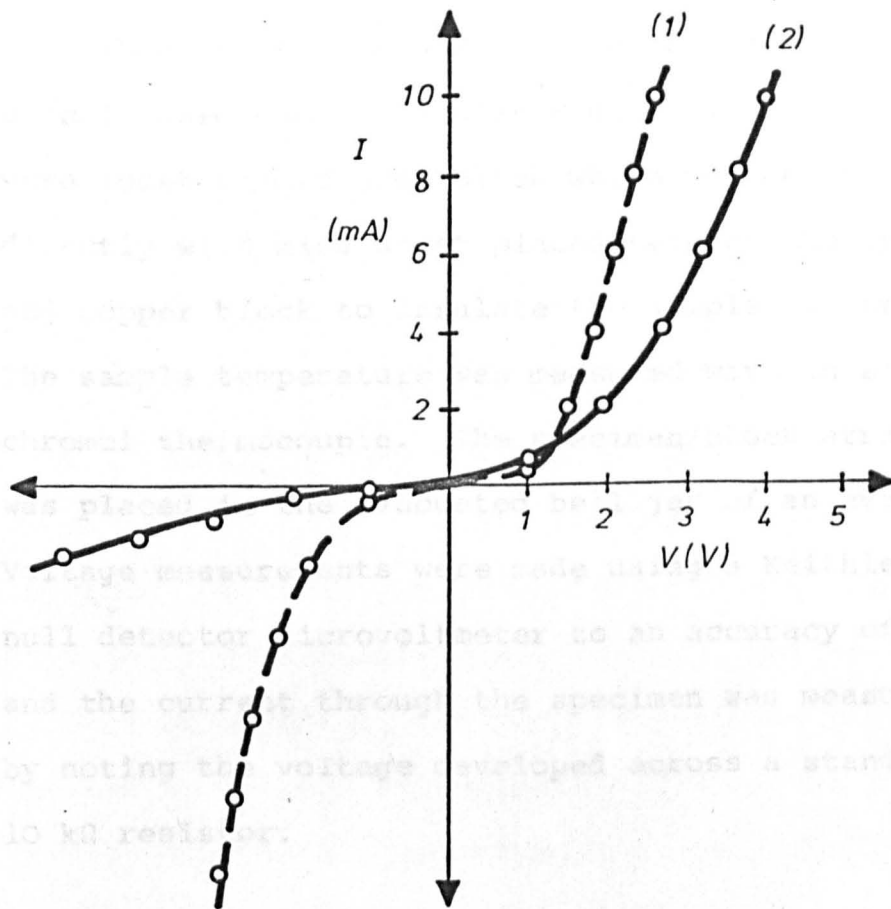
3.3.1 Barrier Height Theoretical Considerations

Fig.3-5).I-V Characteristics of Sn-Sn contacts on SnS.
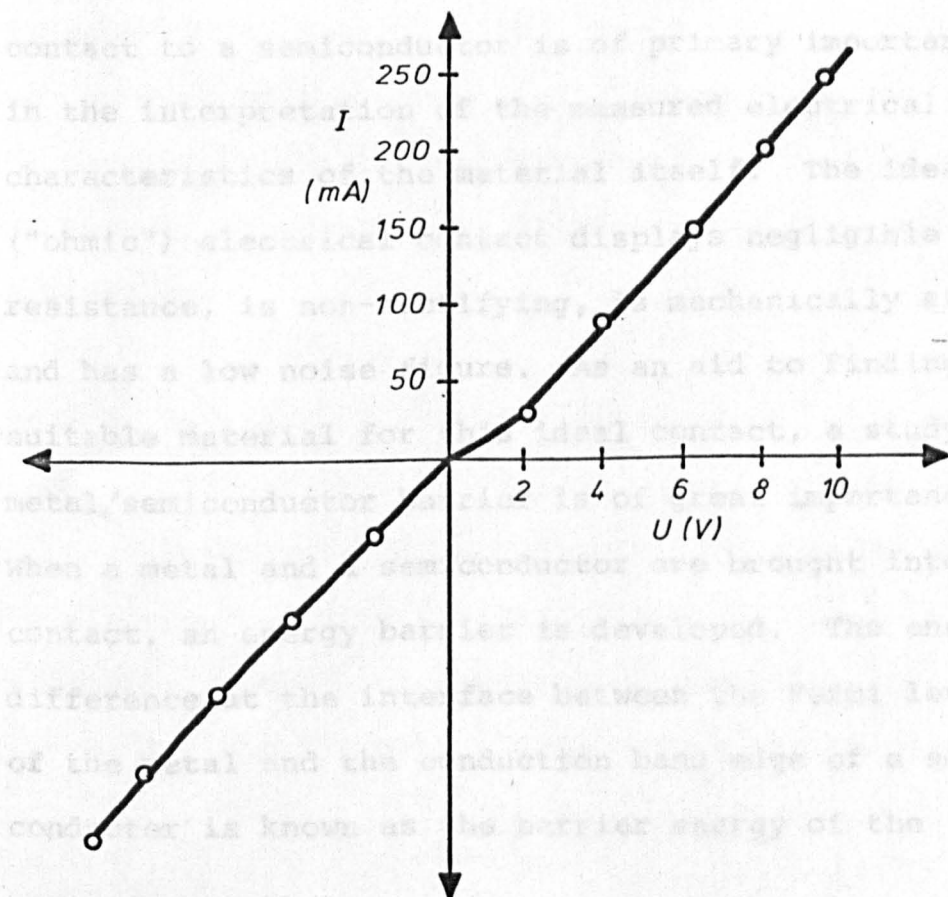
described in section 3.2. The general lay-out of
circuit used can be seen in Fig. 3.6. Specimens
were located on a copper block which was heated in-
directly with mica sheet placed between the specimen
and copper block to insulate the sample electrically.
The sample temperature was measured with an alumel-
chromel thermocouple. The specimen/block arrangement
was placed in the evacuated bell jar of an evaporator.
Voltage measurements were made using a Keithley 155
null detector microvoltmeter to an accuracy of $\pm 1\mu V$,
and the current through the specimen was measured
by noting the voltage developed across a standard
10 kΩ resistor.

3.3.1 Barrier Height Theoretical Considerations

An understanding of the nature of the electrical
contact to a semiconductor is of primary importance
in the interpretation of the measured electrical
characteristics of the material itself. The ideal
("ohmic") electrical contact displays negligible
resistance, is non-rectifying, is mechanically strong
and has a low noise figure. As an aid to finding a
suitable material for this ideal contact, a study of
metal/semiconductor barrier is of great importance.
When a metal and a semiconductor are brought into
contact, an energy barrier is developed. The energy
difference at the interface between the Fermi level
of the metal and the conduction band edge of a semi-
conductor is known as the barrier energy of the

particular metal/semiconductor interface. The study
of electrical interface barriers starts in 1874 with
Braun who observed rectification at an interface formed
by a metal and a PbS crystal. Since then many experi-
mental and theoretical investigations of barrier heights
at metal/insulator interfaces have been carried out.
The physics of metal/semiconductor interfaces, and the
general properties of ohmic contacts have been analysed
and reviewed by Mead (1969), and Bube (1960) has
discussed the formation of ohmic contact to semiconductors.
It is an experimentally observed fact that the size of
the barrier height ϕ_B for the covalent semiconductors is
with few exceptions approximately 2/3 of the band gap
for n-type materials and approximately 1/3 of the band
gap for p-type materials (Mead 1964, 1969, Rideout 1975).
Although the barrier height for covalent semiconductors
is approximately independent of the contact metal used
(Rideout, 1975; McGill, 1974), for highly ionic materials
such as most of the group 11-V1 compound semiconductors
the barrier height is strongly dependent on the work
function of the metal. In this case the barrier height
is given by

$$\phi_B = \phi_W - \chi_S$$

where ϕ_W is the work function of metal and χ_S is the
electron affinity of the semiconductor. Due to diffi-
culties in measuring ϕ_W accurately, we make use of
the electronegativity (Pauling, 1960) of the metal which
is related to the work funciton through the expression
$\chi_m = 0.44\phi_W - 0.15$ (Bube, 1960). Thus the barrier

height can be written (McGill, 1974) for ionic semi-conductors:

$$\phi_B \simeq \chi_m - \chi_s + \text{constant}$$

One can conclude from above equation that the barrier energy increases linearly with the electronegativity of the contact metal used, as has been shown by Rideout (1975). So we might write that

$$\phi_B \simeq S\chi_m + \text{constant}$$

where S is the so called Fermi-level stabilization parameter

$$S = \frac{d\phi_B}{d\chi_m} \quad , \quad \text{(Kurtin, McGill and Mead 1969)}.$$

The relationship of S to the electronegativity difference between the constituent elements of a compound semiconductor, ΔX, is shown in Fig. 3.13.

Several methods have been used to determine the barrier height ϕ_B, but the results are usually consistent (Mead, 1966). The methods include analysing the I-V characteristics of the contact/semiconductor junction, investigating the metal/semiconductor interface capacitance as a function of frequency, determining the photoresponse threshold (Spitzer and Mead, 1961) and observing the behaviour of tunneling electrons at liquid helium temperature (Guinet, 1974). The simplest measurement technique (measuring the I-V curves) was chosen in this case. Since the analysis used here is not given in any standard texts or publications we present it in full.

3.3.2 Measurement Technique

Consider an n-type material with two contacts which have unequal barrier heights and assume there is only one type of carrier as shown in Fig. 3.7.

The Richardson current over a barrier B is given by

$$J_B = AT^2 \exp(-B/kT)$$

where A is the Richardson constant. When an electric field is applied, a current I, passes through the sample. If the voltage between the terminals is V, and across the bulk of the semiconductor is V_R, then the current I will be written as:

$$I = \frac{V_R}{R}$$

where R is the resistance of bulk.

If the contact connected to the negative terminal of the battery has area a_1 and barrier b_1 the Richardson current for this contact will be:

$$I_{b_1} = a_1 J_{b_1} = a_1 AT^2 \exp(-b_1/kT)$$

If the applied current $I \ll I_{b_1}$; then $V_R = V$. Similarly if an applied field is reversed:

$$V_R = V \quad \text{if} \quad I \ll I_{b_2}$$

In general, if the current passing through the semiconductor is much less than the Richardson current (which may be of the order of tens of milliamps), the voltage drop will be symmetrical no matter what the barrier height is.
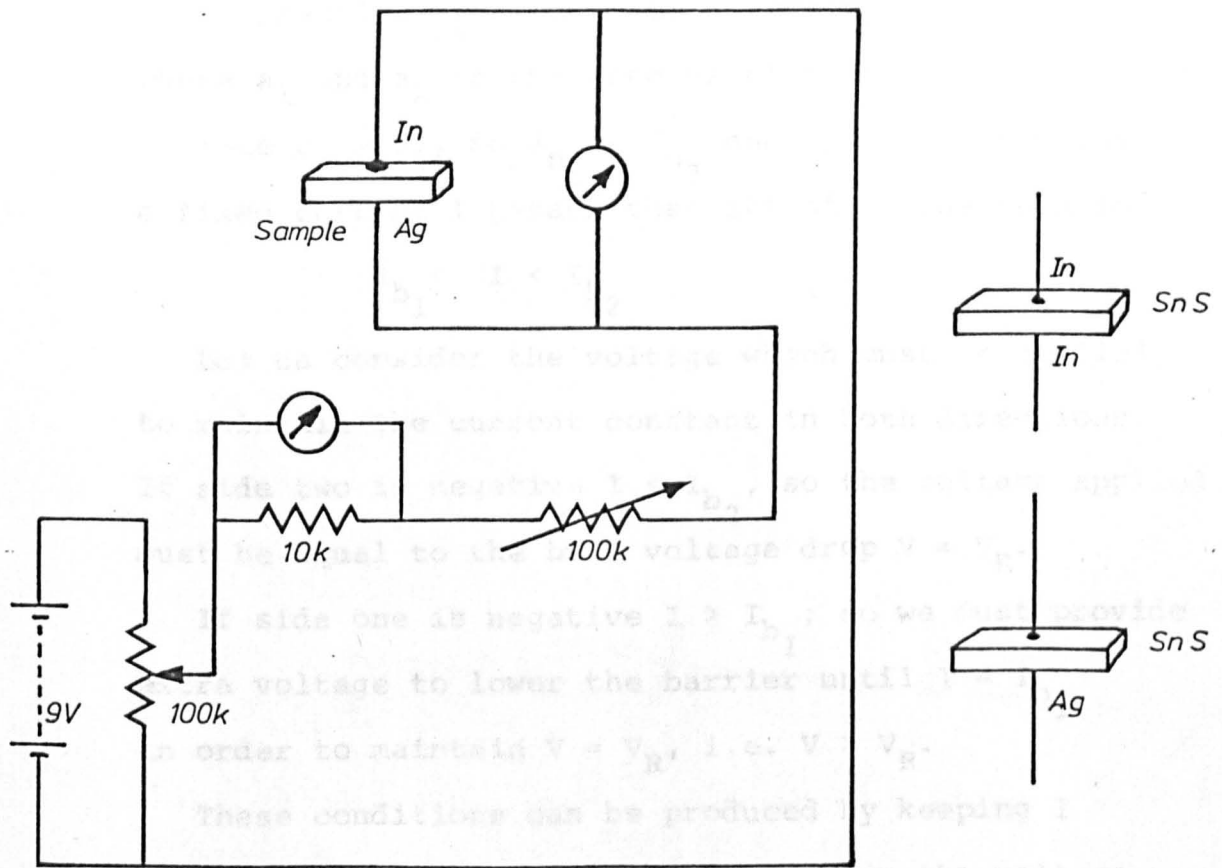
Fig.3-6).Circuit for barrier height measurements.
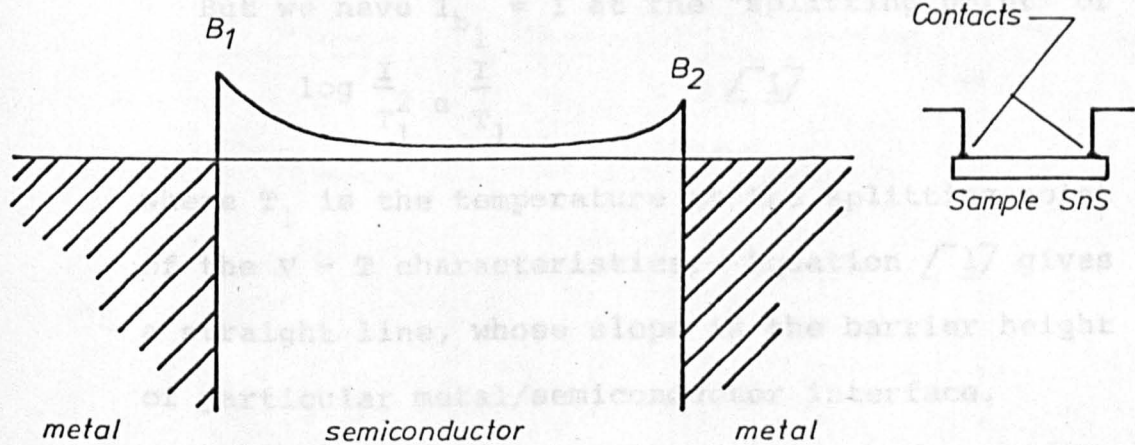
Fig.3-7).Schematic representation of two Schottky barrier

diodes.

In practice $a_1 \simeq a_2$ but the barrier height $b_1 \neq b_2$, where a_1 and a_2 is the area of contact made.

Take $b_1 > b_2$, so $J_{b_1} < J_{b_2}$ and $I_{b_1} < I_{b_2}$. Suppose a fixed current I passes that satisfies the relation

$$I_{b_1} < I < I_{b_2}$$

Let us consider the voltage which must be applied to maintain the current constant in both directions. If side two is negative $I < I_{b_2}$, so the voltage applied must be equal to the bulk voltage drop $V = V_R$.

If side one is negative $I > I_{b_1}$; so we must provide extra voltage to lower the barrier until $I = I_{b_1}$ in order to maintain $V = V_R$, i.e. $V > V_R$.

These conditions can be produced by keeping I constant and varying temperature. When the voltage between the terminals is plotted as a function of the temperature of the sample for several constant current values, one obtains the type of the graph shown in Fig. 3.8.

But we have $I_{b_1} = I$ at the "splitting point" or

$$\log \frac{I}{T_1^2} \; \alpha \; \frac{I}{T_1} \qquad \qquad \underline{/17}$$

where T_1 is the temperature at the splitting point of the V - T characteristics. Equation $\underline{/17}$ gives a straight line, whose slope is the barrier height of particular metal/semiconductor interface.

In practice the small voltage levels invoked in this determination can present measurement problems. For example, thermoelectric voltages will appear
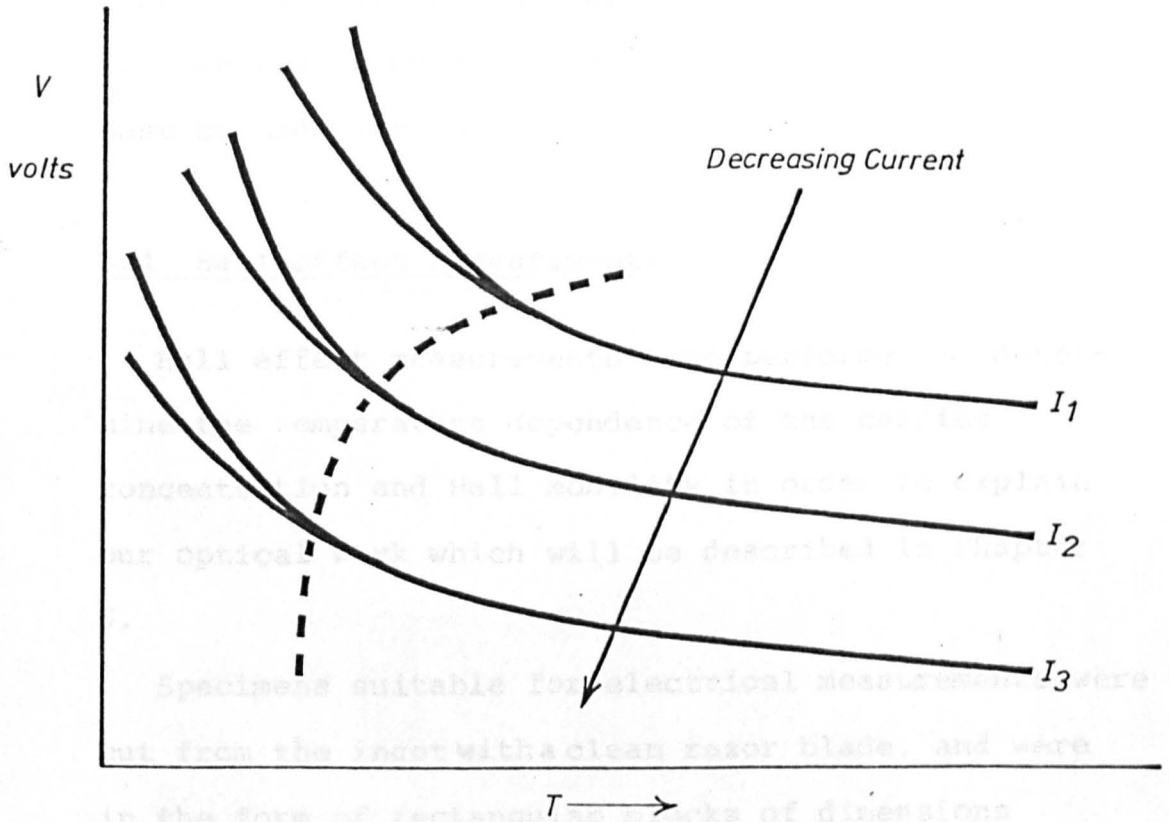
Fig.3-8).Typical voltage-temperature variation of
Schottky barrier diode.
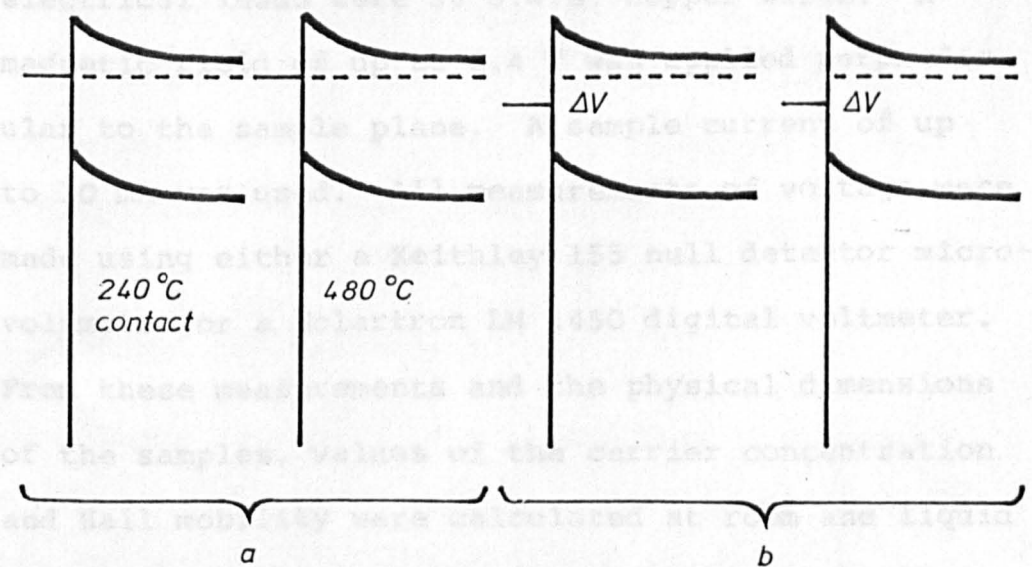
Fig.3-9).Energy diagrams of Schottky barrier diodes
before and after applied electric field.

across the temperature drop along the pin seals used in the evacuated chamber, and due allowance must be made for this.

3.4 Hall Effect Measurements

Hall effect measurements were performed to determine the temperature dependence of the carrier concentration and Hall mobility in order to explain our optical work which will be described in Chapter 6.

Specimens suitable for electrical measurements were cut from the ingot with a clean razor blade, and were in the form of rectangular blocks of dimensions 10 x 4 x 0.3 mm. Four and six contacts were made to the sample as described in section 3.2.4. The specimens were then stuck onto a sample holder with Durefix. The sample holder was made of teflon; the electrical leads were 36 S.W.G. copper wires. A magnetic field of up to 0.4 T was applied perpendicular to the sample plane. A sample current of up to 10 mA was used. All measurements of voltage were made using either a Keithley 155 null detector microvoltmeter or a Solartron LM 1450 digital voltmeter. From these measurements and the physical dimensions of the samples, values of the carrier concentration and Hall mobility were calculated at room and liquid nitrogen temperature using the equations below for a single one-carrier system.

The usual precautions of reversing magnetic field and current were carried out in order to minimise errors of interpretation due to contact misalignment and sample magnetoresistance.

The simple theory of the Hall effect is well known. Our data here analysed in the one carrier approximation for which:

$$R = - \frac{r}{ne} \qquad ; \qquad r = 1$$

$$R = \frac{V_H \cdot t}{B_Z \cdot I_X}$$

$$\sigma = ne\mu_H \qquad ;$$

$$\mu_H B_Z = \frac{E_H}{E_X}$$

where we have considered a sample oriented until a current I_X passing down its major axis: E_H is the Hall electric field; V_H the Hall voltage, B_Z the applied field and t the sample thickness. The carrier concentration is n, the Hall mobility μ_H and, the Hall coefficient (r) is assigned at unity. Other symbols have their usual meanings.

3.5   Results and Discussions

Specimens of single crystal SnS were prepared as described in Chapter 2 (see also Nikolić et al. 1976) using the Bridgman technique. The crystals can be easily cleaved into thin plates perpendicular to the c-axis due to its layer-type structure. X-ray analysis,

laue-photography and X-ray diffractograms confirmed that the ingots were single crystal. We do, however, have reason to believe that inhomogenities (local regions of impurity excess) exist in some samples, and this may explain the enormous variety of electrical contact behaviour observed.

3.5.1 Contact Properties; discussion

The contacts made by silver paint or lead-tin soldering were electrically noisy although sometimes mechanically strong. We therefore concentrate on the reproducible results obtained with alloyed metal contacts which as shown in Figs. 3.2-5. Figure 3.2 shows a non-linear characteristic which is typical of many obtained for n-type specimens, whereas Fig. 3.3 displays typical results for alloyed In-contacts on p-type SnS, showing apparently ohmic behaviour. The contacts on both materials were made at 240 $^{\circ}$C, and the characteristics measured by the same d.c. procedure. The contacts to the n-type material usually became noisy and the characteristics unreproducible for higher currents than displayed in Fig. 3.2. The sample of Fig. 3.3 was extensively used for transport measurements. Fig. 3.4 shows two curves for another n-type sample with alloyed In contacts made at 450 $^{\circ}$C (curve 1) and 400 $^{\circ}$C (curve 2). At low currents and voltages both curves show the non-linear behaviour exhibited by the forward portion of

Fig. 3.2, but the curves are symmetric in this
case. The entire curve (1) is symmetric up to the
maximum voltage ($\pm$ 5V), whereas this is not the
case for the curve (2).

In attempting to explain the observed contact
properties of indium alloyed onto SnS, we suggest
that in the alloying process the indium diffuses
a small distance into the material and acts as an
acceptor impurity, the distance of diffusion being
a function of alloying temperature. This is
deduced from thermopower measurements made on the
small area around the In contacts on n-SnS, which
indicate a p-type region. This introduction of the
acceptor impurity would then lower E_F in the p-type
material, producing an ohmic contact as seen in Fig.
3.3. This behaviour is in accordance with the well
known 'rule of thumb' that a diffused contact impurity
must have the same conductivity characteristic as
the host semiconductor to produce 'ohmic' contact
i.e., acceptor for p-type material and a donor for
n-type material. The non-linear behaviour frequently
observed as in Fig. 3.2 can be represented by an
equivalent circuit of a diode and resistor in series,
i.e., the contact made at this temperature (240 $^\circ$C)
to n-type material has produced one rectifying and
one non-rectifying contact.

One possible explanation for this behaviour would
be the existence of some gross sample inhomogenity

e.g. one end (the 'ohmic' contact end) being p-type
and the other end being n-type due, presumably, to
sulphur excess /Anderson and Morton, 1945; Albers
et al., 1961/.

This seems unlikely,
however, as the behaviour is noted for a number of
n-type samples with Indium contacts alloyed at this
temperature. Fig. 3-4 shows a symmetrical I-V curve
for Indium contacts made at a higher temperature
(450 ^{O}C), the low voltage (high resistance)portions of
which are identical with the non-linear section of
curve 3.2 (this is not shown explicitly in Fig. 3.4).
About $|Vc| = 1.2$ V, however, the conductivity charac-
teristic changes significantly, and for $|V| > |Vc|$ a lower
resistance is symmetrically displayed by the material.
One can explain this low voltage behaviour of Fig. 3.4
by two 'back to back' diodes, i.e., two non-ohmic
contacts to n-type material as found in the reverse
characteristic of Fig. 3.2. We suggest that the curves
for $|V| > |Vc|$ may be explained by increased carrier
injection from one (or possibly two) deeper acceptor
states of Indium in SnS, which are only created by
diffusion of Indium at the higher temperature of contact
formation (450 ^{O}C). We invoke the presence of these
levels in the observed near infrared photoresponse
(see Chapter 4) and remark that similar are found for
CdS (Kröger, Vink and Volger, 1955; Bube and Thomsen,
1955) and Ge (Morton, Hahn and Schultz 1956; Bube 1960).
Above about 1.2 volts we envisage that ionisation of the
deeper acceptor by energetic electrons proceeds by an

impact ionisation process, leading to an increased electron population and increased sample conductivity. The behaviour is displayed by each contact. This process may be alternatively thought of in terms of the measured Fermi levels in 'doped' and 'undoped' samples, i.e., n-type samples with contacts formed at 450 $^{\circ}$C and 240 $^{\circ}$C. Fig. 3-9 (a) shows the two situations before a forward bias is applied and Fig. 3-9 (b) after the application of a bias voltage. It may be seen that the barrier for flow into the metal is reduced significantly for the 'doped' specimen under bias, thus giving the higher conductivity as observed experimentally. The curve (2) evidently displays a greater V_c for the onset of this behaviour in the forward direction, which is compatible with a smaller population of acceptors being created in the semiconductor by the lower diffusion rate observed at the lower contact temperature (400 $^{\circ}$C). This curve, however, exhibits a non-symmetric characteristic for $|V| > |V_c|$. We suggest therefore that in the case of contacts formed by alloying of Indium at lower temperatures, the existence of sample inhomogenities becomes more significant, yielding unsymmetric contact behaviour.

The properties of alloyed tin and tin/Indium contacts were also studied as it was felt that these

might produce non-rectifying behaviour in n-type specimens. A typical curve produced for an n-type specimen with Sn contacts alloyed at 450 ^{o}C is shown in Fig. 3.5. The characteristics obtained with this contact material were noise free and repeatable up to the larger voltages applied, and display linear behaviour in one current direction with the same slope (40 Ω) as found for the linear section of Fig. 3.2. This value is evidently significant as it is obtained for a number of contact materials, and is to be interpreted as the bulk conductance of the n-type samples at room temperature. We would suggest that the change of slope in the forward characteristic of Fig. 3.5 is accounted for by the presence of a rectifying surface oxide layer between the tin contact and the semiconductor. At low voltages (< 2V) this leads to an increased resistance, but above 2V breakdown occurs and the conductivity is that of the bulk material i.e. the slopes of each side of the characteristic are the same.

Other alloy contact materials investigated were cadmium, lead and antimony. Lead sometimes formed ohmic contacts onto n-type SnS, which is understandable if one assumes that lead diffuses as a donor into SnS. However, the procedure was not always reliable, it is being noted that frequently SnS would melt before the 5-nines pure lead contact. Similar problems were

encountered with cadmium and antimony. Some
success was obtained with evaporated antimony
and cadmium contacts, but here problems arose with
fixing suitable connecting wires to these metals.

The study of electrical contacts to a new semi-
conductor such as SnS could occupy a thesis in itself,
so this brief investigation is far from exhaustive.
The object was to determine experimentally how low
noise, low resistance contacts may be obtained to
n- and p-type material which are mechanically sound
down to at least 77 ^{O}K. The effects of contact
ageing have not been thoroughly examined, neither
have the surface conditions been as carefully con-
trolled as would be necessary in such a study. However,
we conclude that contacts approaching this performance
criterion may be repeatedly obtained for p-SnS by
alloying with Indium at 250 ^{O}C under vacuum, and for
n-SnS with a lead alloy, but that the repeatability
for lead contacts is less good.

3.5.2 Barrier Height Discussion

Barrier height measurements were made as described
in section 3.3. In Figs. 3.10 and 3.11 the log V
versus T graphs are shown for silver paint and for
both alloyed and soldered In contacts made to p-SnS.
The barrier heights are obtained as explained in
section 3.3.2 from the slope of the log $^{I}/_{T}2$ versus
$^{I}/_{T}$ graphs for each type of contact. These values
are 0.1 eV for alloyed In contacts, and approximately

0.6 eV for both soldered In and silver paint contacts. Barrier height measurements are not easy to make, and we assign an uncertainty of $\pm$ 0.1 eV to these values.

The very low value of the barrier measured for alloyed contacts confirms the behaviour noted from the linear I-V characteristics. This is understandable if we imagine the Indium alloy contacts diffusing a short way into the p-SnS and acting as acceptors, as has been discussed in the previous sections. The high and approximately equal barriers observed for the silver (paint) and soldered Indium contacts may well represent the height over an oxide layer present in both systems between the metal and the semiconductor. This oxide layer would not be destroyed as it might be in the alloy-contact forming process, where a higher sample surface temperature and an acid flux are used.

A full study of barrier heights for a range of contact materials was not possible for SnS. This is because of the relatively low melting point ($\sim$881.5°C) which precluded evaporation of many metals as contact materials. Thus, had it been possible to produce gold and magnesium contacts, one would have been able to obtain a graph of barrier height (ϕ_B) versus electronegativity (X) for four contact materials (i.e. Mg, In, Ag, Au, for which X = 1.2, 1.7, 1.9 and 2.4 respectively). This would have then enabled a value for the Fermi level stabilisation parameter

$\dfrac{d\phi_B}{dx_m}$ and the electronegativity difference ΔX of the species of a compound semiconductor ($\Delta X = 0.2$ in this case). This value is not inconsistent with another interpretation of the present barrier height measurements for silver paint and (soldered) Indium contacts, namely that the values $\phi_B = 0.5$ and $\phi_B = 0.7$ eV for Indium and silver respectively, yielding

$$\frac{d\phi_B}{dX_m} \approx \frac{0.7 - 0.5}{1.9 - 1.7} = 1$$

as a maximal value, i.e.

$$0 < \frac{d\phi_B}{dX_m} < 1.$$

In conclusion, barrier height measurements for SnS have been made by analysing I - V characteristics in the temperature range 20 - 150 °C. The analysis assumes current flow over the barriers by a Richardson emission process, but this must remain an approximation since other processes (e.g. tunneling and field emission) are known to occur. Nevertheless, the major conclusion that reduced barrier heights may be obtained with Indium contacts to p-SnS is confirmed by observation of the I-V curves, and tends to support the basic correctness of the assumption of thermionic emission as being the dominant barrier crossing mechanism.
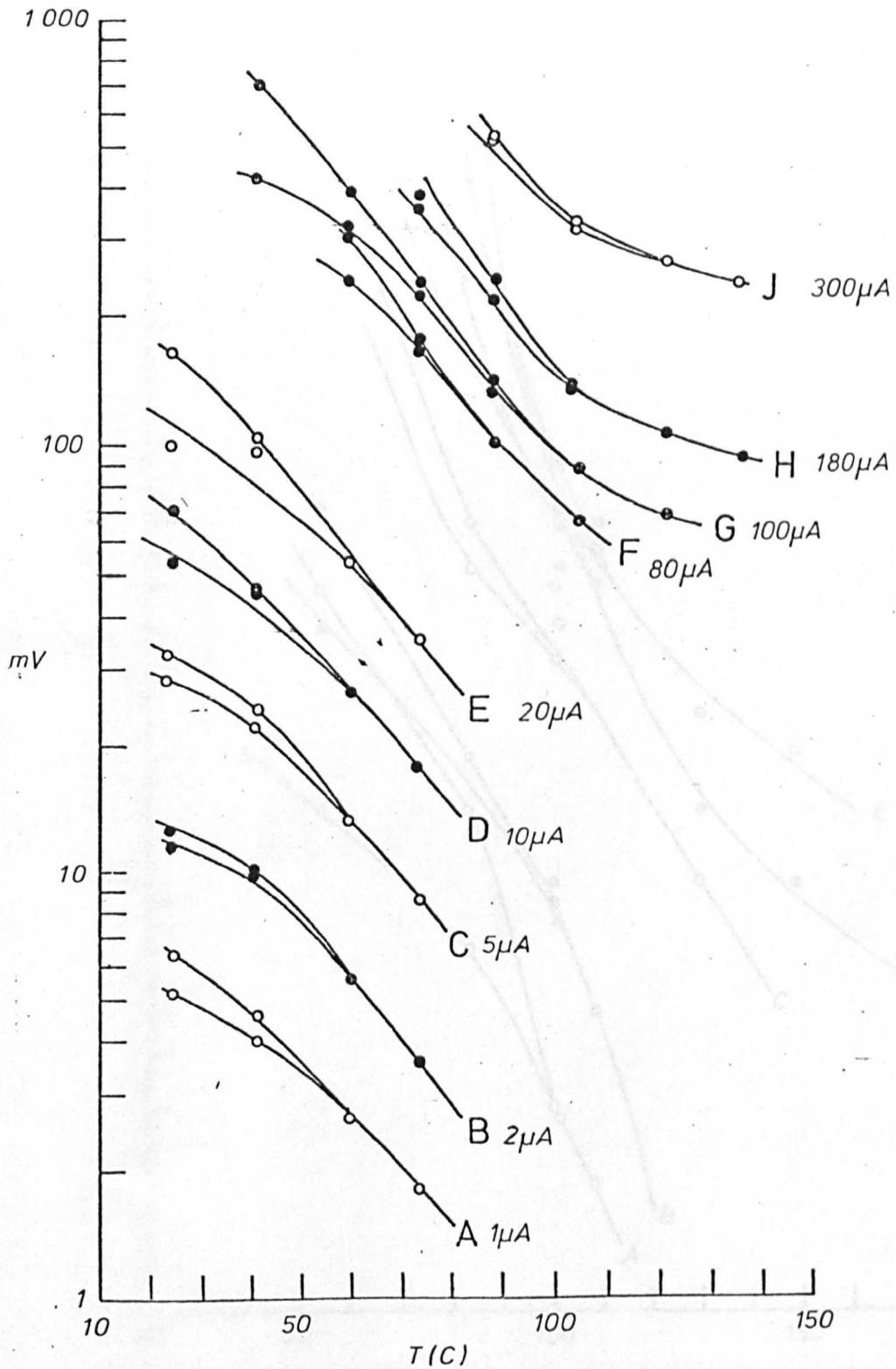
Fig.3-10).Voltage-Temperature variation of alloyed

In contact on p-type SnS.
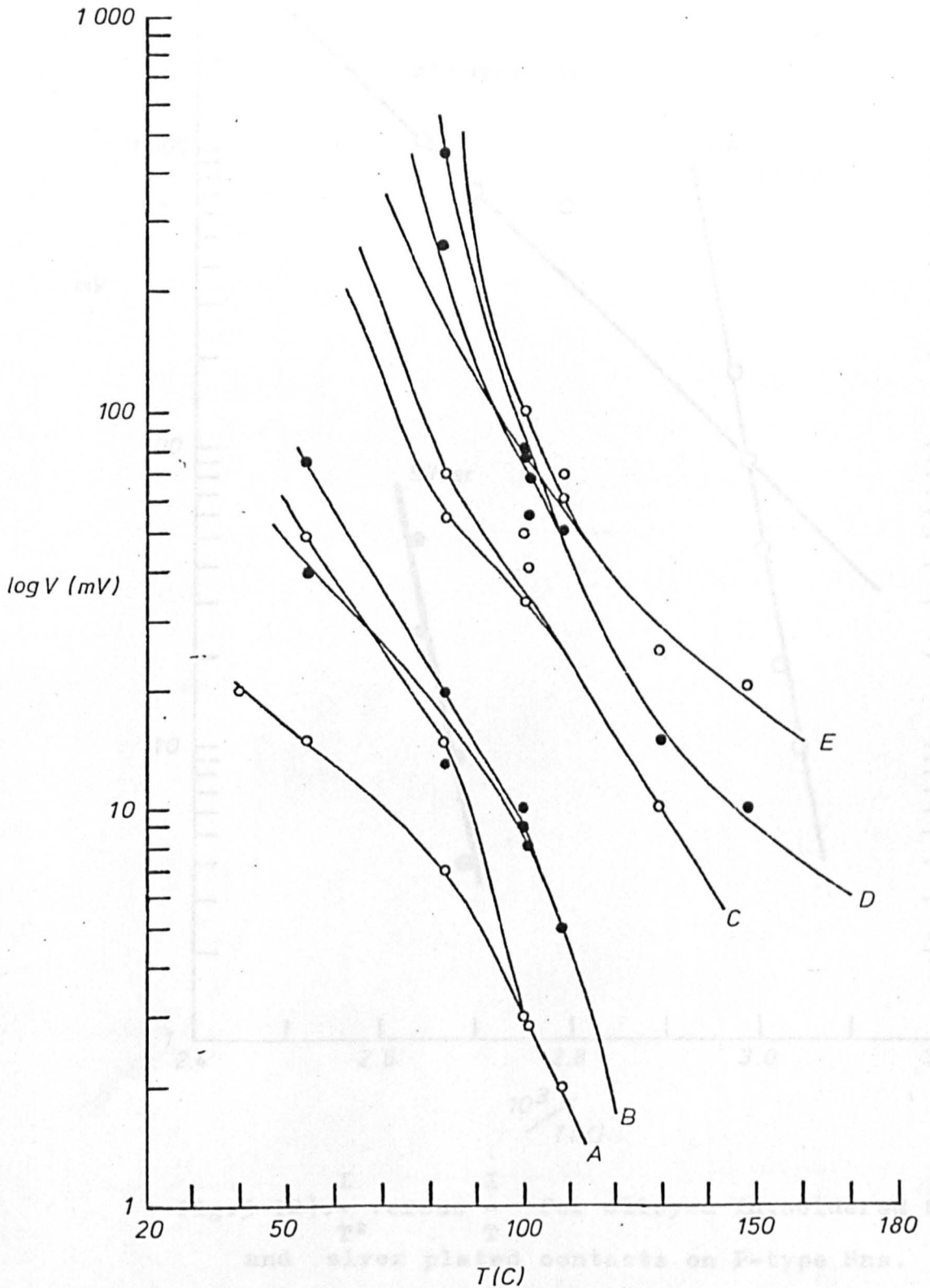
Fig.3-11).Voltage-Temperature variation of silver

plated contact on p-type SnS.
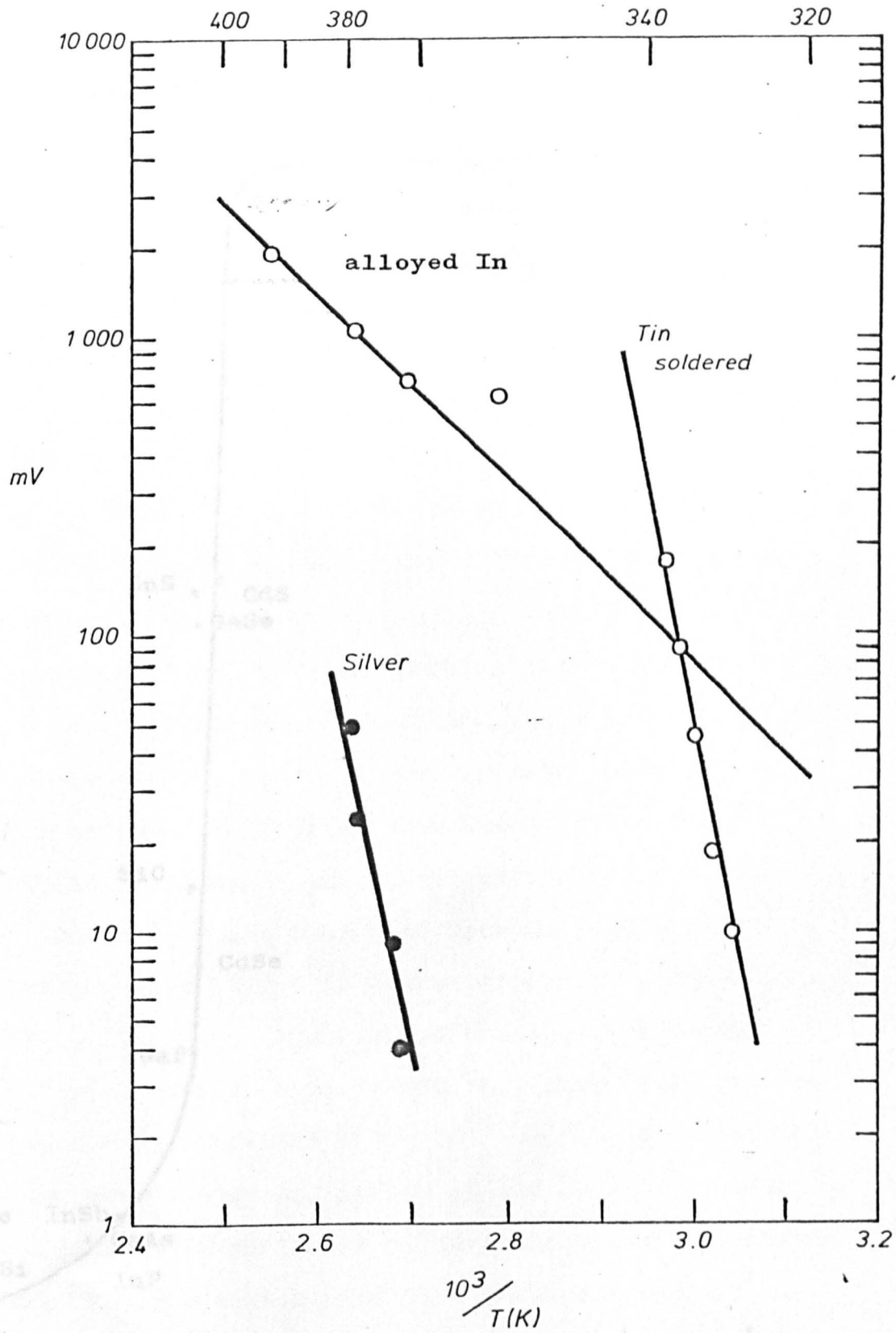
Fig.3-12).- $\dfrac{I}{T^2}$ versus $\dfrac{I}{T}$ for alloyed In, soldered Sn and slver plated contacts on P-type Sns.

Fig.3-13).Index of interface behavior,s,vs electronegativity
        difference, x, between the species of a compound
        semiconductor (after Kurtin et al,1969)

3.5.3 Hall Effect and Mobility Measurements

Temperature dependent Hall effect and carrier conductivity measurements have been made on crystalline n-and p-type specimens. Serious problems were encountered with contacts to the sample which limited the temperature range in which measurements could be made. The results which were obtained are displayed in table 3.1. As is well known, values for carrier concentration are obtainable without low resistance contacts, since current drawn from the Hall contacts is vanishingly small. Mobility determinations, however, require the bulk conductivity of the material to be known, and hence low resistance, non-rectifying contacts are required in this case. The range of carrier concentration obtained for a variety of samples are indicated in brackets.

The only other published data on Hall effect measurements in SnS is due to Albers et al (1960, 1961, 1962) who investigated transport in p-type material in the range 77-600 $^\circ$K. They found carrier concentration ranges $10^{17}- 10^{19}$ cm^{-3}, and typical room temperature mobilities of 100 cm^2/V-sec rising to 1000 cm^2/V-sec at 77°K. Evidently our own figures are consistent with this data and would suggest, if anything, a higher mobility in our samples than in those used by Albers et al. Presumably the variation of carrier mobility with temperature is best explained by the usual judicious mixture of (high temperature) ionised impurity scattering, although the lack of

comprehensive low temperature data (due to contact problems) limits these conclusions in our case.

In the case of n-type material the contacts gave extreme problems, and it was only possible to extract carrier concentration data at 77 ^{O}K and 300 ^{O}K for a small number of samples. We remark, however, that in the same temperature range, the freeze-out in the two materials is essentially the same $((n/p)_{300} / (n/p)_{77} \sim 2.5)$, indicating approximately equal depths for substituted acceptors and donors. In view of the obvious crystallographic assymmetries in this material it was decided to investigate mobilities in a, b and c directions for a p-type sample. The preparation of a suitable sample for c-axis work presented such materials problems that it was finally abandoned, leaving measurements in the a and b directions which yielded identical values for mobility within the limits of experimental error. Evidently one may expect significant variation in mobility between the c-axis and the other two in view of the differences in physical properties in this direction, and it is regrettable that this measurement could not be made.

In conclusion, the present transport measurements may be considered to indicate the range of sample mobilities and carrier concentrations used in our experiments. They represent a limited study, however, which must await further improvements in contact fabrication before further conclusions can be made.

Sample No:	Temperature ($^\circ$K)	Carier Concentration (cm^{-3})	Hall Mobility (cm^{-2}/V.Sec)
A(p-type)	3C0	1.15×10^{19}	146
	77	6.54×10^{18}	1512
B ,,	300	7.49×10^{18}	169
	77	5.50×10^{18}	1500
C ,,	300	5.62×10^{19}	-
	77	4.85×10^{18}	-
	50	1.25×10^{18}	-
D(n-type)	300	6.25×10^{18}	236
E ,,	300	3.83×10^{18}	354

CHAPTER FOUR

PHOTOCONDUCTIVITY AND RELATED PHENOMENON ON CRYSTALLINE SnS

4.1 Introduction

A study of photoconductivity and the photovoltaic effect in semiconductors allow us to explore semiconductor band structure, recombination processes, impurity levels and the properties of metal-semiconductor interfaces.

In the present work, photoconductivity and photovoltaic effects were investigated for the first time as a function of sample temperature, (40 $^{\circ}K$ - 300 $^{\circ}K$) energy of incident radiation (0.4 - 2 eV), sample bias and illumination intensity for a variety of both n- and p-type crystalline SnS samples. The determination of the temperature and energy variation of photoconductivity and photovoltaic effect involved three sets of apparatus. One, for determining the room temperature photoconductivity and photovoltaic spectrum covering the region approximately 0.99-1.50 eV, was used for n-type crystalline SnS samples. Two further systems were used for measurements on p-type material; one for 77 $^{\circ}K$ and 300 $^{\circ}K$ measurements in the range 0.99-2.10 eV, and one for 40-300 $^{\circ}K$ measurements in the spectral range 0.4-1.3 eV. We confine the details of

these arrangements to the appendix to this chapter, A.

4.2 Photoconductivity Measurement Technique

In each case a fairly conventional photoconductivity measurement was used; a wide band quartz-halogen lamp illuminates the entrance slit of a monochromator, the output of which is focussed by a quartz-lens or aluminium mirror train onto the specimen which is placed in the cryostat. A mechanical chopper and reference assembly (10 hz - 800 hz) is used and phase-sensitive detection of the photo-response is employed. The results are displayed on a chart recorder as the monochromator is scanned automatically. By varying the chopper frequency, the signal can be measured away from the region of mechanical and flicker noise frequencies, specific contact noise frequencies and even noise from fluctuations in the density of photocurrent carriers. (Rose 1955).

Specimens suitable for photoconductive measurements were cut from the ingot. Each time four contacts were made on freshly cleaved and oriented samples as described in chapter 3. On most specimens two-contact and four-contact measurements were attempted, and in addition a number of simple combinations of biassing circuits and transformer/preamplifier arrangements were used to optimise sample photosignal. In all cases extensive shielding precautions were taken. Simple masks were also made up to shield or expose various parts of the sample and contacts. The analogue records of the photosignal which were ultimately obtained

were ratioed to the monochramator instrument function. This was obtained by measuring the monochromator output with a thermopile (Hilger-Schwarz FT - 9008) and pre-amplifier arrangement.

A certain amount of confusion exists in the literature over the terms 'photoconductive' and 'photovoltaic' effects. In a perfectly homogeneous sample provided with two barrier contacts the action of illuminating radiation $h\nu > E_g$ is to create electron-hole pairs in the conduction and valence band respectively, thereby changing the sample resistance. Evidently this change may be observed as a change in voltage across the specimen, or across a resistance in series with it, when the specimen is placed in a simple bias circuit. This, strictly speaking, is the photoconductive effect. An alternative method of measuring this phenomena of bulk-generated photoconductivity is to measure the voltage change across the inner pair of four contacts, the outer pair being connected to a constant-current supply. In many practical cases, however, an inhomogeneous sample, or a sample with partially or totally rectifying contacts implies the existence of space charges at barriers. Photoproduced carriers will under these circumstances migrate, ultimately producing an e.m.f. This, strictly speaking, is the photovoltaic effect, and is measured in a two-contact geometry. In most of our experiments, it is this effect which is measured, since it is often orders of magnitude greater than pure photoconductivity. The a.c. photovoltages generated are of the order of 10 μv. Evidently the measurement of such small signals

requires careful impedance matching of amplifiers and
transformers and the extensive use of screening.

4.3   Results and Discussion

4.3.1   n-SnS for 0.9 < hν < 1.5 eV

Figures 4-1 to 4-5 inclusive show typical photo-
conductive characteristics obtained for n-type samples
at 300 °K in this frequency range. Two photo-conductive
response characteristics for a sample with Sn-Sn contacts
(1) and Sn-In contacts (2) are shown in Figure 4.1.
Although the scales of these graphs are different, the
shape of the response is broadly similar. For curve (1)
illumination of the bulk (contacts shielded) and illumi-
nation of the contacts produced essentially the same
results. With In-Sn mixed contacts, however, the photo-
current intensity was much higher if the indium contact
was exposed. Using the Moss criteria for obtaining the
excitation gap from curve (2) we obtained 1.13±0.02 eV,
(1.09μ) and if we regard the curve (1) as essentially
curve (2) at long-wavelengths (i.e. λ > 0.9μ) the same
result is obtained. We justify this procedure later,
but remark now that E_g = (1.13±0.02) eV almost certainly
corresponds to the indirect transition observed in
absorption by Lambros et.al (1974). The higher intensity
of curve (2) compared to (1) is explained by carrier
injection from the acceptor level created in n-SnS by
indium diffusion at the contact. It is not, perhaps,
therefore surprising to find that two indium contacts

('B', Fig. 4.2) give an even larger photoresponse, as
may be seen from the relevant scales on these diagrams.
The long-wavelength edge of this curve again provides
us with a value for the indirect gap, but the curve
peaks at 0.84μ with a point of inflexion at 0.95μ. We
suggest that the peak in our curve at 0.84μ may be
interpreted as a transition to another level at 1.46 eV.
Lambros et al (1974) have invoked the presence of a
phonon-involved transition at 1.42 eV to explain their
transmission data, and this is certainly in good agreement
with the present data. We remark that the difference in
shape of curves 4.1 and 4.2 (B) are almost certainly att-
ributable to different surface recombination properties
in these samples. This type of variance is not unknown
in, for example, CdS (e.g. Görlich, photoconductivity
of solids p.48).

Curves 4.2 (A), 4.3, 4.4 and 4.5 were all obtained
with rather thin specimens, t < L where L is the diffusion
length. Under these conditions we may expect moderate
to high surface recombination, giving a sharp peak in the
region of the gap. An investigation of this type of
response was made, for example, in GaAs by Frederikse
and Blunt (1955). Moss (1965) has also analysed the
photoresponse under these conditions, and has shown that
the short-wavelength sensitivity is inversely proportional
to the surface recombination velocity. The sharp peak
observed in these samples provides a value 1.09 ± 0.02 eV
for the indirect transition energy which is consistent
with that obtained from the previous curves. In addition,
a small peak is observed at 0.84μ (i.e. 1.46 eV) which
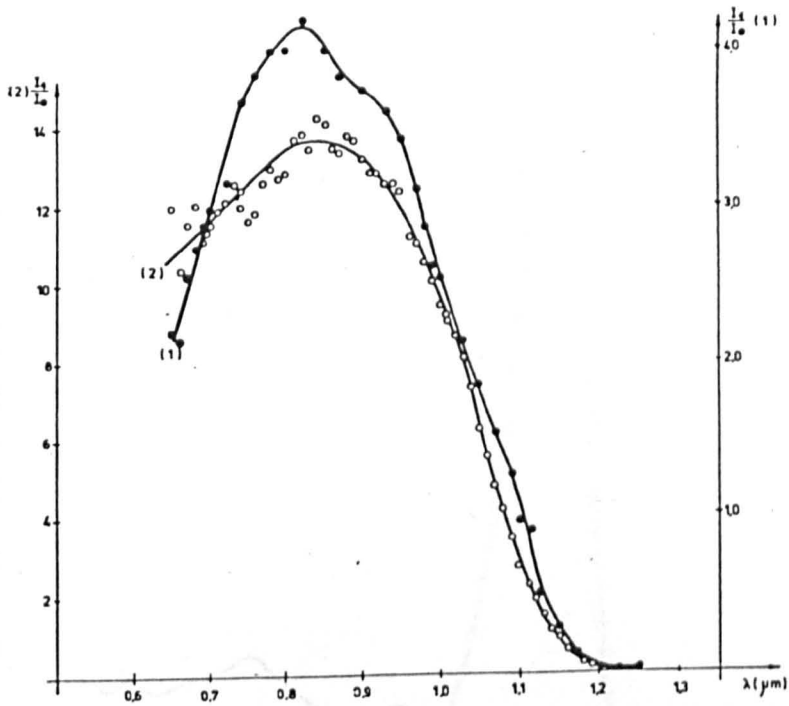
Fig.4-1). Photo response curve of n-type SnS.
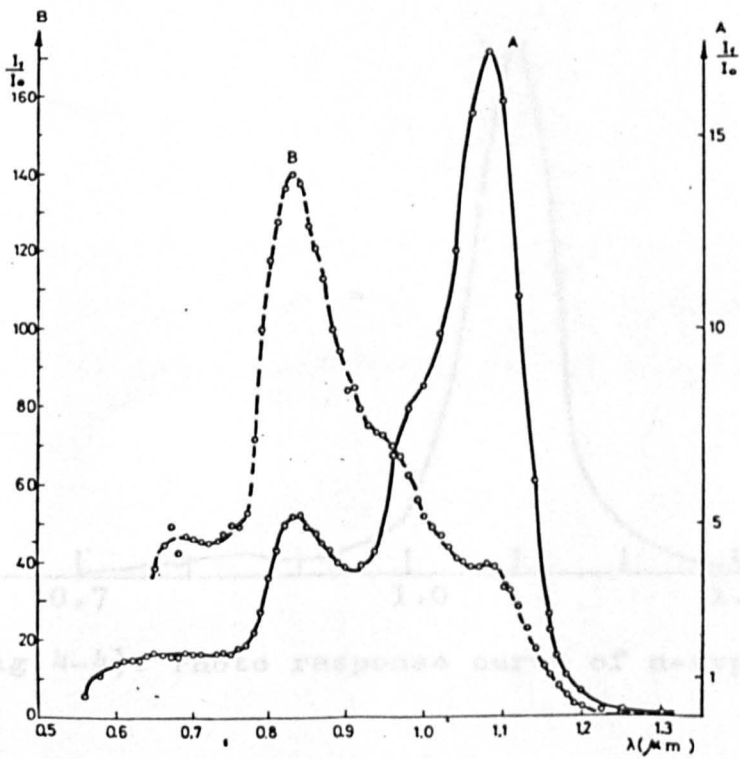
Fig.4-2). Photo response curve of n-type SnS.
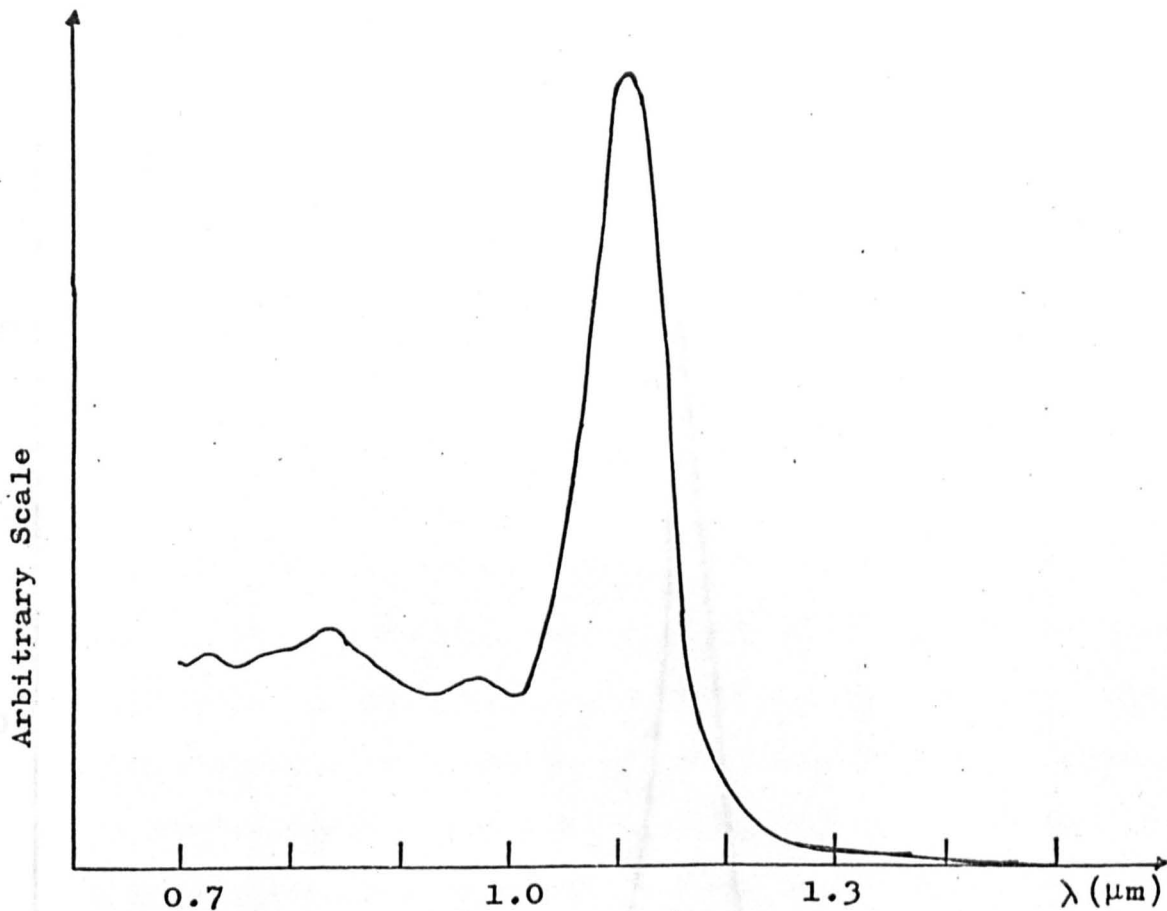
Fig.4-3). Photo response curve of n-type SnS.
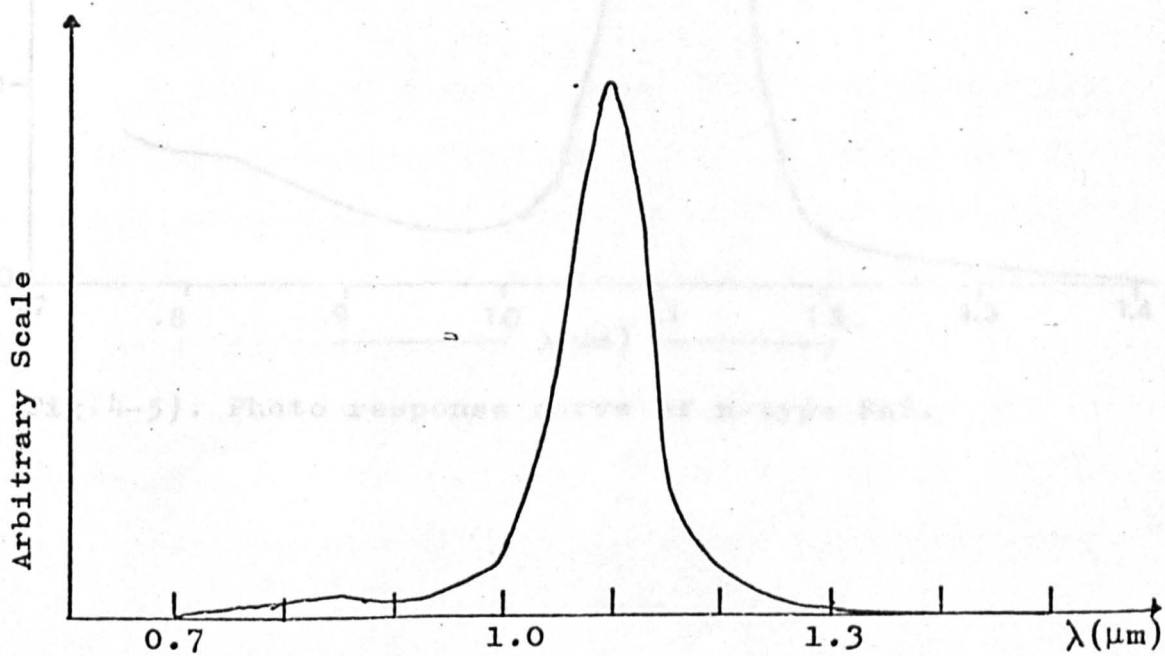
Fig.4-4). Photo response curve of n-type SnS.
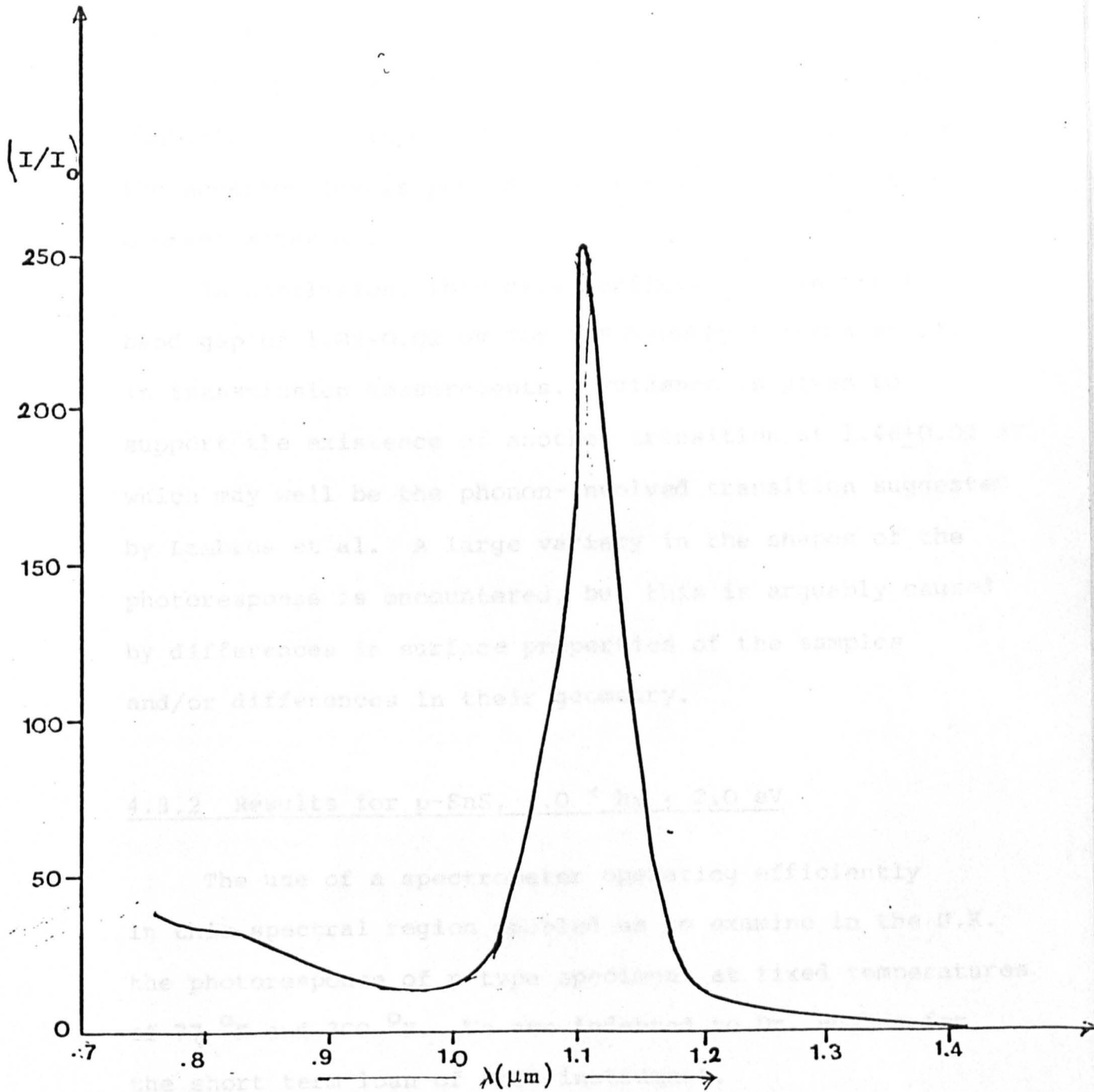
Fig.4-5). Photo response curve of n-type SnS.

is again explained in terms of another transition in
the material. The relative size of the response for
Figures 4.3 (bulk only illuminated) and 4.4 (bulk plus
contacts) is again explained in terms of injection from
the acceptor levels provided by the diffusing of indium
contact material.

In conclusion, this data confirms the (indirect)
band gap of 1.09±0.02 eV for SnS found by Lambros et al.
in transmission measurements. Evidence is given to
support the existence of another transition at 1.46±0.02 eV
which may well be the phonon-involved transition suggested
by Lambros et al. A large variety in the shapes of the
photoresponse is encountered, but this is arguably caused
by differences in surface properties of the samples
and/or differences in their geometry.

4.3.2 Results for p-SnS, $1.0 < h\nu < 2.0$ eV

The use of a spectrometer operating efficiently
in this spectral region enabled us to examine in the U.K.
the photoresponse of p-type specimens at fixed temperatures
of 77 $^{\circ}$K and 300 $^{\circ}$K. We are indebted to Dr. Hughes for
the short term loan of this instrument.

Indium contacts were made to these specimens as
described in chapter three. The bias current (dark
current) passing through the sample was of the order of
the Richardson barrier current, for which values the
contacts were non-rectifying. Both the room temperature
data, and the 77 $^{\circ}$K data of necessity, were taken with

the specimen in vacuo. Effects of the ambient atmosphere, producing changes in the surface recombination velocity which have been mentioned in the previous section in connection with the short-wavelength response should not, therefore, be of importance in this case (Bock et al, 1958; Bube 1953, 1960).

We analyse the photoresponse band edge in terms of an indirect transition and a direct transition. The inflexion point F_2 occuring in Fig. 4.6 at 1.13 ± 0.02 eV and 1.22 ± 0.02 eV for 300 ^{O}K and 77 ^{O}K respectively is associated with the indirect transition and the temperature independent peak E_1 in Fig. 4.7 (1.43 ± 0.02 eV) is, in our opinion, an indication of a direct valence-band to conduction band transition. We suggest that one of these transitions is direct and the other indirect from the difference in the slopes θ_1 and θ_2 of the photoresponse vs. energy curves. An analysis by the author for this material suggests that for indirect transitions the slope of this graph is greater than for direct transitions. Finally, we remark that the shift of the indirect band edge from (1.13 ± 0.02) eV at 300 ^{O}K to (1.22 ± 0.02) eV at 77 ^{O}K is consistent with the shift of (0.18 ± 0.05) eV found for the shift of the absorption edge between 300 ^{O}K and 100 ^{O}K by Lambros et al. The photoresponse for $h\nu > F_g$ in semiconductors is not frequently investigated. As has been remarked earlier the surface properties are of great importance in this régime, and effects due to atmospheric change (Bube, 1953, 1960; Bock, et al. 1958) or the disposition of contacts (Bock) are not unknown. As yet, no band structure is available for SnS and
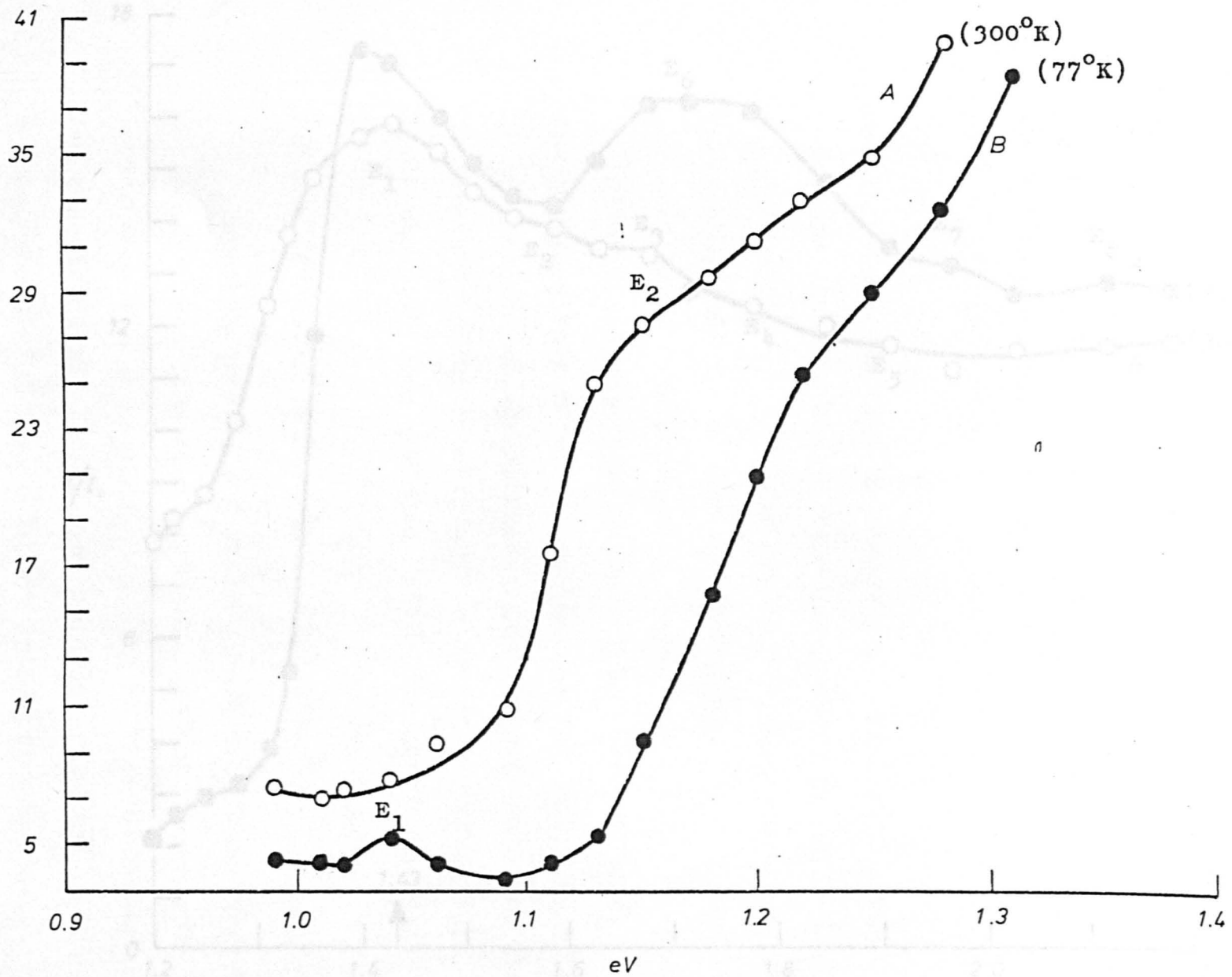
Fig. 4-6). Photo response curve of p-type SnS.
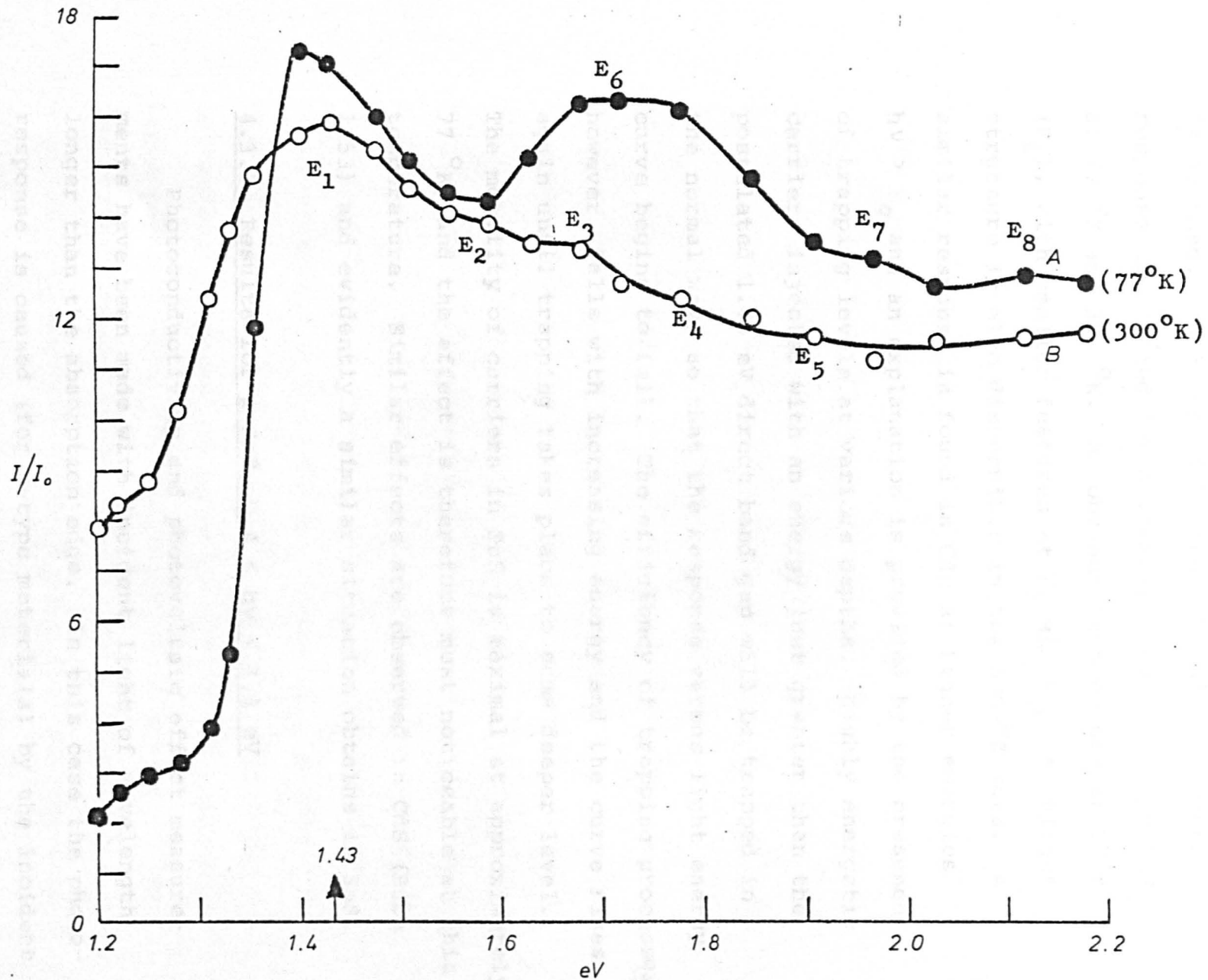
Fig. 4-7). Photo response curve of p-type SnS.

therefore no theoretical evidence for other bands
which might show up in the high energy photoresponse
is to hand. In Figure 4.7, the typical high-energy
response is plotted for a freshly cleaved p-type SnS
at 77 ^{O}K and 300 ^{O}K. An obvious bump occurs at 77°K
(F_6), with smaller features at F_7 and F_8; some slight
structure is also discernible in the 300 ^{O}K data. A
similar response is found in CdS at higher energies
$h\nu > E_g$ and an explanation is provided by the presence
of trapping levels at various depths. Highly energetic
carriers injected with an energy just greater than the
postulated 1.43 eV direct band gap will be trapped in
the normal way, so that the response versus light energy
curve begins to fall. The efficiency of trapping processes,
however, falls with increasing energy and the curve rises
again until trapping takes place to some deeper level.
The mobility of carriers in SnS is maximal at approximately
77 ^{O}K, and the effect is therefore most noticeable at this
temperature. Similar effects are observed in CdS (Bube
1953) and evidently a similar situation obtains in SnS.

4.3.3 Results for p-SnS, 0.4 < hν < 1.1 eV

Photoconductivity and photovoltaic effect measure-
ments have been made with incident light of wavelength
longer than the absorption edge. In this case the photo-
response is caused (for p-type materials) by the incident
photon producing a free hole and an electron bound in
the neighbourhood of the acceptor impurity. The photo-

current density will be determined, in the normal way,
by the total excess carrier concentrations and their
mobilities

with $\Delta p = \tau.f;$

where Δp is the steady state increase in the density
of free carriers generated at an excitation rate f/second
per unit volume, with τ the free-state lifetime of the
carriers. This is the simplest and most general photo-
conductivity relation.

In this section, we review the photoresponse of
p-type SnS samples in the temperature range 40-300 ^{O}K
for incident radiation of energy less than the band gap.
Although several measurements were made down to 10 ^{O}K
in the cold finger cryostat system, severe contact noise
problems were encountered. The 'below gap' photoresponse
of semiconductors is not widely investigated, except for
the notable exceptions of Ge, Si and CdS. This is perhaps
surprising as the technique forms an invaluable complement
to absorption spectroscopy and photoluminescense in
investigating semiconductor impurities. This ability to
resolve structure to a greater extent than is possible
with, for example, the absorption spectroscopy technique
is reviewed by Kogan and Lifshits (1977) and Collins and
Lightowlers (1968). We remark that in the case of SnS
the present photoresponse data are significantly better
than the only absorption data to hand in this spectral
region.

Figure 4.8 shows averaged traces of the photoresponse
from a typical p-type SnS sample between 40 ^{O}K and 300 ^{O}K.
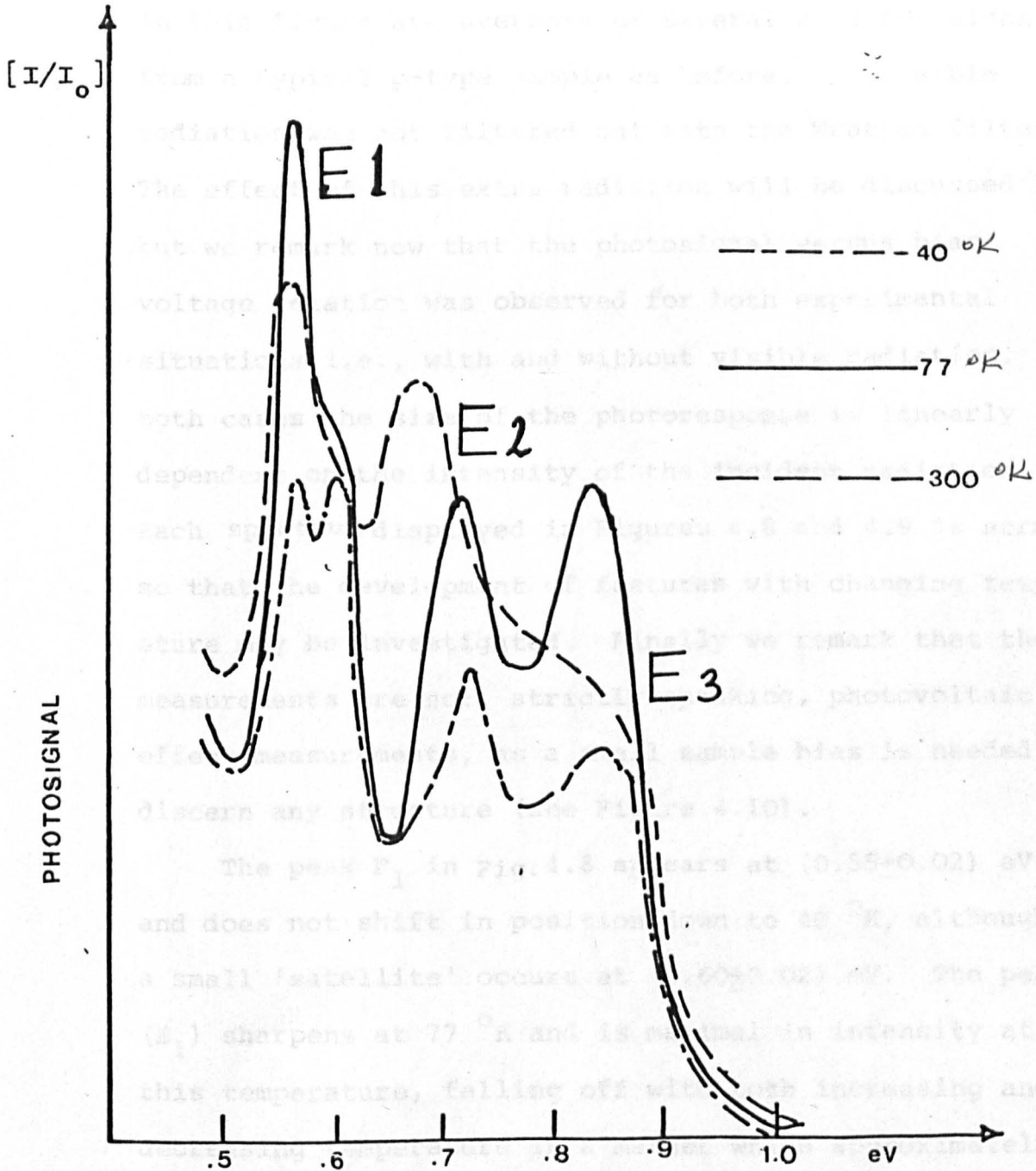
Fig.4-8). Photo response curve of p-type SnS.

A wratten 70 filter was used in these experiments, which had the effect of cutting out visible ($\lambda < 700$ nm) light. For low sample bias voltage a linear relation is found between the size of the photosignal and the sample bias, as may be seen in Figure 4.9. The traces in this figure are averages of several runs for signals from a typical p-type sample as before, but visible radiation was not filtered out with the Wratten filter. The effect of this extra radiation will be discussed later but we remark now that the photosignal versus bias voltage relation was observed for both experimental situations i.e., with and without visible radiation. In both cases the size of the photoresponse is linearly dependent on the intensity of the incident radiation. Each spectrum displayed in Figures 4.8 and 4.9 is normalised so that the development of features with changing temperature may be investigated. Finally we remark that these measurements are not, strictly speaking, photovoltaic effect measurements, as a small sample bias is needed to discern any structure (see Figure 4.10).

The peak F_1 in Fig.4.8 appears at (0.55 ± 0.02) eV and does not shift in position down to 40 $^{\circ}$K, although a small 'satellite' occurs at (0.60 ± 0.02) eV. The peak (E_1) sharpens at 77 $^{\circ}$K and is maximal in intensity at this temperature, falling off with both increasing and decreasing temperature in a manner which approximately follows the Hall mobility versus temperature behaviour noted by ourselves and Albers (1961). We discuss the
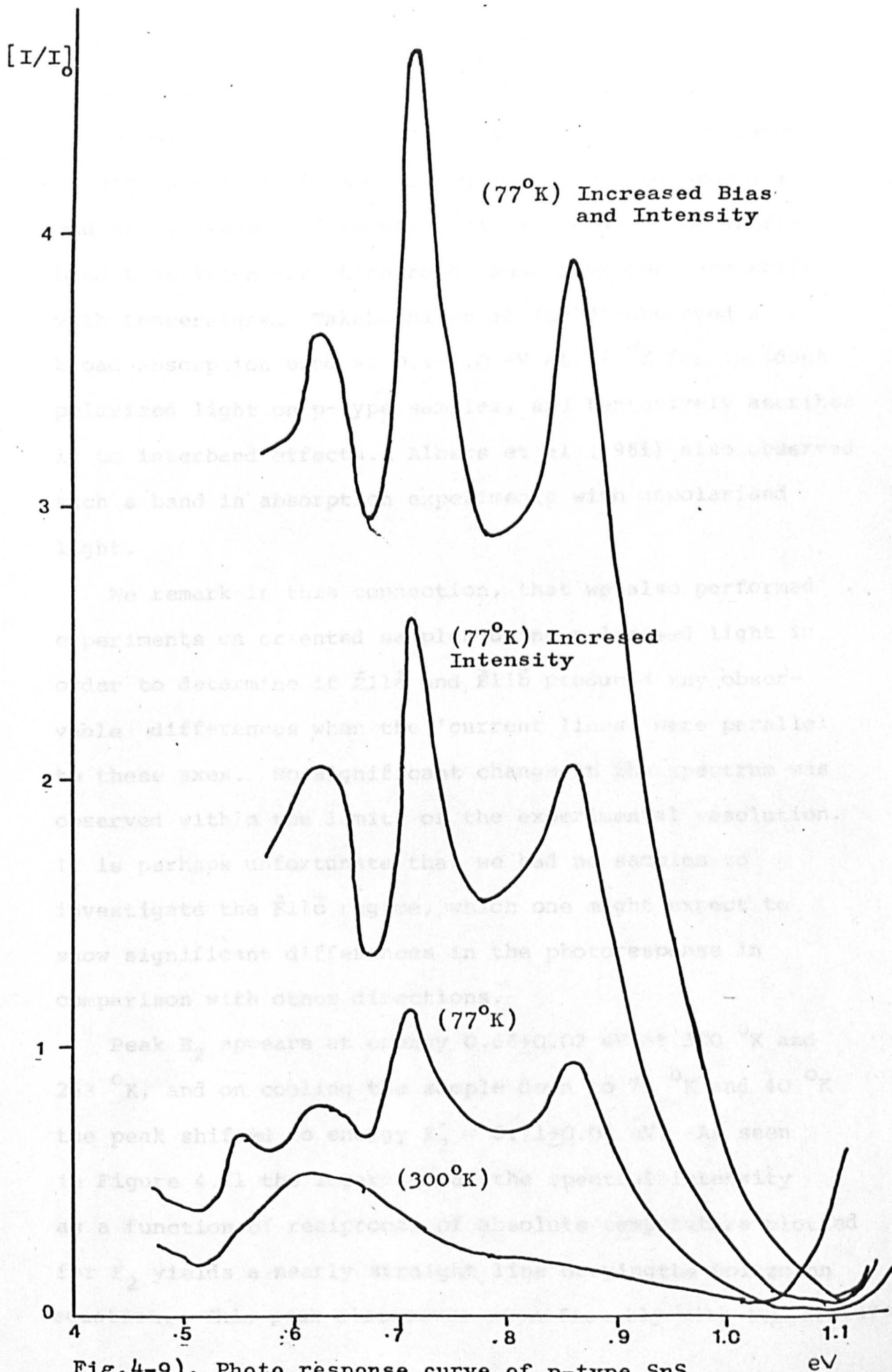
Fig.4-9). Photo response curve of p-type SnS.
(Visible radiations unfiltered)

possible origins of this peak later, but remark now
that the apparent lack of a temperature shift implies
a transition between two states moving with temperature
at approximately the same rate, e.g. a (deep) acceptor
and the valence band to which it is bound, or an inter-
band transition for which both bands have the same shift
with temperature. Takahashi et al (1972) observed a
broad absorption band at 0.4-1.0 eV at 77 ^{o}K for incident
polarised light on p-type samples, and tentatively ascribes
it to interband effects. Albers et al (1961) also observed
such a band in absorption experiments with unpolarised
light.

We remark in this connection, that we also performed
experiments on oriented samples using polarised light in
order to determine if $\vec{E} \| \vec{a}$ and $\vec{E} \| \vec{b}$ produced any obser-
vable differences when the 'current lines' were parallel
to these axes. No significant change in the spectrum was
observed within the limits of the experimental resolution.
It is perhaps unfortunate that we had no samples to
investigate the $\vec{E} \| \vec{c}$ regime, which one might expect to
show significant differences in the photoresponse in
comparison with other directions.

Peak E_2 appears at energy 0.66$\pm$0.02 eV at 300 ^{o}K and
263 ^{o}K, and on cooling the sample down to 77 ^{o}K and 40 ^{o}K
the peak shifted to energy $E_2' = 0.71 \pm 0.02$ eV. As seen
in Figure 4.11 the logarithm of the spectral intensity
as a function of reciprocal of absolute temperature plotted
for E_2 yields a nearly straight line obeying the Boltzmann
equation. This peak also moves significantly with temperature.

Fig.4-11). Log(I/I₀)versus I/T characteristic of photoresponse
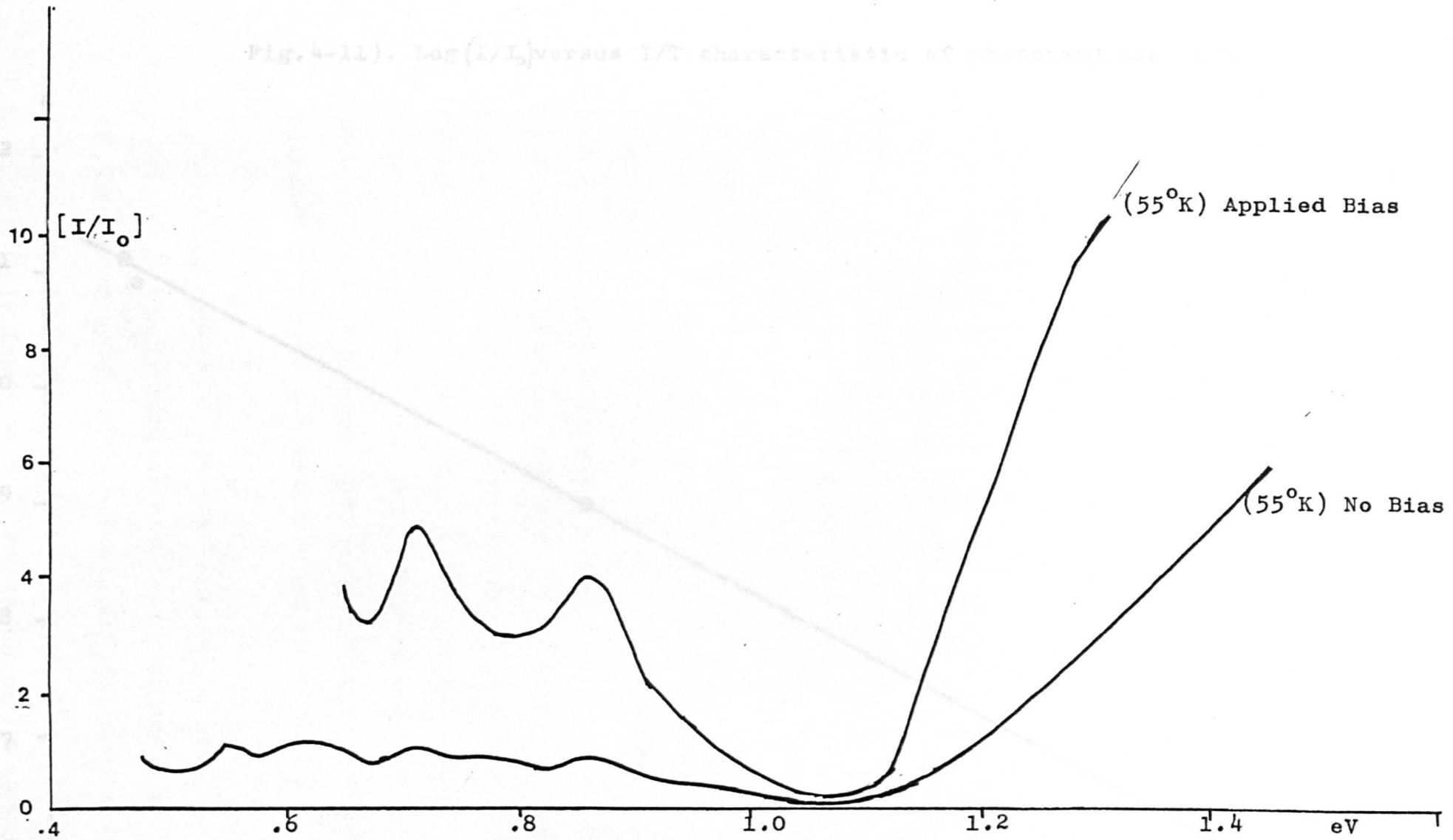
Fig.4-10). Photo response curve of p-type SnS.(Visible radiations unfiltered)

Fig.4-11). Log(I/I_0) versus I/T characteristic of photoresponse of SnS.
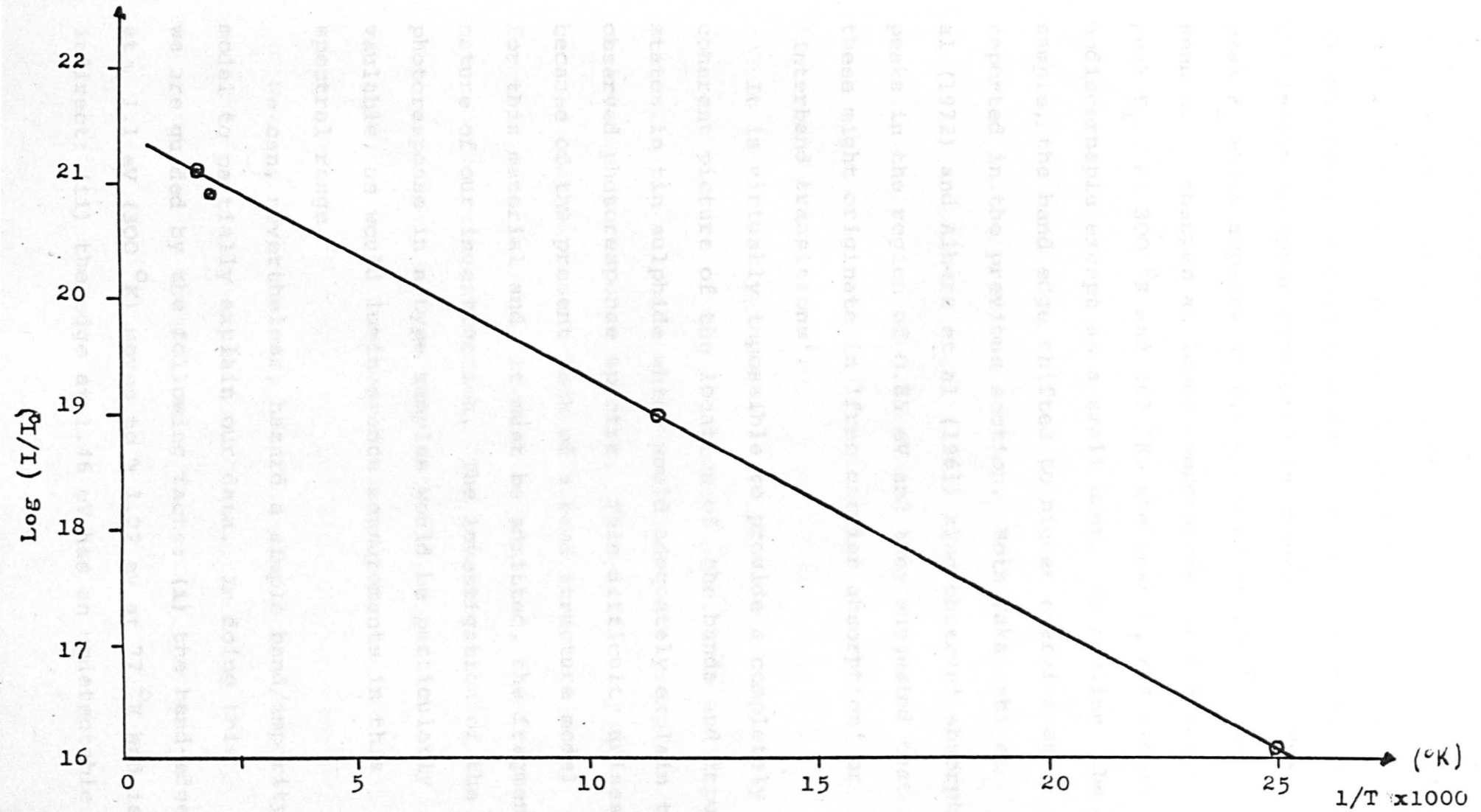
This peak is therefore probably due to the transition of an electron from the valence band to localized levels in the forbidden band gap leaving behind a hole in valence band. A good candidate for this level may be the indium acceptor mentioned in chapter three. The peak F_3 which appears at 0.83 ± 0.02 eV at 300 ^{O}K was seen to sharpen at lower temperatures as did the peak F_1. At 300 ^{O}K and 263 ^{O}K, the peak F_3 was almost undiscernable except as a small hump. On cooling the sample, the band edge shifted to higher energies as reported in the previous section. Both Takahashi et al (1972) and Albers et al (1961) also observed absorption peaks in the region of 0.85 eV and they suggested that these might originate in 'free carrier absorption' or 'interband transitions'.

It is virtually impossible to provide a completely coherent picture of the location of the bands and impurity states in tin sulphide which would adequately explain the observed photoresponse spectra. This difficulty arises because of the present lack of a band structure model for this material and, it must be admitted, the fragmentary nature of our investigation. The investigation of the photoresponse in n-type samples would be particularly vaulable, as would luminescence measurements in this spectral range.

We can, nevertheless, hazard a simple band/impurity model to partially explain our data. In doing this we are guided by the following facts: (i) the band-edge at $\sim$ 1.1 eV (300 ^{O}K) moves to $\sim$ 1.22 eV at 77 ^{O}K and is indirect; (ii) the edge at 1.46 eV has an undetectable

shift with temperature and is direct; (iii) the low energy peaks at 0.55 eV and 0.83 eV (77 ^{O}K) do not shift significantly with temperature (although they change in size); (iv) the peak at 0.66 eV (300 ^{O}K) moves to 0.71 eV (77 ^{O}K); (v) the effect of additional irradiation with intrinsic radiation (i.e., F_g < hν, no wratten 70 filter) is to accentuate some of the low energy peaks and diminish others. The theoretical information that can be brought to bear on the problem is limited; Albers et al (1961) in an analysis of density-of-states masses obtained from free carrier absorption data suggests that there must be at least four equivalent maxima in the valence band. As has been remarked earlier, no band structures are available for the GeSe, GeS, SnS, SnSe members of the IV-VI family. For the other members of the group (e.g. SnTe) the band structure models are legion (see for example, Ota and Rabii, 1974) but a common feature of many of these is the presence of a 'second' valence band, which is not continuous with the first. Such a band may have several equivalent maxima.

In any band/impurity level scheme we must also remember that absorption data imply the presence of broad bands at approximately 0.4 eV and 0.85 eV in contactless samples. These samples were p-type (as were ours) due to the presence of a doubly charged acceptor caused by Sn vacancies and S excess. Our own samples, however, had indium contacts which diffused a little way into the bulk, probably resulting in an indium acceptor in this material. We therefore tentatively suggest that the photoresponse

peaks at 0.55 eV and 0.85 eV may be associated with the doubly charged acceptor, whereas the feature at 0.66 eV is a result of transitions involving the indium impurity.

A diagram showing a suggested impurity level/band model is shown in Figure 4.12. The transitions A(0.83 eV) and B(0.55 eV) are shown between a deep level which we believe may be the second charged state of the doubly charged acceptor, the first charged state occurring at very small energies possibly in the far infrared régime. A similar mechanism has been suggested to explain the photoconductivity of CdS; in this case the presence of a 'deep' (0.9 eV) second charged state of the A_2 doubly-charged acceptor (due to S excess) is invoked to account for the photoresponse both with and without additional radiation with $h\nu > F_g$. This radiation (Honig, Moscow conference p.1170, 1968) will clear (or partially clear) the deep trap state of electrons, with the consequent reduction in size of the low energy peak compared with the high energy peak (see Fig. 4.9). The band gap deduced from this scheme is 1.38 ± 0.04 eV which is consistent with 1.43 ± 0.02 eV observed from the photoresponse at higher energies. Furthermore, the lack of a shift in peak positions is consistent with the constancy of the edge which is also found experimentally. Further experiments with n-type samples (which should not display these doubly-charged acceptor transitions) and with p-type samples in the far infrared régime at low temperatures are clearly indicated in order to test the doubly-charged acceptor hypothesis. In the latter case, the photothermalisation technique would be used to investigate the level of the first state

of the doubly-charged acceptor; to perform such experiments, however, would require better contacts to the specimens than are presently obtainable.

The central peak at 0.66 eV (300 $^{\circ}K$) moves significantly with temperature, as does the indirect band edge at 1.08 eV. We therefore associate this peak with a transition from an indirect valence band to an indium acceptor state. The other possible transitions from this level to the 'main' valence and conduction bands are either too low (0.4 eV) for our present instrumentation or they lie in the energy range of the indirect edge at 1.1 eV. These are many shortcomings of this model; for example, the small shoulder peak at 0.6 eV is not explained, neither is the shift of peaks F_1 and F_3 (but not E_2) in the presence of additional visible light. In the absence of a suitable band structure, however, we propose this scheme as a reasonable possibility.

C.B.

C.B.

β

Indium Acceptor
Excited State Level

C

A

Ground State of
Doubly Charged
Acceptor Level

V.B.
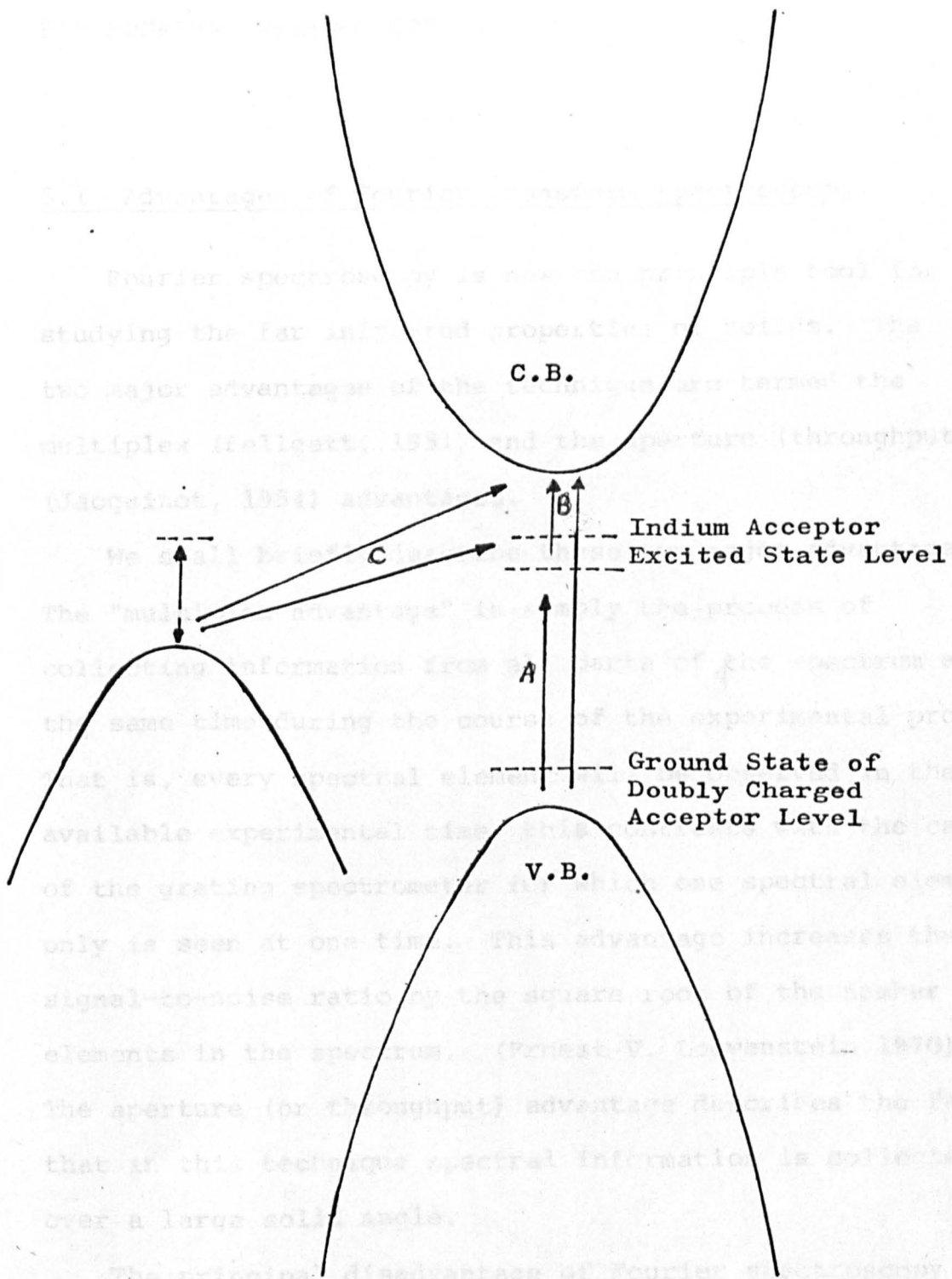
Fig. 4-12). Suggested Band Structure of SnS.

CHAPTER FIVE

EXPERIMENTAL TECHNIQUE AND DESCRIPTION OF APPARATUS
FOR FOURIER SPECTROSCOPY

5.1 Advantages of Fourier Transform Spectroscopy

Fourier spectroscopy is now the principle tool for
studying the far infra-red properties of solids. The
two major advantages of the technique are termed the
multiplex (Fellgett, 1951) and the aperture (throughput)
(Jacquinot, 1954) advantages.

We shall briefly describe these two major advantages.
The "multiplex advantage" is simply the process of
collecting information from all parts of the spectrum at
the same time during the course of the experimental process.
That is, every spectral element will be observed in the
available experimental time; this contrasts with the case
of the grating spectrometer for which one spectral element
only is seen at one time. This advantage increases the
signal-to-noise ratio by the square root of the number of
elements in the spectrum. (Ernest V. Loewenstein 1970).
The aperture (or throughput) advantage describes the fact
that in this technique spectral information is collected
over a large solid angle.

The principal disadvantage of Fourier spectroscopy
is that the spectrum of interest is not immediately
observable, but the "interferogram" has to be analysed
by a computer to produce the required spectrum. This
delay in computing the final spectrum makes it difficult

to monitor the progress of an experiment and constitutes
a significant disadvantage. Nevertheless, with a little
experience one can deduce the final spectrum, at least
approximately, by careful examination of the recorded-
interferogram that is obtained in the time domain. In
our own laboratory a small computer is available on a
time-sharing basis and this enables us to analyse the
spectrum while the experiment is going on.

5.2 Simple Derivation of Fourier Transform Integrals

Consider first the simple case of incident monochro-
matic radiation. Let the incident wave be:

$$y = A \exp i(\omega t - 2\pi\sigma_o x) \qquad (5.1)$$

where σ_o is the wavenumber of monochromatic wave. The
radiation from the source is split into two beams, either
by the beam divider in the Michelson interferometer or
by the two sets of mirrors in the Lameller grating inter-
ferometer. Before recombination, the beams travel distances
x_1 and x_2, where x_1 and x_2 are the "round trip" distances
from the beam divider to the mirrors M_1 and M_2 respectively.
(See figure 5.1).

The resultant amplitude in the direction of the
detector will be:

$$A_{det} = A(rt)\left[\exp i(\omega t - 2\pi\sigma_o x_1) + \exp i(\omega t - 2\pi\sigma_o x_2)\right] \qquad (5.2)$$

where r and t are the reflection and transmission
coefficients (of the beam splitter) respectively.

Static Mirror

Dielectric
Beam-Splitter

Poly-
Lens

Moving Mirror
and Drive

Chopper Disc

Source

Diode

Chopper

Lamp

Chopper
Motor

Source P.S.U
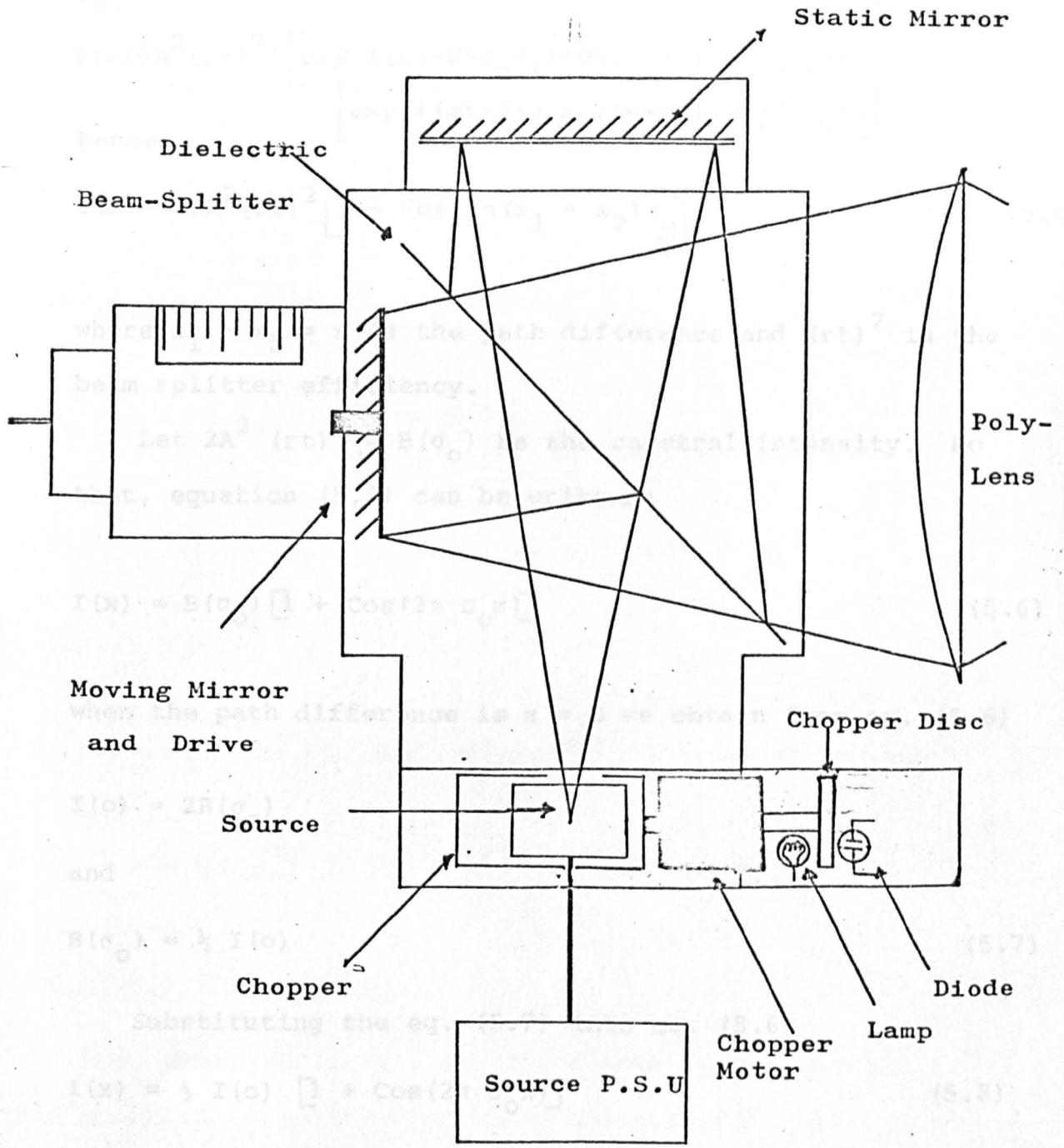
Fig.5-1). A Schematic diagram of Interferometer

The resultant intensity can thus be written:

$$I(x)=/A_{det}/^2=A^2/rt/^2 \left[\exp i(\omega t-2\pi\sigma_o x_1)+\exp i(\omega t-2\pi\sigma_o x_2)\right]^2 \quad (5.3)$$

So,

$$I(x)=A^2(rt)^2 \{ \left[\exp i(\omega t-2\pi\sigma_o x_1)+\exp i(\omega t-2\pi\sigma_o x_2)\right]$$
$$\left[\exp i(\omega t-2\pi\sigma_o x_1)+\exp i(\omega t-2\pi\sigma_o x_2)\right] \}$$

Hence,

$$I(x) = 2A^2(rt)^2 \left[1 + \cos 2\pi(x_1 - x_2)\sigma_o\right] \quad (5.5)$$

where $x_1 - x_2 = x$ is the path difference and $(rt)^2$ is the beam splitter efficiency.

Let $2A^2(rt)^2 = B(\sigma_o)$ be the spectral intensity. So that, equation (5.5) can be written:

$$I(x) = B(\sigma_o)\left[1 + \cos(2\pi \sigma_o x)\right] \quad (5.6)$$

when the path difference is $x = 0$ we obtain from eq. (5.6)

$$I(o) = 2B(\sigma_o)$$

and

$$B(\sigma_o) = \tfrac{1}{2} I(o) \quad (5.7)$$

Substituting the eq. (5.7) into eq. (5.6)

$$I(x) = \tfrac{1}{2} I(o) \left[1 + \cos(2\pi \sigma_o x)\right] \quad (5.8)$$

Up to here, the radiation has been considered to be monochromatic. In fact, the beam is not monochromatic (being provided by a mercury arc source), and thus expression (5.6) becomes in a more general form:

$$I(x) = \int_{-\infty}^{\infty} B(\sigma) \left[1 + \cos(2\pi\sigma x) \right] d\sigma \tag{5.9}$$

which can be re-written as

$$I(x) = \int_{-\infty}^{\infty} B(\sigma) \, d\sigma + \int_{-\infty}^{\infty} B(\sigma) \cos(2\pi\sigma x) \, d\sigma \tag{5.10}$$

or

$$I(x) = \tfrac{1}{2} I(o) \pm \int_{-\infty}^{\infty} B(\sigma) \cos(2\pi\sigma x) d\sigma$$

hence

$$2\left[I(x) - \tfrac{1}{2} I(o) \right] = \int_{0}^{\infty} B(\sigma) \cos(2\pi\sigma x) d\sigma$$

Finally using the Fourier integral transformation we have

$$B(\sigma) = (Const) \int_{0}^{\infty} \left[I(x) - \tfrac{1}{2} I(o) \right] \cos(2\pi\sigma x) d\sigma \tag{5.11}$$

5.3 Computing Techniques

From equation (5.11), it can be seen that to obtain the spectral intensity $B(\sigma_1)$ from the recorded output $I(x)$ (the "interferogram") one must perform a Fourier transformation of the form

$$B(\sigma_1) = \int_{0}^{\infty} \left[I(x) - \tfrac{1}{2} I(o) \right] \cos(2\pi\sigma_1 x) dx \tag{5.12}$$

In practice, interferograms $I(x)$ are recorded against the sampled output at regular intervals Δx between the zero path position and some finite maximum path difference L_1 (which is equal to twice the moving mirror displacement in a Michelson interferometer) and thus equation (5.12) is approximated by a summation

$$B(\sigma) \underset{\sigma=\sigma_1}{\overset{L}{=\Sigma}} \underset{x=0}{} \left[I(x) - \tfrac{1}{2}I(0)\right] \text{Cos } (2\pi\sigma_1 x) \Delta x \qquad (5.13)$$

where $x=h.\Delta x$ and $h=0,1,2....\dfrac{L}{\Delta x}$

and so on.

We do not discuss in here how digital computers are programmed to analyse the Fourier transformation of digitized interferograms from equation (5.13). These methods are standard and can be supplied by the manufacturers of interferometer. We remark, however, that the interferometer has to be aligned very accurately to get symmetric interferograms, otherwise artefacts are frequently obtained in the computed spectrum, particularly when "single sided" cosine transforms are performed. It cannot be emphasised too strongly that the computed spectrum is sensitive to even one misrecorded data point.

5.4 Description of Apparatus used for Fourier Spectroscopy

In this section the apparatus used for obtaining the far infrared reflectivity and transmission spectrum in the range of temperature 10-300 $^\circ$K will be described. Figure 5.2 shows a block diagram of the system as a whole, and each stage is described in detail in the subsequent sections.

Figure. 5.2: A Block Diagram of the System for Reflectivity Measurements
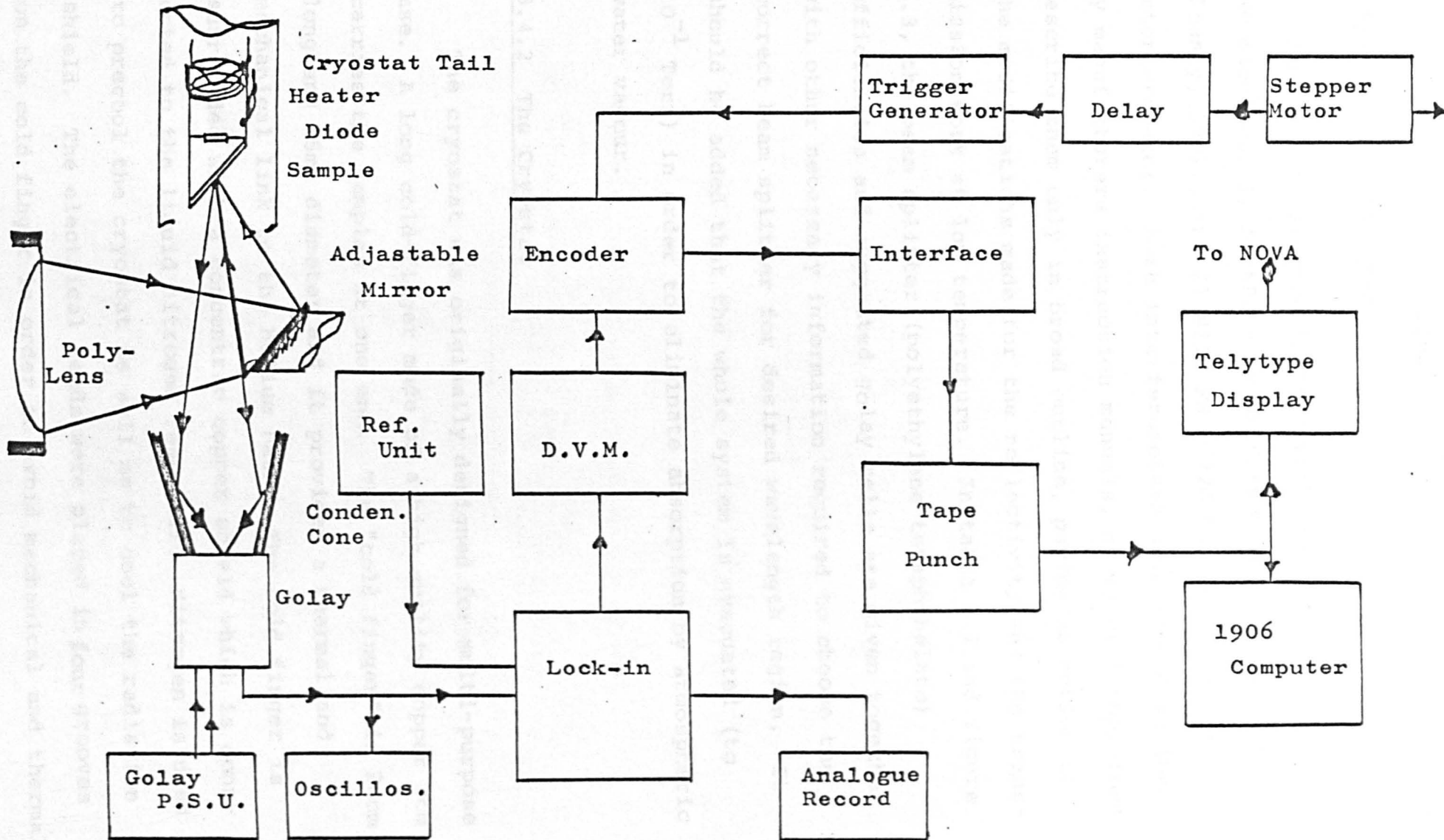
5.4.1 The Interferometer

The optical spectra in this work were measured on two machines, 1) An NPL - Grubb Parson modular Michelson (Chanty, 1971), and 2) R11C FS - 720 Fourier transform interferometer. Both interferometers have been described by manufacturers instruction manuals, so we will therefore describe them only in broad outline, paying attention to the modifications made for the reflectivity and the transmission work at low temperature. In table 5.1 and figure 5.3, the beam splitter (polyethylene teraphthalate) efficiencies and suggested golay cells are given together with other necessary information required to choose the correct beam splitter for desired wavelength region. It should be added that the whole system is evacuated (to 10^{-1} Torr) in order to eliminate absorption by atmospheric water vapour.

5.4.2 The Cryostat

The cryostat was originally designed for multi-purpose use. A long cold-finger made of a high quality copper rod carries the samples at one end. The "cold finger" is 20cm long and 15mm diameter and it provides a thermal and mechanical link to the helium bath. The cold finger is surrounded with a concentric copper shield which is connected to the liquid nitrogen reservoir. Nitrogen is used to precool the cryostat as well as to cool the radiation shield. The electrical leads were placed in four grooves on the cold finger in order to avoid mechanical and thermal contact with the outer shield. The temperature is measured with two thermocouples (copper against constantan and

GENERAL RANGE WORKING CONDITIONS

Range	Beamsplitter Thickness	Golay Detector Type
$10 - 50cm^{-1}$	50μ	Quartz or Diamond *
$20 - 100cm^{-1}$	25μ	Quartz or Diamond *
$40 - 200cm^{-1}$	12.5μ	Quartz or Diamond *
$80 - 400cm^{-1}$	6.25μ	Diamond
$120 - 660cm^{-1}$	3.75μ	Diamond
$325 - 425cm^{-1}$	12.5μ (second peak)	Diamond
$600 - 800cm^{-1}$	6.25μ (second peak)	Diamond

* If a diamond Golay is used here it is recommended that a special wedged quartz filter is interposed in the beam together with the other filtration.

TAPE DATA FOR 5μ PATH DIFFERENCE STEPPING INTERVAL

Resolution cm^{-1}	Path Diff. (1 side) mm	Mirror Movement (1 side) mm	Points (1 side)	Tape length (1 side) 3 digit	Tape length (1 side) 4 digit	Time (1 side) mins.
0.1	100	50	20,000	666' 8"	833' 4"	333.30 x t
0.2	50	25	10,000	333' 4"	416' 8"	166.65 x t
0.25	40	20	8,000	266' 8"	333' 4"	133.34 x t
0.5	20	10	4,000	133' 4"	166' 8"	66.67 x t
1.0	10	5	2,000	66' 8"	83' 4"	33.33 x t
2.0	5	2.5	1,000	33' 4"	41' 8"	16.67 x t
2.5	4	2	800	26' 8"	33' 4"	13.33 x t
5.0	2	1	400	13' 4"	16' 8"	6.67 x t
10.0	1	0.5	200	6' 8"	8' 4"	3.33 x t

NOTE: (1) t (column 7) is Pulse Interval in secs.

(2) In general, time/mm of mirror movement = $6\frac{2}{3}$ x t mins.

Optical Path Difference

$$L = 2nd/(1 - \frac{1}{2n^2})^{\frac{1}{2}}$$

Interference Condition

For RI and RII

Minima when $K = \frac{N}{L}$

Maxima when $K = \frac{N - \frac{1}{2}}{L}$

Where $N = 1, 2, 3, 4,$
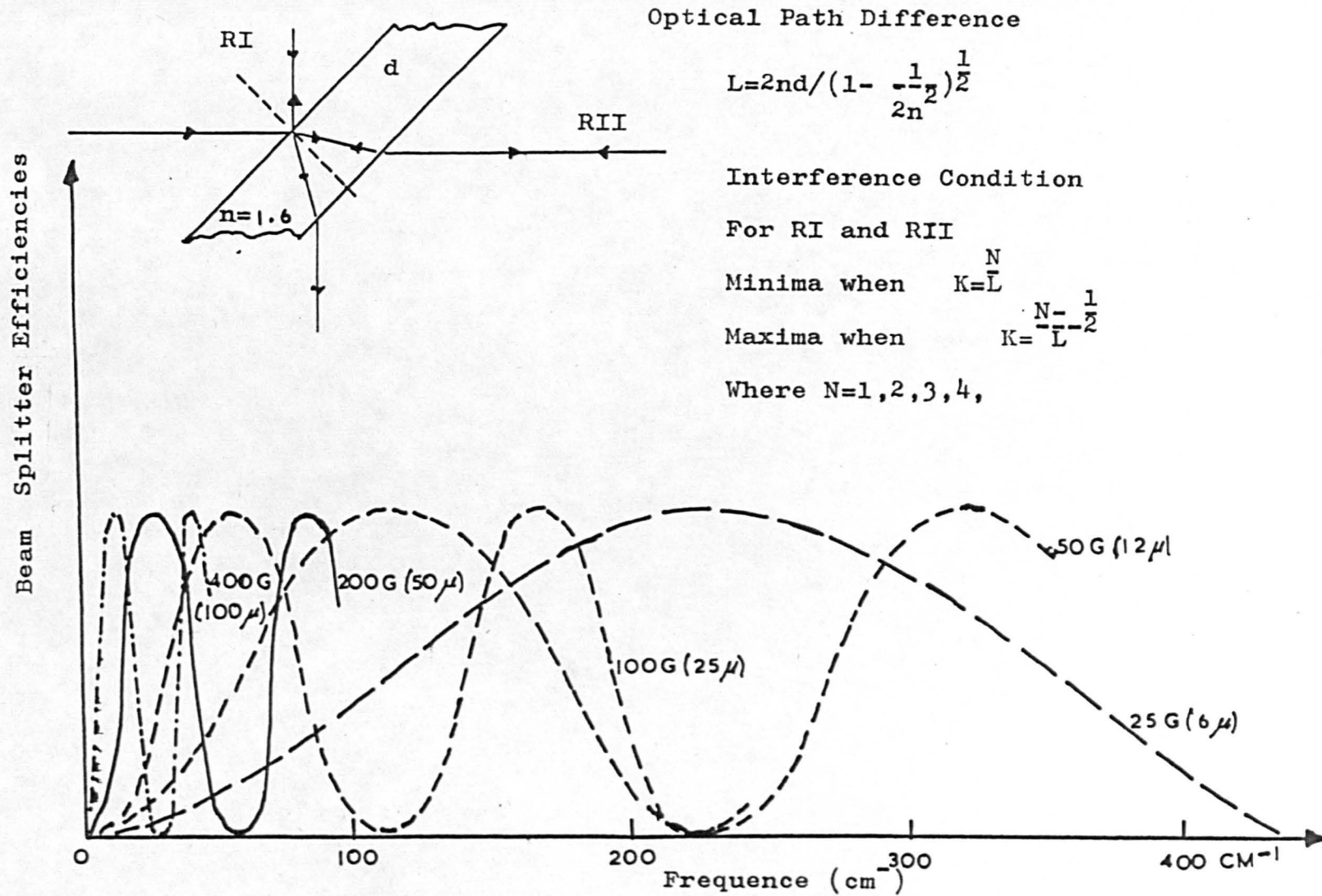
Figure -5.3 : Relative Beam Splitter Efficiencies

Au + 0.03 at o/o Fe against chromel) and one reverse-biassed diode (1S44) which is also used as a temperature sensor in the temperature controller. A heater is placed between the specimen and helium bath, made of 30 SWG cotton covered chromel wire of about 40 ohm resistance. The temperature at the end of the cold finger was no more than 5 $^\circ$K warmer than that of the helium bath. The far end of the cold finger is cut to make a 22.5° angle for reflection measurements. The samples under investigation were mounted on extended cold finger of cryostat using a single blob of durofix. It is to be noted that no collimating optics are employed in the interferometer, so that the divergent light output was focussed on to the specimen using a suitable polyethylene lens (mounted at the interferometer exit) and a freshly aluminised plane mirror.

To avoid unwanted (visible and near infrared) radiation falling on the detector a sufficient thickness of white and black polyethylene windows were used as filters. These filters also acted as windows holding the samples under the desired cryostat vacuum ($\sim 10^{-5}$ torr or better). Black polyethylene serves to filter out visible and U.V. radiation and white polyethylene acts as a near infrared filter. However, these materials have disadvantages, due to lattice absorptions in the far infrared which are mentioned in chapter six. The losses in the sample chamber and the guiding system (condensing cone) are negligible compared with the other losses occurring in windows and lenses.

In order to minimise the mechanical vibrations arising from external sources such as pumps the cryostat together with the sample chamber is placed on a soft plastic foam, while the interferometer is placed on a heavy table

supported by four "mini" valve springs.

5.4.3 Temperature Controller

The precise control of sample temperature using a heater working against a thermal link to a cryostat containing a cryogenic fluid requires complicated electronic circuitry.

Precise temperature controllers have been described previously by Rohlin (1970); Pries and Moore (1970); Gluyas, Hughes and James (1970). These have resistance sensors in one arm of an AC bridge. Temperature controllers using the DC method are described by Fletcher (1971); Plesiewicz and Swiercz (1974); and Jones (1974). Temperature controllers are available commercially, and most of these utilise the DC method.

The system described here is very simple to construct and operate and less expensive than conventional units. It can be used over a wide temperature range, although the control is more precise over some temperature intervals than others.

The heart of the system is the temperature sensing diode (1S44); the forward voltage drop on the diode varies inversely with the surrounding temperature. The voltage across it goes to the input of the first "operational amplifier" 741. (This operational amplifier 741 had a gain unity for simplicity). The inverted output of this 741 is compared with a reference voltage (set externally, according to the desired temperature) at the second (inverting) 741. The output of the second inverting operational amplifier 741 biasses an NPN BD121 type trans-

Figure.5.4 : TEMPERATURE CONTROLLER
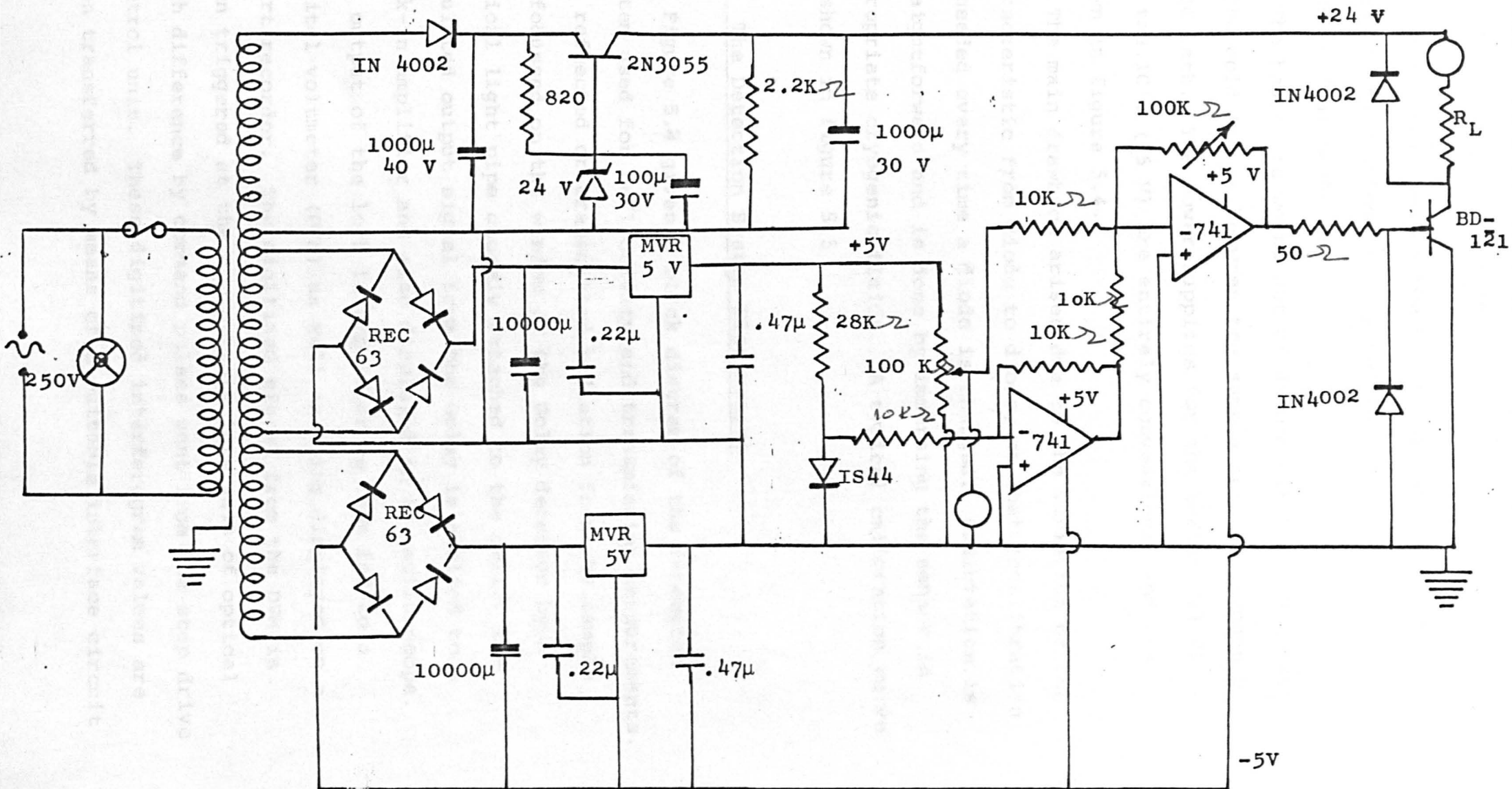
istor which switches on the heater as required. The
heater is thus automatically controlled, and switches
on and off as necessary.

The heater is wound out of 40 ohm wire and is located
on the cold finger between the sample and the cryogenic
fluid bath. The power supplies for the heater (24 V)
and the IC's (±5 V) are entirely conventional and are
shown in figure 5.4.

The main drawback arises due to the variation of the
characteristic from diode to diode, so that recalibration
is needed every time a diode is changed. Calibration is
straightforward and is done by immersing the sensor in
appropriate cryogenic fluids. A typical calibration curve
is shown in figure 5.5

5.5 The Detection System Electronics

Figure 5.2 gives a block diagram of the detection
system used for reflectivity and transmission measurements.
The reflected or transmitted radiation from the sample
is focussed on the window of the Golay detector by a
conical light pipe closely attached to the cell. The
modulated output signal from the Golay is applied to a
lock-in amplifier and also displayed on an oscilooscope.
The output of the lock-in amplifier is then fed to a
digital voltmeter (DVM) as well as being displayed on a
chart recorder. The digitized signal from the DVM is
then triggered at the appropriate intervals of optical
path difference by command pulses sent from the step drive
control unit. These digitized interferogram values are
then transferred by means of a suitable interface circuit
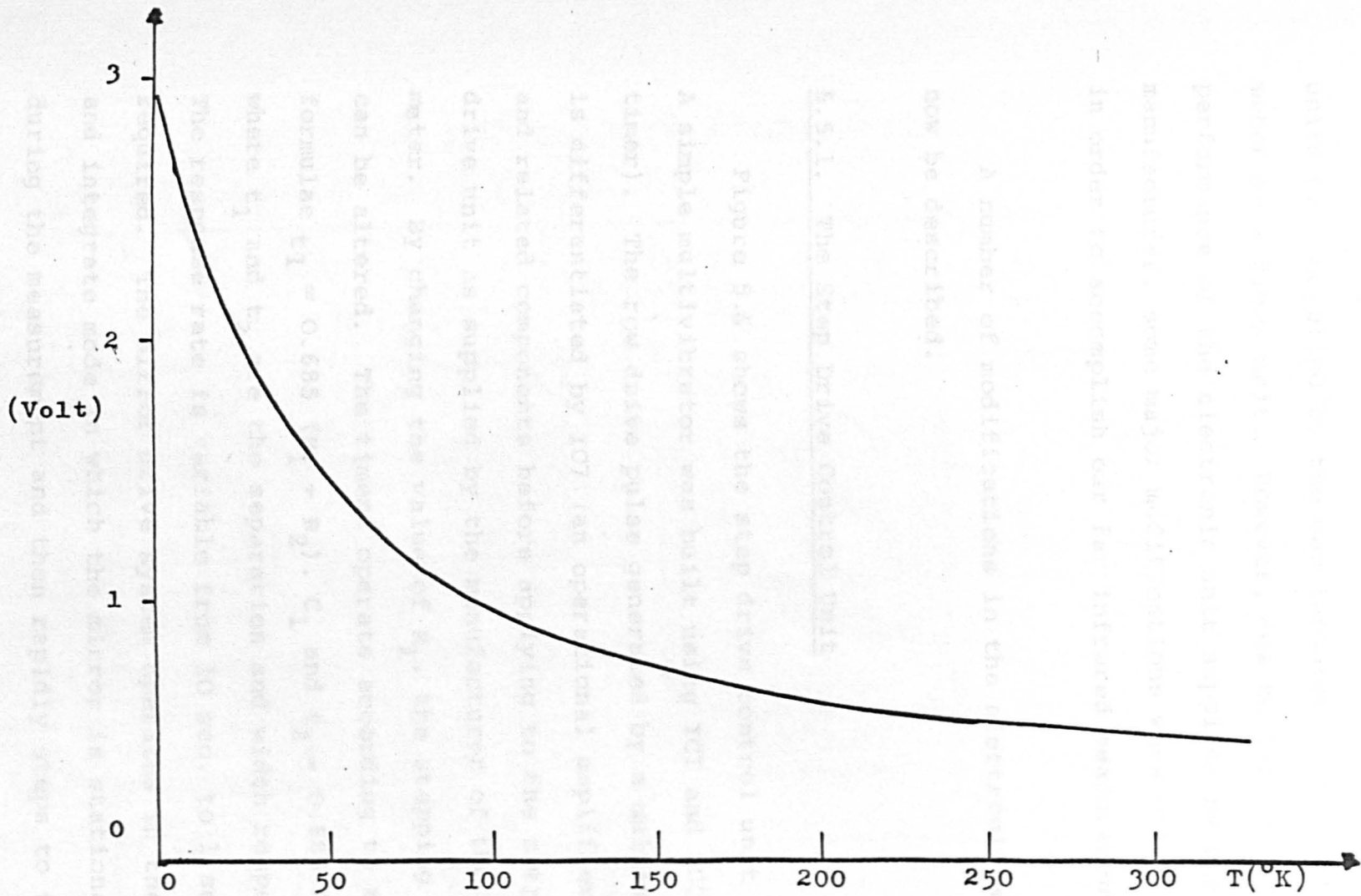
Fig.5-5). A typical calibration curve for diode used for temperature sensor

unit to a punched paper tape to he read into a digital
computer.

Originally, as mentioned earlier, all the electronic
units were supplied by the manufacturer of the interfero-
meter as a block unit. However, due to lack of adequate
performance of the electronic unit supplied by the
manufacturer, some major modifications were undertaken
in order to accomplish our far infrared measurements.

A number of modifications in the electronic system will
now be described.

5.5.1. The Step Drive Control Unit

Figure 5.6 shows the step drive control unit circuit.
A simple multivibrator was built using ICI and IC2 (555
timer). The row drive pulse generated by a multivibrator
is differentiated by IC7 (an operational amplifier 741)
and related components before applying to the stepper motor
drive unit as supplied by the manufacturer of the interfero-
meter. By changing the value of R_1, the stepping rating
can be altered. The timers operate according to the
formulae $t_1 = 0.685 (R_1 + R_2) . C_1$ and $t_2 = 0.685 R_2 . C_1$,
where t_1 and t_2 are the separation and width respectively.
The response rate is variable from 10 sec. to 1 sec. as
required. The mirror drive system operates in the step
and integrate mode in which the mirror is stationary
during the measurement and then rapidly steps to the next
position. The mirror step is 2.5 m.

The second part of the circuit consists of a schmidt
trigger which provides a well-defined square wave pulse,

FIG. 5.6). STEP DRIVE CONTROL UNIT
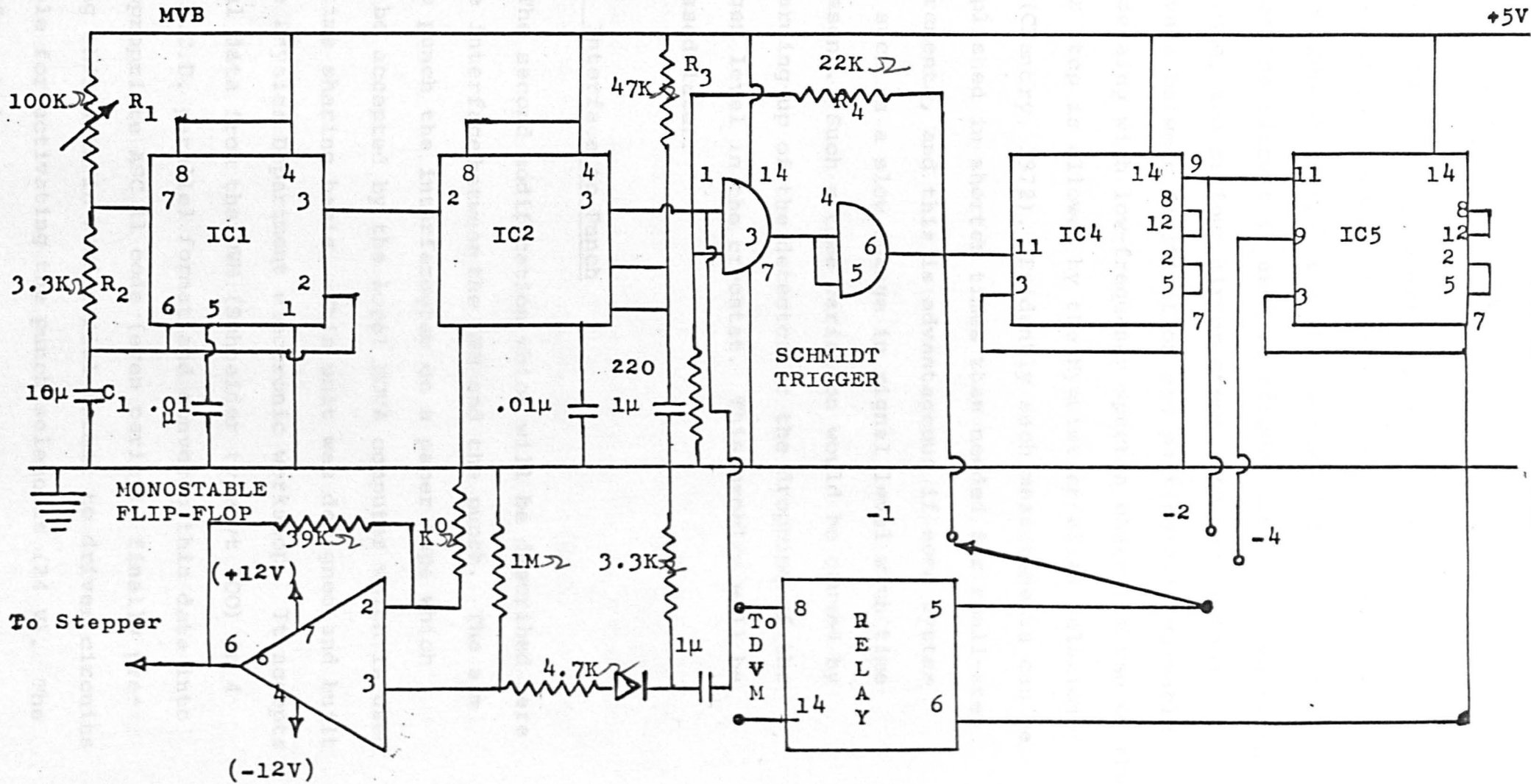
and two IC4 (7474) integrated circuit chips for delaying
the signal provided by the schmidt trigger together with
a relay IC6 which triggers the digital voltmeter. This
part of the circuit is used to trigger the digitized signal
after one, two or four mirror steps. Longer spatial
intervals between digitisation are particularly valuable
when delaing with low-frequency spectra where the use of the
longer step is allowed by the Nyquist or alias relation-
ship (Chantry, 1972). Evidently such measurements can be
accomplished in shorter times than needed for small-step
measurements, and this is advantageous if some system
fault such as a slow change in signal level with time
is present. Such a time variation would be caused by
the warming-up of the detector or the dropping of the
nitrogen level in the cryostat. This problem will be
discussed later.

5.5.2 Interface to Punch

The second modification which will be described here
is the interface between the DVM and the punch. The aim
was to punch the interferogram on a paper tape which
could be accepted by the local NOVA computer which is used
on a time sharing basis. This unit was designed and built
in the Physics Department electronic workshop. It accepts
digital data from the DVM (Schneider type vt 300) in 4·
digit B.C.D. parallel format and converts this data into
the appropriate ASC 11 code (even parity), finally pre-
senting this data in word serial format to driver circuits
suitable for activating the punch selenoids (24 V). The
punch format is:

```
NULL
1st data digit (most significant magnitude digit)
2nd data digit (next       "          "        "  )
3rd   "     "   (next       "          "        "  )
4th   "     "   (least      "          "        "  )
CR  carriage return
LF  line feed
```

This unit provides the facility that after approximately 50 data points are obtained, in a run the tape which has been produced is fed to the NOVA through our own teletype. The resultant spectrum is then immediately analysed and displayed on the teletype. Thus one can see the resultant spectrum roughly and decide at what point to terminate the experiment.

5.5.3   Reference Signal

The third modification in the electronic unit which will be described here is the reference signal supply to the lock-in amplifier. Originally, the reference signal was driven from a small generator (as supplied by the manufacturer of the interferometer) driven by the chopper motor, but slipping of the linkage between the motor and generator caused a changing phase shift between the chopper and reference signal, which - if it occurred in the middle of an experimental run - could upset whole sets of experimental results. Wheeler and Hill, (1966) also reported the same problem with the Grubb Parson's unit, so they also modified the original reference signal drive. In our case, the generator was removed and a reference signal for the lock-in amplifier was generated by using the same chopper motor to interrupt a light beam

provided by a small lamp illuminating a high sensitive RS photo-diode which has been placed in the chopper unit housing of the interferometer. A schematic diagram of the reference signal supply is given in figure 5.7; this provides a convenient square-wave signal to our lock-in amplifier reference channel.

5.5.4 Power Supply to the Golay Cell

For all measurements a Golay cell with a diamond window was used as the detector; although, in our opinion, a more sensitive low temperature detector was really needed for some of the reflectivity and trans- mission experiments which were carried out. Originally, the Golay cell power supply unit was housed in the lock- in amplifier unit supplied by the manufacturers. This lock-in was replaced by a more sensitive (Brookdeal type 9501) unit offering better signal to noise ratios. The Golay cell power supply was thus rebuilt in a separate unit and this is shown in fugure 5.8. The +4V power unit is a highly regulated supply obtained from Coutant Instruments. The +90V power unit is home-made and the simple circuit diagram is shown in figure 5.8. The +90V is derived from bridge rectification (Rec 50, RS) of the 125V secondary of a transformer. Simple zener (IS 3082) stabilisation is used; only sufficient current for the Golay cathode follower is needed and this is provided by the circuit shown.

5.6 Optics

Several different sample cell and focussing arrange-
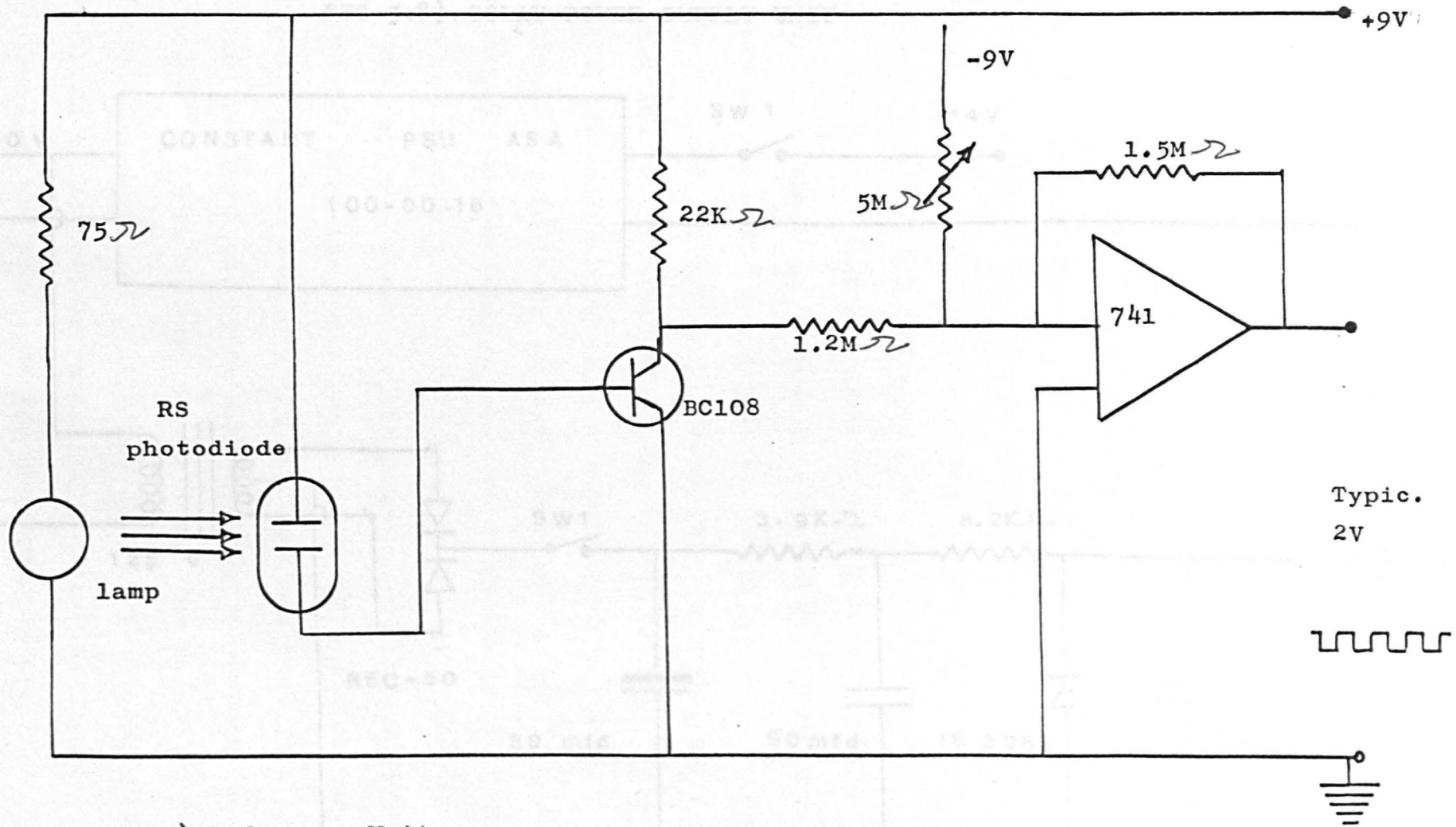
Fig.5-7).Reference Unit.

FIG 5.8). GOLAY POWER SUPPLY UNIT
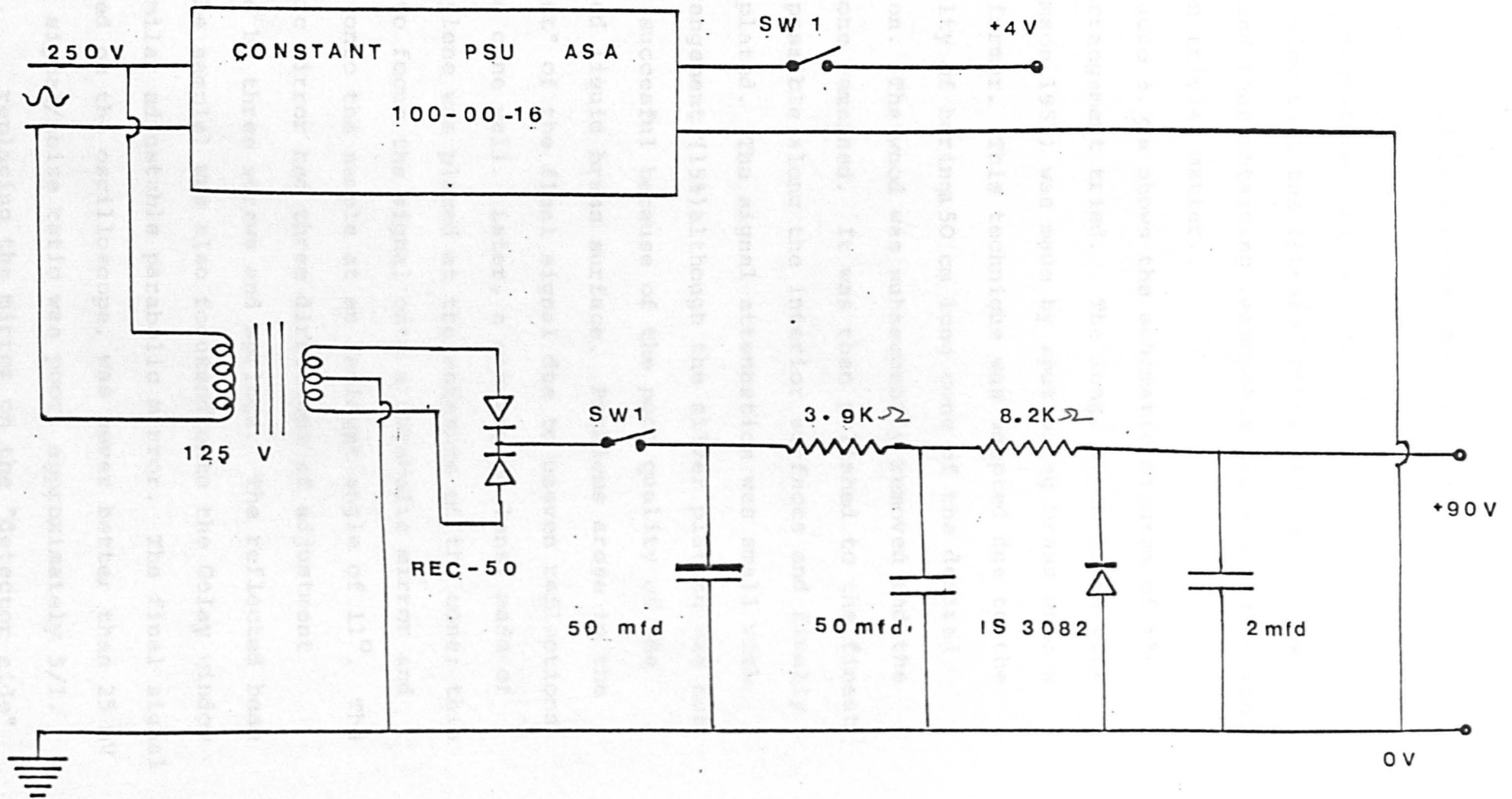
ments were tried in a search for an efficient optical
system for measuring sample transmission and reflection
in the temperature range 4 - 300 ^{O}K. It is essential to
bear in mind that the infrared power levels are low
(μW's) and thus obtaining reasonable signal:noise ratios
is a non trivial matter.

Figure 5. 9.a shows the schematic diagram of the
first arrangement tried. The long, 50 cm brass cone
(Williamson 1952) was made by sputtering brass onto a
wooden former. This technique was adopted due to the
difficulty of boringa 50 cm long cone of the desired
dimension. The wood was subsequently removed and the
metal cone remained. It was then polished to the finest
finish possible along the interior surfaces and finally
silver plated. The signal attenuation was small with
this arrangement (15%)although the silver plating was not
totally succesful because of the poor quality of the
sputtered liquid brass surface. Problems arose in the
"contrast" of the final signal due to uneven reflections
from the cone wall. Later, a converging lens, made of
polyethylene was placed at the entrance of the cone; this
helped to focus the signal onto a parabolic mirror and
finally onto the sample at an incident angle of 11°. The
parabolic mirror had three directions of adjustment
provided by three screws and springs. The reflected beam
(from the sample) was also focussed onto the Golay window
by a similar adjustable parabolic mirror. The final signal
displayed on the oscilloscope, was never better than 25 mV
and the signal/noise ratio was poor, approximately 5/1.
However,   replacing the mirror on the "detector side"
with a torroidal mirror (Fletcher, 1975) slightly

Cold Finger

to pump

Sample

Inlet

Golay

(a)

A

B

Cold Finger

Golay

(b)

Cold Finger

(c)

A

B

Golay

not to scale

Fig.5-9).Sample cell arrangements.

improved the signal to noise ratio but not enough to make the system routinely useable. Finally an arrangement seen in figure 5..9c was used to give a better signal to noise ratio with high contrast and high efficiency. The disadvantage of the system was that the angle of incidence was higher than in the first two arrangements, being 22.5°. Typical final signals were 2 - 300 mV with noise less than one per cent. The 10 cm long cone A, (see fig. 5..9c) was made of aluminium and a polyethylene lens was placed at the entrance. The reflected beam was collected by a condensing cone B, made of electro-formed copper etched with a solution of 33 ml nitric acid + 33 ml orthophosphoric acid + 33 ml glacial acetic acid, with 1-2 min. in order to improve the surface reflection. Total losses on the cone were negligible in comparison with the losses on the windows.

5.7 Problems

The disadvantage of Fourier spectroscopy - namely the delay between obtaining data and the computed output - has been discussed earlier. Although some partial solution of the problem has been achieved through the use of a time sharing computer, the computer is not always available in this mode. The length of time required to take an actual spectrum can also lead to experimental problems. Typically this can be three hours in high resolution (< 1 cm^{-1}) work, and during this time a 10 o/o decrease can occur in the signal, presumably due to the warming up of the Golay cell. In addition this time lag can create problems if the cryogenic fluid is used up

during the experimental time. An attempt was made to cool the Golay cell with running water using a tank which was fitted under the Golay base. This created additional noise, however. In order to improve signal to noise ratios, the use of a longer time constant is advisable; however, this also implies an increased sampling interval and a longer experimental run with the concomitant problems discussed above.

The raw data on the punched tape was heavily modulated with the instrumental function. The digitized spectra had to be corrected for this by ratioing to a background tape obtained by replacing the sample with a freshly aluminised mirror.

CHAPTER SIX

OPTICAL MEASUREMENTS ON SnS

6.1 Introduction

    The IV-VI semiconductors SnS, SnSe, GeSe and GeS
form an interesting class of isomorphic materials which
are in many ways intermediate between two-dimensional
(layer-type) systems and three dimensional crystals.
SnS is a fairly typical member of this series: it
crystallises into distorted rock-salt structure units
arranged in layers with a strong intra-layer (mostly
covalent) and weak interlayer coupling (the nature of
the weak interlayer forces is poorly understood for all
layered crystals, although the assumption of Van der
Waals forces is widely made in the absence of better
information). These crystals have the appearance of
shiny platelets which are easily cleaved in a direction
perpendicular to the c-axis.

    We have prepared single-crystal specimens of SnS
as described in chapter two and performed polarised
far infrared reflection and transmission measurements
in the temperature range 10-300 $^{\circ}$K in order to deter-

mine the fundamental lattice vibrations, and to
compare our findings with recent group theoretical
predictions (Wiley et al 1976). In addition, far
infrared reflection measurements have also been
made using partially polarised light (due to the
interferometer design) down to 10 $^\circ$K in order to
determine the existence and magnitude of any poss-
ible plasma effects. No direct measurements of the
phonon frequencies have been previously made in this
material. We note, however, that Lambros et al (1974)
suggest a phonon frequency of approximately 320 cm^{-1}
which is involved in an indirect band gap transition
obtained optically.

6.2 Experimental Details

A study of the infrared reflectivity and trans-
mission spectra of semiconductors allows us to
explore, amongst other things, their fundamental
lattice vibrations and free carrier dispersion.
The first measurement of the far infrared reflec-
tivity spectrum in the range 50 - 350 cm^{-1} of SnS
was that of Nikolic et al (1974). These authors
measured the room temperature reflectivity spectrum
of p-type crystalline SnS at normal incidence and
calculated the optical constants of SnS using
Kramers-Krönig analysis. The present investigation
adds to this earlier study by extending the measure-
ments to lower temperatures using both partially
polarised (due to the interferometer design) and

polarized light (Chamberlain et al 1976). We now
have a fairly clear interpretation of our results
in terms of a straightforward lattice mode reflection.

Single crystals of SnS were grown by the Bridgman
technique. The details of these preparations have
been given elsewhere (Nikolic et al 1974, and in
chapter two in this thesis). Samples in this work
had a surface area $0.5 - 1$ cm^2. Our samples were
analysed by x-ray techniques and confirmed to be
single crystal. Subsequent electrical character-
ization measurements indicated that our specimens
were both n- and p-type, with carrier concentrations
in the range $10^{17} - 10^{19}$ cm^{-3} (see chapter three).
Measurements with $\vec{E}\|\vec{a}$ and $\vec{E}\|\vec{b}$ were performed on
(040) cleavage faces, the cleavage being done
simply by peeling off with sellotape one of the
layers from SnS plates which had been cut from the
ingot, thereby exposing a fresh face. Samples of
$2 - 5$ μm thickness for transmission experiments were
prepared by bonding the crystal with a cyanoacrylate
.ester adhesive to a polythene substrate, and then
peeling off successive layers with sellotape. In
this way relatively strain-free specimens were
obtained.

Near normal incidence polarized far infrared
reflectivity and transmission measurements were made
in the frequency range $10 - 500$ cm^{-1} using conven-
tional Fourier transform techniques. A commercial

optical cryostat DN 70, (Oxford Instruments Ltd.)
was used for the measurements in the range 77 -
300 ^{O}K, and the home made cold-finger cryostat was
used for both polarized and partially polarized light
studies in the lower temperature range 10 - 77 ^{O}K.
In the case of the polarized light measurements
wire-grid polariser (Auton, 1967) was used to
polarise the light falling on the specimen.

Samples were oriented to locate $\vec{a}$ and $\vec{b}$ axes
before insertion into the spectrometer by X-ray tech-
nique. The specimens were simply mounted using
Durofix. A block diagram of the apparatus used
for the reflectivity and transmission measurements
has been given in chapter five together with a
detailed description of the experimental technique.

6.3   Results

The reflection spectrum of the n-type SnS samples
was measured from 50 to 350 cm^{-1} with $\vec{E}$11 to $\vec{a}$, $\vec{b}$
and $\vec{c}$, axis at room temperature, displayed in figure
6.1.   These measurements were performed on either
FS - 720 Beckman or a NPL - Grubb Parsons modular
Michelson interferometer (Chantry et al 1969).
The frequency resolution was 2.5 cm^{-1}, sufficient
to resolve all the structure observed in the spectra,
and the data presented are averaged over many spectra.
The spectra $\vec{E}$11$\vec{a}$ and $\vec{E}$11$\vec{b}$ were taken on an oriented
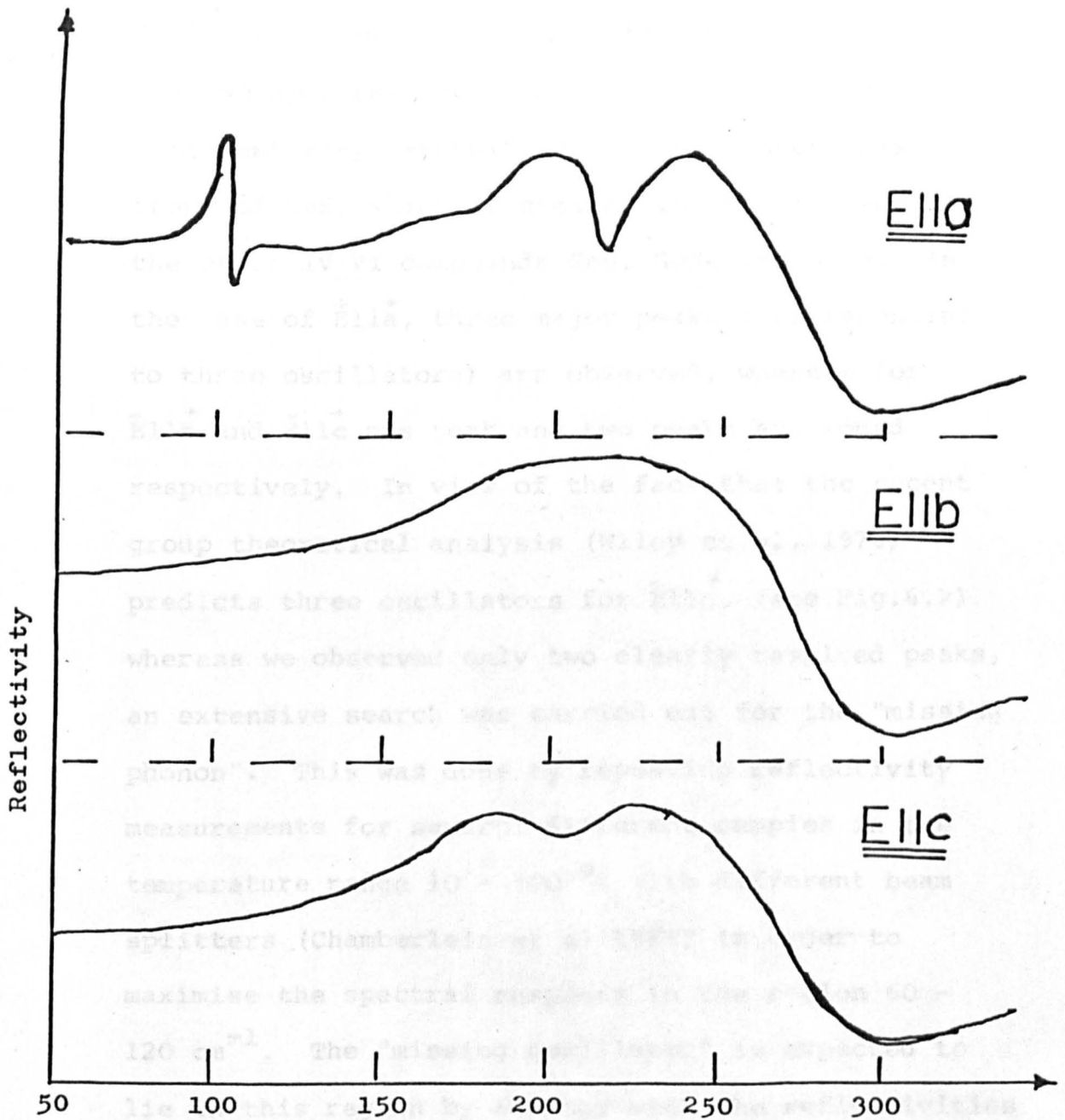
Fig.6-1). Averaged reflectivity versus wavenumber curves
for E∥a, E∥b and E∥c for an n-type SnS sample at
300K.

cleavage face using a wire-grid polarizer (Auton, 1967) which could be rotated by $90°$ for recording the two spectra. It is necessary to perform this alignment very carefully due to the large aniso- tropy of SnS, which is similar in this respect to the other IV-VI compounds GeS, GeSe and SnSe. In the case of $\vec{E}\|\vec{a}$, three major peaks (corresponding to three oscillators) are observed, whereas for $\vec{E}\|\vec{b}$ and $\vec{E}\|\vec{c}$ one peak and two peaks are found respectively. In view of the fact that the recent group theoretical analysis (Wiley et al, 1976) predicts three oscillators for $\vec{E}\|\vec{c}$, (see Fig.6.2) whereas we observed only two clearly resolved peaks, an extensive search was carried out for the "missing phonon". This was done by repeating reflectivity measurements for several different samples in the temperature range 10 - 300 $°K$ with different beam splitters (Chamberlain et al 1966) in order to maximise the spectral response in the region 60 - 120 cm^{-1}. The "missing oscillator" is expected to lie in this region by analogy with the reflectivities of the isomorphs GeSe and GeS (Wiley et al 1976, Chandrasekhar and Zwick 1976). However, despite careful sample surface preparation, interferometer optimization and (in addition) transmission measure- ments over the 50 - 350 cm^{-1} range, we cannot conclusively observe the presence of an oscillator in this region with a strength greater than one- hundredth of the strength of the other two oscillators

LAYER SYMMETRY	CRYSTAL SYMMETRY	ACTIVITY

$3A_1$ → $3A_g$ —————— R[c(bb)c̄]

$3B_{1u}$ —————— ir[E ∥ a]

$2A_2$ → $2B_{1g}$ —————— R[a(bc)ā]

$2A_u$ —————— INACTIVE

$3B_1$ → $3B_{2g}$ —————— R[b(ac)b̄]

$3B_{3u}$ —————— ir[E ∥c]

$1B_2$ → $1B_{3g}$ —————— R[c(ab)c̄]

$1B_{2u}$ —————— ir[E ∥b]

$1B_{3g}$ —————— R[c(ab)c̄]

$1B_{2g}$ —————— R[b(ac)b̄]

$1A_g$ —————— R[c(bb)c̄]

$1A_1 + 1B_1 + 1B_2$ → $1B_{1u} + 1B_{2u} + 1B_{3u}$ —————— ACOUSTIC
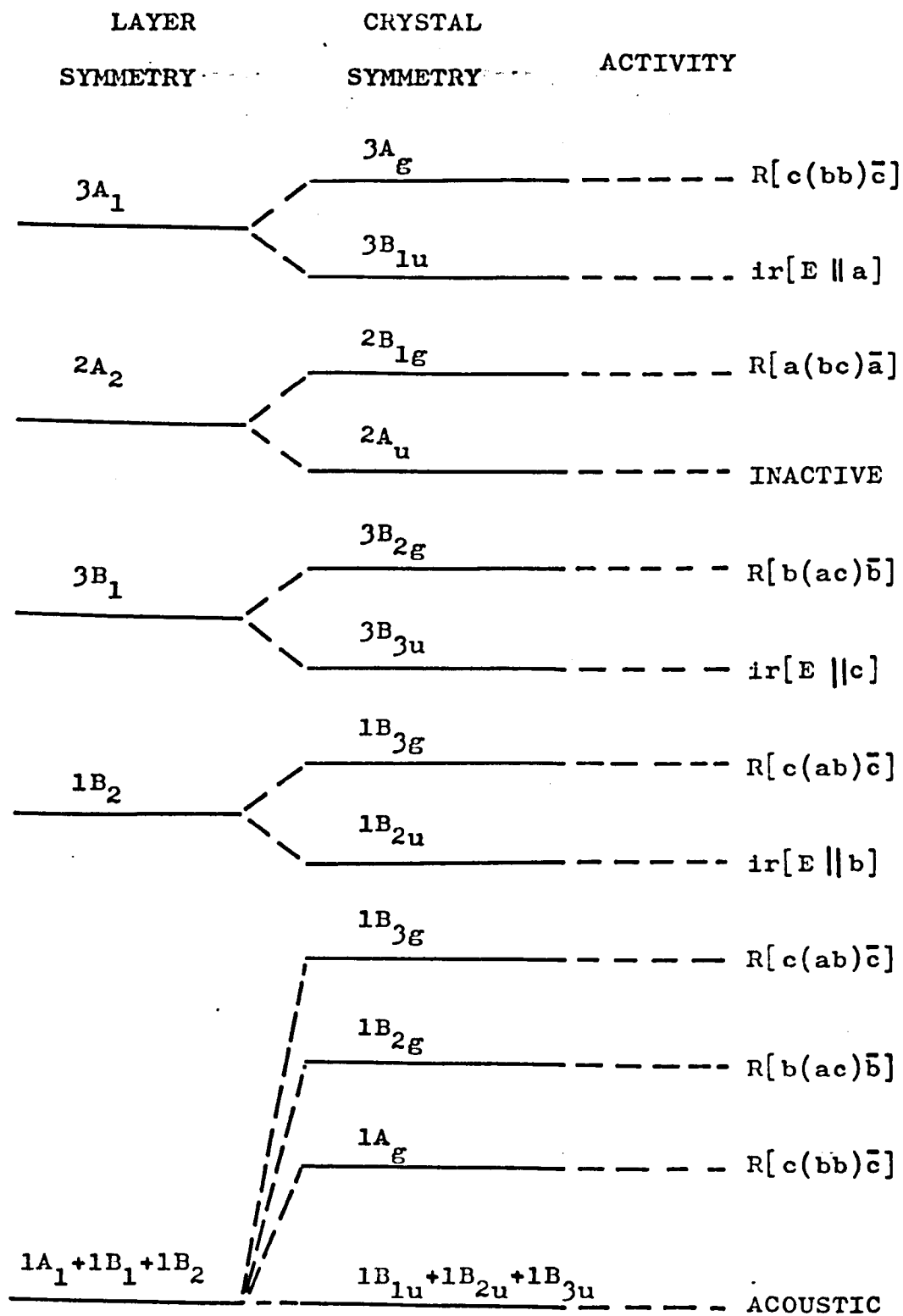
Fig.6-2). Diagram showing the relations among phonons for individual layers and three dimensional crystals of GeS. (After Wiley et al ,1976)

observed for $\vec{F} \| \vec{c}$. In order to obtain the optical

constants of SnS, the experimental reflectivity

curves measured by Fourier transform spectroscopy

for $\vec{F} \| \vec{a}$ and $\vec{F} \| \vec{b}$ directions were analysed by means

of   Kramers-Krönig techniques: the results of

this analysis are displayed in Figure 6.3 and in

table one, which also displays the phonon mode

assignments based on Wiley's recent group theoretical

treatment. The computer programs used in this laboratory

for the Fourier transform and Kramers-Krönig analysis

has been given elsewhere (Doran, 1974). Table two

displays the oscillator parameters and dielectric

constants for the three polarization directions which

have been deduced from a least-squares computer fit to

the experimental reflectivity data. This program

(together with an explanation of its physical basis) is

given as an appendix B to this chapter . Table three

shows the changes in transverse optical phonon frequencies

ω_T (for the $\vec{F} \| \vec{a}$ and $\vec{F} \| \vec{b}$ directions) in the temperature

range 10 - 300 $^{\circ}$K, as deduced from the shift in

the reflectivity peak positions over this temperature

range, and from the results of the room temperature

Kramers-Krönig analysis. $\vec{F} \| \vec{c}$ data values of the

frequency shifts are not displayed because of the

uncertainty in this direction of polarization. As

seen from the numerical values of the transverse

optical phonons there is a negligible change down

to 50°K. One might say, that transverse optical
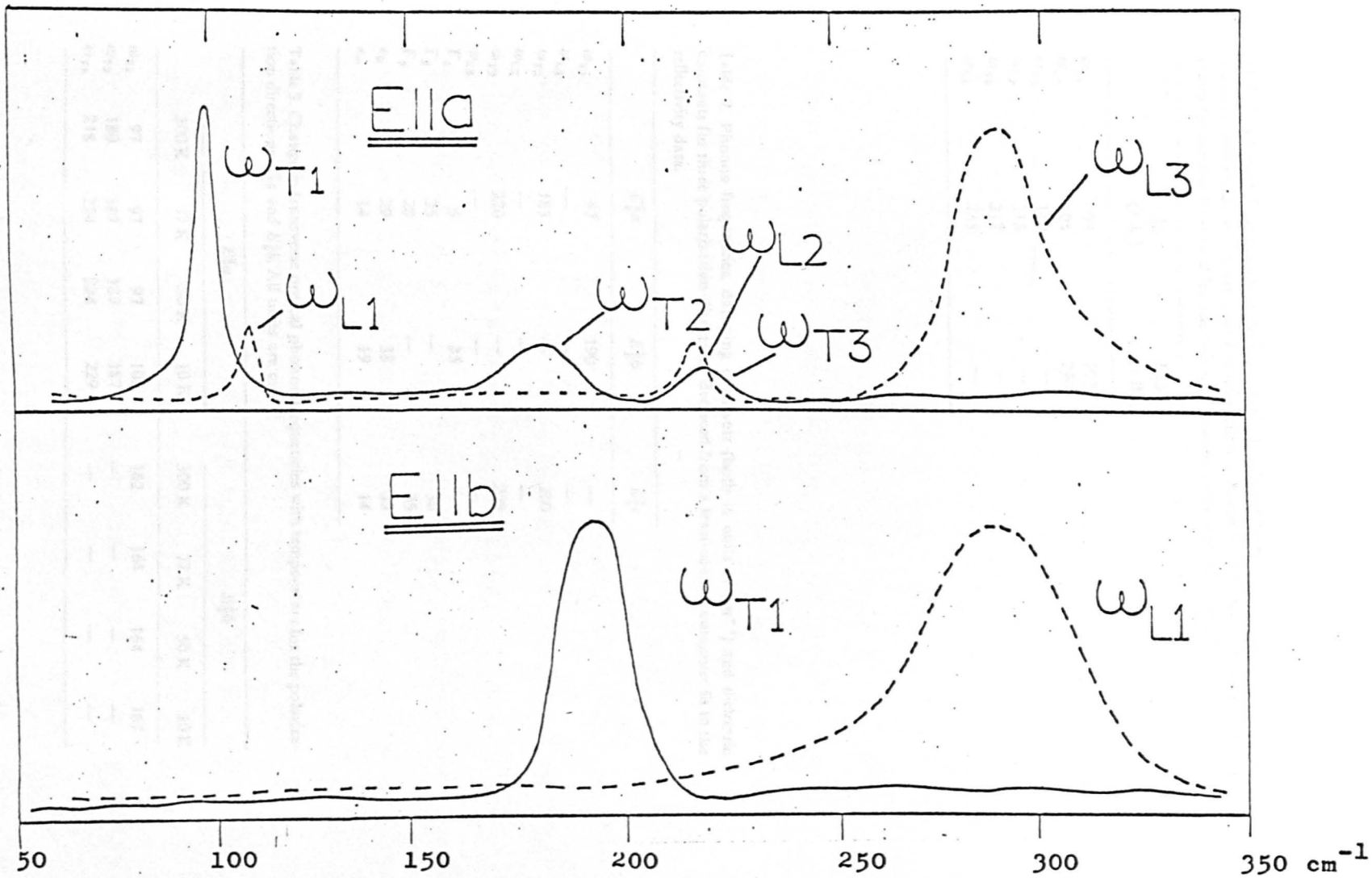
Fig.6-3). Kramers-Kronig analysis of the reflectivity spectra.

Table 1. Phonon frequencies (in units of cm^{-1}) deduced from Kramers-Krönig analysis, together with mode assignments and multiplicities deduced from Wiley's (Wiley *et al* 1976) group theoretical treatment for the two polarization directions $E\|a$ and $E\|b$.

	$E\|a$ (3 A_g)	$E\|b$ (1 B_{2u})
ω_{T1}	97	192
ω_{L1}	105	290
ω_{T2}	180	—
ω_{L2}	215	—
ω_{T3}	217	—
ω_{L3}	285	—

Table 2. Phonon frequencies, damping constants (both in units of cm^{-1}) and dielectric constants for three polarization directions deduced from a least-squares computer fit to the reflectivity data.

	$E\|a$	$E\|b$	$E\|c$
ω_{T1}	97	190	—
ω_{L1}	—	—	—
ω_{T2}	183	—	200
ω_{L2}	—	—	—
ω_{T3}	220	—	229
ω_{L3}	—	—	—
Γ_1	5	35	—
Γ_2	25	—	30
Γ_3	20	—	35
ϵ_0	29	38	33
ϵ_∞	14	19	14

Table 3. Change in transverse optical phonon frequencies with temperature for the polarization directions $E\|a$ and $E\|b$. All units are cm^{-1}.

	$E\|a$				$E\|b$			
	300 K	77 K	50 K	10 K	300 K	77 K	50 K	10 K
ω_{T1}	97	97	97	102	162	164	164	167
ω_{T2}	180	187	187	187	—	—	—	—
ω_{T3}	218	224	224	229	—	—	—	—

phonon frequencies of SnS are temperature-independent in the range 50 - 300 $^{\circ}$K.

A typical room temperature absorption curve for a thin n-type sample with $\vec{E} \| \vec{a}$ (suitably corrected for surface reflectivity changes) is shown in Figure 6.4. Three oscillator peaks corresponding to the transverse optical frequencies are displayed clearly. A peak appearing about at 100 cm^{-1} is sharper than those of two others; these results are very sensitive to orientation of the sample. In addition, transmission data were also taken at room temperature on this specimen in the spectral range 500 - 4000 cm^{-1} using a Perkin-Elmer monochromator system. This data showed interference fringes, from which a value of the high-frequency dielectric constant could be deduced as a check on the value obtained from Kramers-Krönig and curve-fitting analysis of the reflectivity data. The thickness of this sample was measured to be 2.5 μm, using a talystep gauge. The reflection spectra for n-type samples are essentially similar in the temperature range 50 - 300 $^{\circ}$K to those obtained at room temperature, and are not therefore displayed separately. In this temperature range the p-type samples also show the same characteristic features.
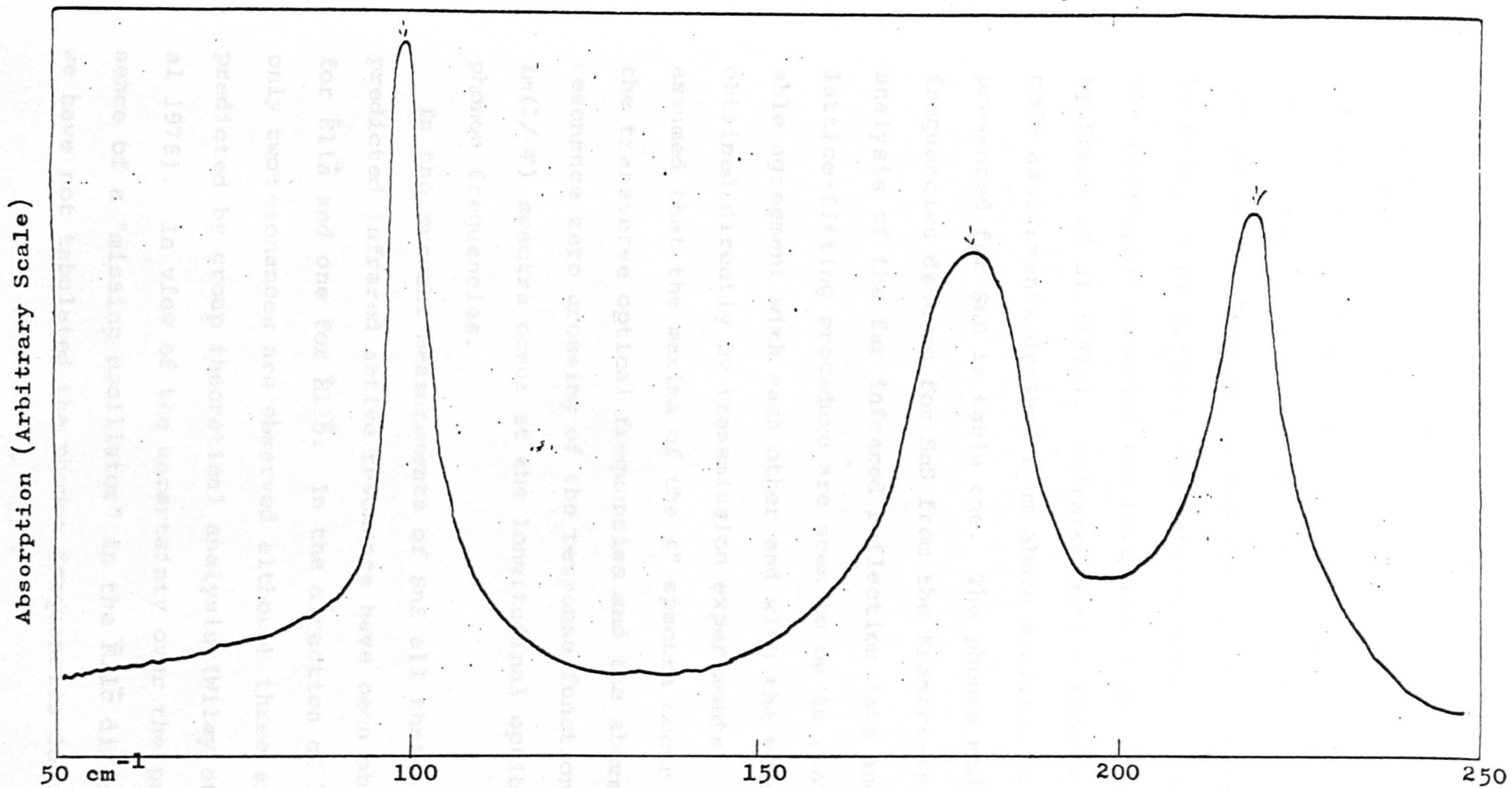
Fig.6-4). Absorption versus wavenumber for a 2.5μm thich sample of
n-SnS at 3ooK with E∥a.

6.7 Discussions

A factor-group analysis of the D_{2h}^{16} space group
of SnS, together with a discussion of the effects
of interlayer forces on the infrared and Raman-
active phonon frequencies has been given recently
by Wiley et al (1976). The lattice dynamics of
the isomorphic material GeS have also been reported
by Kress et al (1976). Infrared active phonon-
mode assignments derived from above analysis are
presented for SnS in table one. The phonon mode
frequencies deduced for SnS from the Kramers-Krönig
analysis of the far infrared reflection data and
lattice-fitting procedure are seen to be in reason-
able agreement with each other and with the values
obtained directly by transmission experiments. We
assumed that the maxima of the ε'' spectra occur at
the transverse optical frequencies and the above
resonance zero crossing of the response function
$Im(1/\varepsilon')$ spectra occur at the longitudinal optical
phonon frequencies.

In the present measurements of SnS all three
predicted infrared active resonance have been observed
for $\vec{E}||\vec{a}$ and one for $\vec{E}||\vec{b}$. In the direction of $\vec{E}||\vec{c}$
only two resonances are observed although three are
predicted by group theoretical analysis (Wiley et
al 1976). In view of the uncertainty over the pre-
sence of a "missing oscillator" in the $\vec{E}||\vec{c}$ direction,
we have not tabulated the phonon frequencies deduced

from the Kramers-Krönig analysis data in this
polarization direction. We have, however, applied
the lattice fitting procedure to our $\vec{E} \| \vec{c}$ reflec-
tivity spectra assuming the presence of two oscill-
ators in order to furnish approximate phonon
frequency and dielectric constant values. We
notice in this connection that Wiley et al (1976)
have similarly failed to observe a predicted phonon
in the $\vec{E} \| \vec{a}$ polarization direction for GeS, although
recently Nikolić and Hughes (1976) have been able
to observe the presence of this oscillator in their
reflection spectra. Evidently, very careful sample
surface preparation techniques are required for
specimens cut perpendicular to the $\vec{c}$ faces because
of scattering effects from irregularities in the
exposed layer ends.

It is of interest to compare the SnS optical
phonon frequencies with those recently obtained
for the isomorphic systems GeSe and GeS (Wiley et
al 1976, Chandrasekhar and Zwick 1976, Siapkas et
al 1976). (See table four). In the case of SnS
the transverse optical phonon modes lie in all cases
between the two corresponding values for the Germanium
chalcogenides. That is, the ratio of the corresponding
frequencies of GeSe and GeS are related by a simple
scaling factor for most of the high frequency phonons
in the layer plane. This frequency ratio,

$$\frac{\gamma(GeSe)}{\gamma(GeS)} \backsim 0.73 \pm 0.06 \quad \text{and} \quad \frac{\gamma(GeSe)}{\gamma(SnS)} \backsim 0.88 \pm 0.07.$$

We may assume that SnS is more layer-like than GeS and
less layer-like than GeSe.

This conclusion was also reached by Chandrasekhar and Zwick (1976) using a similar dynamical argument.

We also attempted to perform Raman Scattering experiments on our samples at Leicester University using a Kr 6371$\overset{o}{A}$ laser system. The combination of Raman and Infrared spectroscopy would here allow us to obtain complete information about the ratio of interlayer to intralayer coupling, as has been done for GeSe (Chandrasekhar and Zwick 1976) and GeS (Wiley et al, 1976). Unfortunately, these experiments were not a success and this was, in our opinion, caused by the poor signal/noise ratios obtainable in the detection system. Finally, we have appended in table four a compendium of room temperature phonon frequencies for the isomorphic systems GeSe, SnS, GeS.

In view of the well-known hazards of using Kramers-Krönig analysis for heavily damped systems, such as SnS (Barker, 1964), we have not presented the dielectric constant values obtained by this technique in table one. The values for this quantity displayed in table two are, however, believed to be reliable in view of the fact that this procedure yields values of ε_∞ in the $\vec{E} \| \vec{a}$ and $\vec{E} \| \vec{b}$ directions which are consistent with those obtained from an analysis of the interference fringe data. For example, with partially polarized light incident on the c face of a 2 μm thick sample, interference fringes were observed in transmission above 700 cm^{-1}. The spacing of these fringes was 500 cm^{-1} at the highest frequencies

of incident light. The value of $\varepsilon_\infty = 16$ deduced from this observation is consistent with the values of $\varepsilon_\infty = 14$ and $\varepsilon_\infty = 19$ obtained by a fitting procedure from the $\vec{E} \| \vec{a}$ and $\vec{E} \| \vec{b}$ data respectively.

One of the original objectives of this work was to search for plasma reflection effects in our specimens in order to determine the carrier susceptibility mass. We see no evidence in our n-type samples of any "plasma edge" (Bradley, 1973) in the wavelength and temperature regions investigated. In the case of our p-type specimens, we are almost equally convinced that the same conclusions hold. Slight doubts, however, are cast by order of magnitude estimates of the plasma-edge position and by certain experimental artefacts that will be discussed later. This order of magnitude estimates will now be considered: if we take the early estimates of hole effective mass ratios for the symmetry directions of SnS (Haas and Corbay, 1961), we obtain

$$\left(\frac{m^*}{m_o}\right)_a \sim \left(\frac{m^*}{m_o}\right)_b \sim 0.2 \quad \text{and} \quad \left(\frac{m^*}{m_o}\right)_c \sim 1$$

from free carrier absorption data. Combining these in the usual way we obtain a hole susceptibility mass of $\sim 0.3m_o$, which taken with an averaged value of ε_∞ over the three symmetry directions of $\langle \varepsilon_\infty \rangle \sim 16$ yields a plasma frequency of $\omega_p \sim 80 \text{ cm}^{-1}$ for typical samples with $N_A - N_D \sim 5 \times 10^{17} \text{ cm}^{-3}$. In conclusion, therefore, complex plasmon-phonon coupling effects should be seen for our p-type samples as this frequency

(ω_p) is in the region of the phonon frequencies measured in our experiments. However, no clear indication is given in our data for such effects. In some of our spectra, it initially appeared that there was an increase in the non-resonant contribution to the reflectivity below 200 cm^{-1} for samples at 10 $^{\circ}$K. However, this observation is inconsistent with the normal movement of plasma edges with temperature in view of the fact that higher temperature samples do not show this response. Careful analysis of the experimental findings leads us to think that this effect is due to "iceing" of the polythylene windows over the course of a day's experimentation. Broadband absorption by the ice at frequencies less than $\sim$150 cm^{-1} would not then be "ratioed out", giving rise to these pseudo-plasma effects. Another critical problem encountered in the measurements of far infrared reflectivity and transmission of SnS is caused by movement with temperature of the polyethylene absorption features. It is well-known that the spectroscopist suffers from a scarcity of components in the far infrared, such as windows and lenses. Polyethylene is widely used as a window material but a problem arises due to its intrinsic absorption. The first feature is observed at 71 cm^{-1} (Davies and Haigh, 1974), (a sharp single phonon absorption) and another at 96 cm^{-1} (Krimm and Bank, 1965, Fleming et al. 1972) the latter being a weak absorption at room temperature shifting to 106 cm^{-1} at liquid nitrogen temperature (Davies and Haigh, 1974). The third feature of note is the

absorption maximum found at 190 cm^{-1} at room temperature, which on cooling to 77 ^{O}K is observed to shift to 215 cm^{-1} for high density and 220 cm^{-1} for the low density material. All three absorptions of polyethylene coincide with the fundamental lattice vibrations of SnS, and it is therefore particularly important to correct the effect of polyethylene on SnS spectrum.

To conclude: six of the seven infrared active modes of SnS have been observed in the reflection in the region 50 to 350 cm^{-1}; in general their positions agree with recent group theoretical analysis by Wiley et al. (1976).

Table 4

	GeS			GeSe			SnS		
	E ∥ a	E ∥ b	E ∥ c	E ∥ a	E ∥ b	E ∥ c	E ∥ a	E ∥ b	E ∥ c
w_{T_1}	117.5	201	105	88 88	150 155		97	192	
w_{T_1}'	117.5	205	105	88	154		97	190	
w_{T_2}	257.5		237	175 173			180		
w_{T_2}'	257.5		237.5	173			183		200
w_{T_3}			280	186 181			217		
w_{T_3}'			280	182			220		229
w_{L_1}	123.5	298	107	91.5 92	210.5 207		105	290	
w_{L_1}'				91	208				
w_{L_2}	325		275	178 178			215		
w_{L_2}'				179					
w_{L_3}			320	224 225			285		
w_{L_3}'				224					
E_O	25.1	29.5	30	21.9 24.5	30.4 23.5			38	33
$E_{O'}$	22.7	27.9	20.9				29		
E_{OO}	14.8	12	10	18.7 13.6	21.9 13				
$E_{OO'}$	13.5	13	10				14	19	14

Lattice mode frequencies of GeS (Wiley et al 1976),
GeSe (Chandrasekhar and Zwick 1976, Siapkas et al 1976
the bottom reference) and SnS.

(Lattice mode frequencies w_T, w_L in cm^{-1})

<u>Foot Note:</u> In any comparison of the strengths of the interlayer forces amongst the members of the SnS subset, it is of great importance to take account of any variations from stoichiometry. This is apparent from the fact that a slightly non stoichiometric material will not cleave as easily as one with perfect stoichiometry.

In this chapter we have compared the corresponding far infra-red lattice mode frequencies of the members of the SnS subset. We have simply assumed that our SnS samples were more layer-like than GeS and less layer-like than GeSe; the data for GeS and GeSe used in this comparison were obtained by Wiley et al(1976) and Chandrasekhar and Zwick(1976). Our arguments will only be true under certain assumptions; namely that the stretching forces between Sn-S and Ge-S are of the same order. However this is not strictly true. Furthermore in previous chapters we discussed the electrical and opto-electrical properties of our samples together with the effects on these properties of the sample quality. In this connection we do not know the sample quality and opto-electrical properties of the GeS and GeSe samples reported by the above authors.

After the preparation of this chapter it has learnt from the literature that Raman spectra had been obtained in SnS, at room temperature only by Nikolic et-al(1977). These authors compared their Raman frequencies with the present infra-red data(Chamberlain et al 1976) to obtain a value for the interlayer coupling factor following the analysis of Zallen and Slade(1971,1974). The parameter $(\nu_0/\nu_\Delta)^2$ representing the strength of the

interlayer coupling is found from this work to be of the order   6. This value indicates that SnS is less layer-like compared with, for example, GeS. This statement is in conflict with our conclusions. We now suggests two possible explanations for this discrepancy. Firstly, some of the crystal growing processes were carried out at Belgrade University(as reported in the acknowledgement section) but there is no evidence that our sample and the Raman sample(Nikolic et al 1977) have the same phys-ical properties. These workers have taken our infra-red data for comparison purposes, and it is almost certain that their sample were not cut from the same ingot as these used by us. Secondly Nikolic et al have made no attempts to calculate the bond stretching force in SnS, which is, of course, given by the expression

$$k_r(Sn,S) = [k_r(Sn,Sn)\ k_r(S,S)]^{\frac{1}{2}}\ (X_{Sn} - X_S)^2$$

[Lucovsky et al 1974]. Where X_{Sn} and X_S are the electro-negativity of Sn and S respectively. It is apparent that using the standard data and the above expression the bond stretching forces in SnS and GeS are fairly different.

APPENDIX A

DESCRIPTION OF APPARATUS USED FOR PHOTOCONDUCTIVITY
MEASUREMENTS.

The first apparatus to be described here is that
used to measure the photoconductivity and the photo-
voltaic effect in the region (0.99-1.5) eV on crystalline
n-type SnS at 300 $^{\circ}$K. A general layout of the apparatus
used is shown in Fig. A.1. A Carlzeiss SPM2 prism
spectrometer with a"Unipan"preamplifier and a selective
microvoltmeter type 203 were the main part of the set-
up, which has been described in detail by Nikolić (1969).
The source was a 12V, 40W, single filament car spot
light bulb acting as a broad band source in the visible and
infrared regions. The incident radiation was mechanically
chopped at a frequency of 10 Hz, and focussed into the
entrance slit of the monochromator by means of combination
of aluminised mirrors. The intensity of the radiation
from the monochromator was adjusted with an adjustable
exit slit and focussed onto the sample using an aluminised
mirror as seen in Fig. A.1. Bias to the specimen was
supplied from a 1.5V battery and no attempt made to
stabilise the current further. An a.c. signal created
on the sample by illuminating it with single wave-
length radiation was fed with a quadruply screened

Source
12 V
40W

Chopper
10 c/s

Monochromator

R
300 Ω

e
1.5V

Sample

T

Pre-amplifier
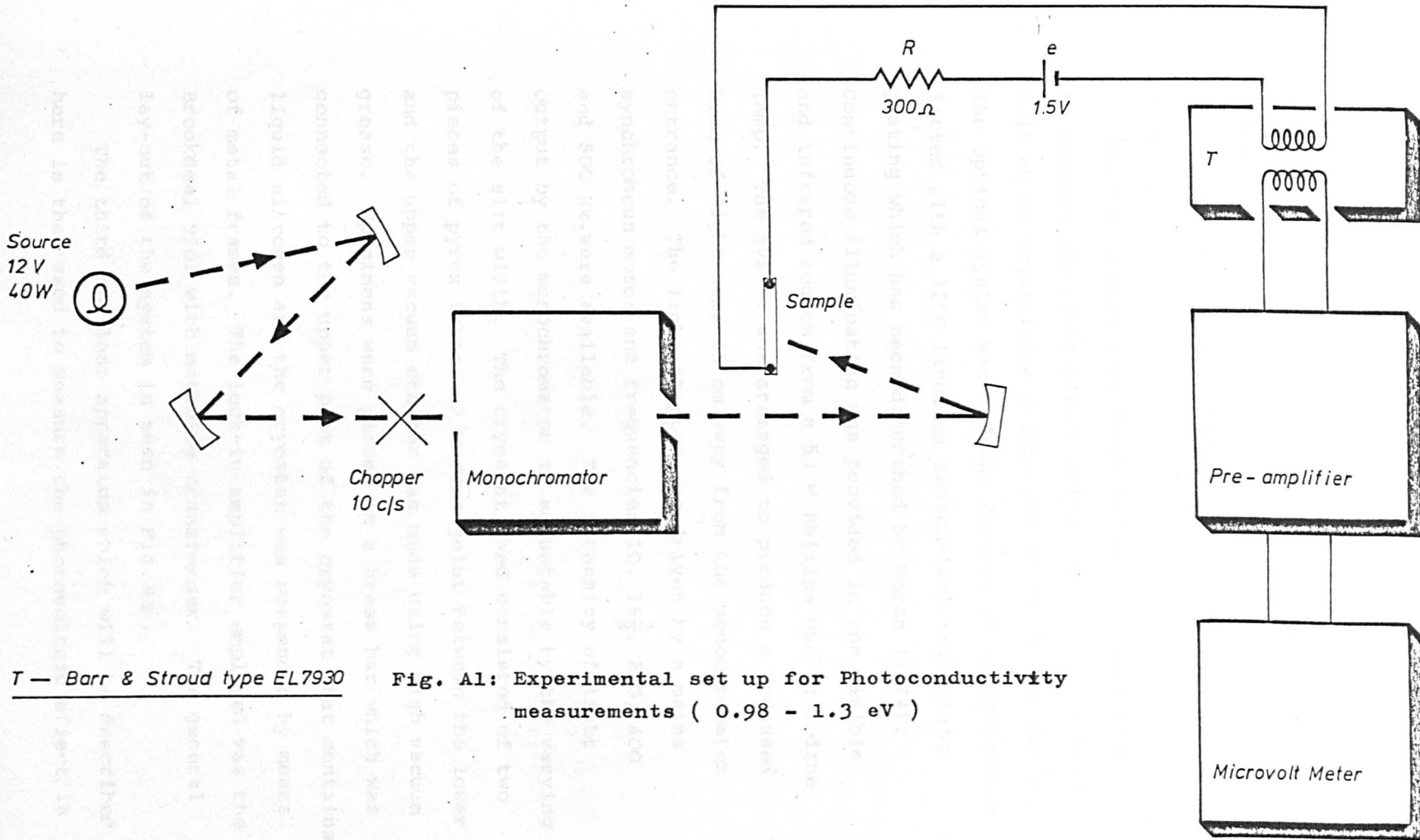
Microvolt Meter

T — Barr & Stroud type EL7930

Fig. A1: Experimental set up for Photoconductivity
measurements (0.98 - 1.3 eV)

matching transformer. (Barr and Stroud, 60 Ω type 7930) to a"Unipan" preamplifier and selective micro-voltmeter with a gain factor of 10^9 and band width of 5 Hz. The output of amplifier was read directly on a meter.

The second apparatus described here is that used to measure the photovoltaic effect in the region 0.99-2.15 eV on crystalline p-type SnS at 77 $^{\circ}K$ and 300 $^{\circ}K$. The optical system was a Grubb Parsons M2 monochromator fitted with a 1200 lines/mm Bausch-Lomb reflecting grating which has been described by Doran (1974). Continuous illumination was provided in the visible and infrared region from a 55 W Philips quartz-iodine lamp. The system was arranged to produce a focussed beam of light some 25 cm away from the monochromator entrance. The light chopper was driven by a mains synchromous motor and frequencies 10, $16\frac{2}{3}$, 200, 400 and 800 Hz were available. The intensity of light output by the monochromator is adjustable by the varying of the slit width. The cryostat used consisted of two pieces of pyrex tubes. A vacuum joint between the lower and the upper vacuum chamber was made using high vacuum grease. Specimens were placed on a brass bar which was connected to the upper part of the cryostat that contains liquid nitrogen and the cryostat was suspended by means of metal frames. The lock-in amplifier employed was the Brookdeal 9501 with matching transformer. The general lay-out of the system is seen in Fig. A2.

The third and last apparatus which will be described here is that used to measure the photovoltaic effect in

the region 0.48-1.3 eV on crystalline p-type SnS at
lower temperatures (40-77) ^{o}K. The monochromator
employed was a Metrospec high radiance monochromator
fitted with a 2000 nm blaze grating with 295 lines/mm.
Both entrance and exit slit widths were adjustable.
A quartz halogen lamp was used as a source. The fila-
ment current and voltage were controlled continuously.
The light was focussed on to the entrance of monochromator
and on to the sample by means of movable quartz lenses.
The wavelength drum on the monochromator was driven
automatically by a motor which is engaged to a clutch,
and could be driven at different speeds. The spectrum
was obtained with and without a Kodak wratten 70 filter
(Doran 1974, and manufacturer) for the infrared region.
This has a low-pass response with cut off at 1.8 eV
as well as high transmission in the pass-band. Electrical
connections from the sample inside the cryostat were
made by covered 36 SWG copper leads. It was found that
to avoid   standing noise it was necessary to carefully
screen all the electrical leads.

Monochromator

Chopper

Sample

Cryostat

9v

5k

1k

47µF

Die Cast Box

Source

Reference Signal

Lock-in Amplifier

Chart Recorder
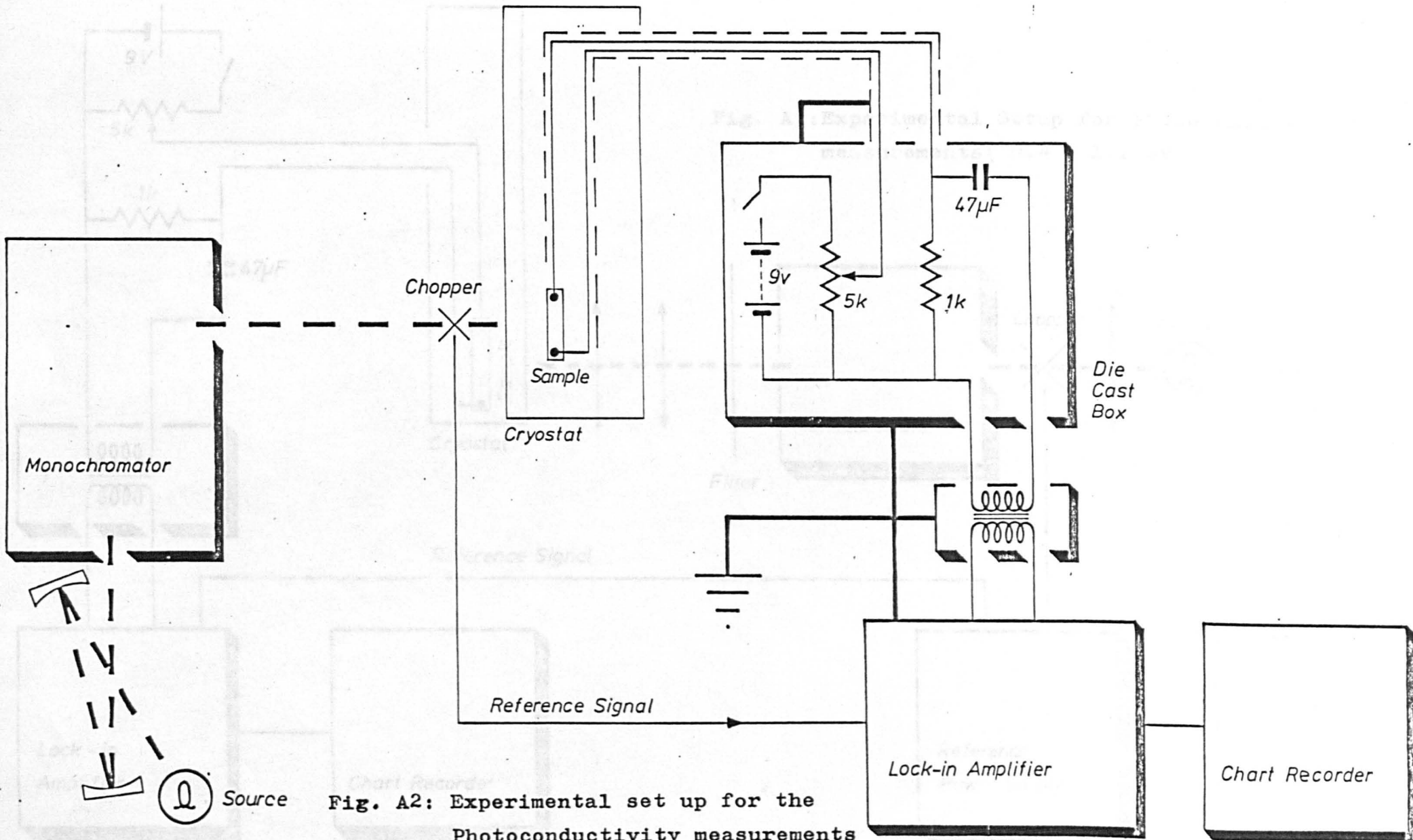
Fig. A2: Experimental set up for the Photoconductivity measurements (0.98- 2.1 eV)
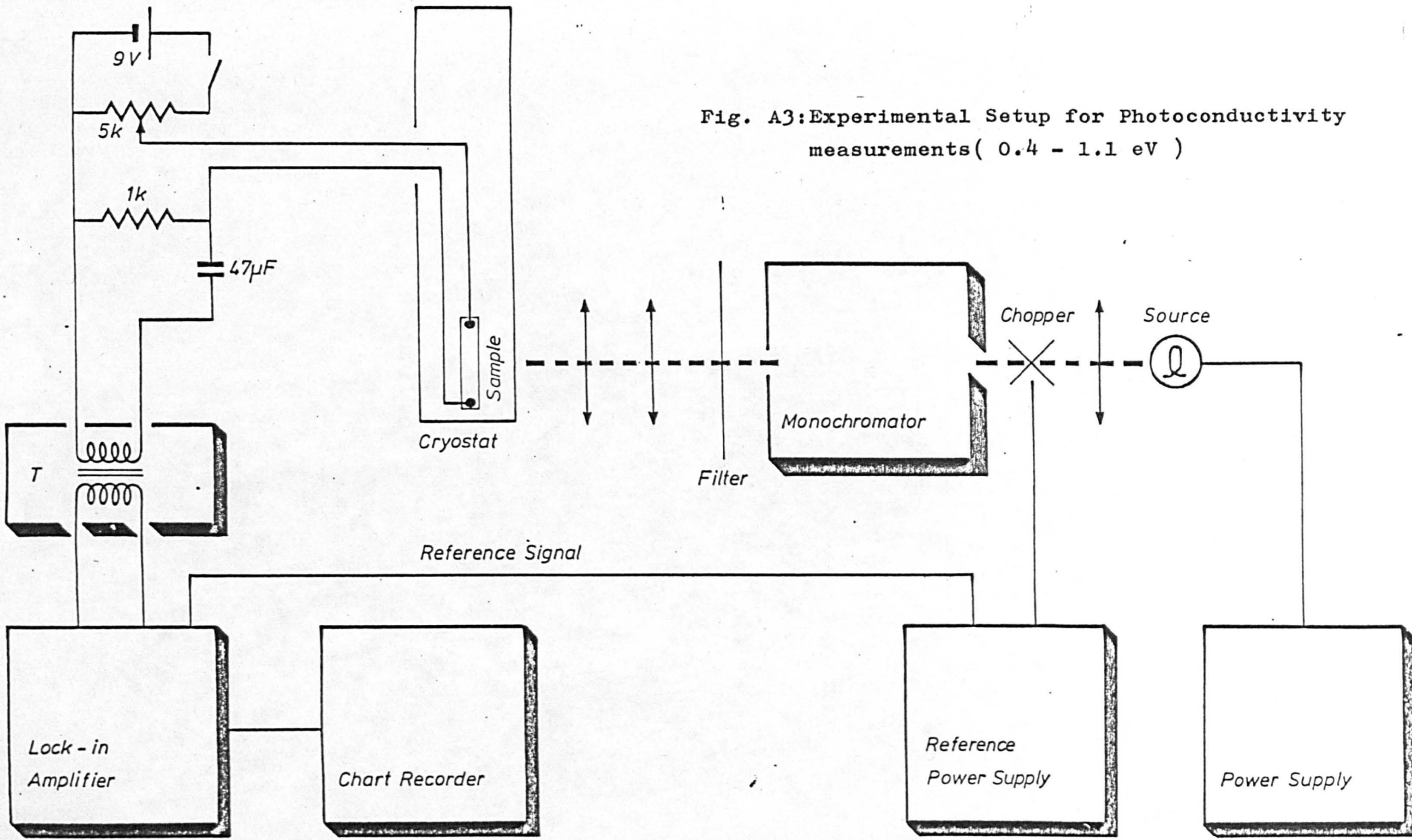
Fig. A3: Experimental Setup for Photoconductivity measurements(0.4 - 1.1 eV)

APPFNDIX B

OSCILLATOR FITTING PROGRAM

Introduction

The reflection at normal incidence is related to
the real and imaginary parts of the dielectric response
function $\varepsilon(\omega)$ through the usual equation

$$R = \left[(n-1)^2 + k^2\right] \Big/ \left[(n+1)^2 + k^2\right] \qquad \underline{/1/}$$

where n and k are the real and imaginary parts of the
refractive index, i.e. $(n+ik)^2 = \varepsilon(\omega) = \varepsilon^1(\omega) + i\varepsilon^{11}(\omega)$.
We use the dynamic argument (Balkanski/Abeles, p.546)
to obtain

$$\varepsilon^1(\omega) = n^2 - k^2 = \varepsilon_\infty + \frac{(\varepsilon_0 - \varepsilon_\infty)(\omega_{TO}^2 - \omega^2)\omega_{TO}^2}{(\omega_{TO}^2 - \omega^2)^2 + \Gamma_a^2 \omega^2} \qquad \underline{/2/}$$

and

$$\varepsilon^{11}(\omega) = 2nk = \frac{(\varepsilon_0 - \varepsilon_\infty)\omega_{TO}^2 \omega \Gamma_a}{(\omega_{TO}^2 - \omega^2)^2 + \Gamma_a^2 \omega^2} \qquad \underline{/3/}$$

where ω_{TO} is the transverse optic phonon frequency.

ε_0 is the "low frequency" dielectric constant;

ε_∞ is the "high frequency" dielectric constant,

and Γ_a refers to the damping of the mode. We extend
the analysis to several lattice modes on the assumption
that these modes are independent and therefore we can

write for n oscillators

$$\epsilon^{1}(\omega) = \epsilon_{\infty} + \sum_{j=1}^{n} \frac{(\epsilon_{o}-\epsilon_{\infty})(\omega_{j}^{2}-\omega^{2})\omega_{j}^{2}}{(\omega_{j}^{2}-\omega^{2})^{2}+\Gamma_{j}^{2}\omega^{2}} \qquad \angle\underline{4}7$$

$$\epsilon^{11}(\omega) = \sum_{j=1}^{n} \frac{(\epsilon_{o}-\epsilon_{\infty})\omega_{j}^{2}\omega\Gamma_{j}}{(\omega_{j}^{2}-\omega^{2})^{2}+\Gamma_{j}^{2}\omega^{2}} \qquad \angle\underline{5}7$$

where the ω_{j}'s and Γ_{j}'s refer to each mode.

Computation Procedure

The experimental reflectivity data points (R versus σ) are fitted to one, two or three lattice oscillators (as seems appropriate) using a least-squares computer fit. The routine used is Peckhams method which is implemented on the Cripps Computer Centre routine FO4FAF. The program used by us is rather cumbersome and can, no doubt, be streamlined as far as input and output is concerned. A compilation for fitting 150 data points to three oscillators is appended. The first segment inputs the data points and notes the "initial guesses" (θ_{1} to θ_{10}) of the variables to be fitting and the accuracy parameters (V_{1} to V_{10}) required by the NAG routine. In the second segment the full expression is given which is to be fitted to the data points provided. This is equation $\angle\underline{1}7$ with n and k subtracted from equation $\angle\underline{2}7$ and $\angle\underline{3}7$ (or in the case of several oscillators

from equation $\angle\bar{4}\bar{7}$ and $\angle\bar{5}\bar{7}$). The smooth working of the routine FO4FAF requires that the physical variables ε_∞, $(\varepsilon_0 - \varepsilon_\infty)_j$, ω_j and Γ_j be of the same numerical order. The computer variables $\theta(1)$, $\theta(2)$ etc. used in our program are therefore chosen in accordance with this requirement using the scheme:

$$\theta_1 = \varepsilon_\infty$$
$$\theta_2 = (\varepsilon_0 - \varepsilon_\infty)$$
$$\theta_3 = \omega_1/10$$
$$\theta_4 = \frac{\Gamma_1}{\omega_1} \times 10^3 \qquad \text{(Contribution from first oscillator.)}$$

and same θ_5, θ_6, θ_7 and θ_8, θ_9, θ_{10} for second and third oscillators.

The third segment calls up the NAG routine FO4FAF which accomplishes the fitting. In this routine we give details of the output format. The final output lists the values of the computer parameters θ_1, θ_2, θ_3 etc. from which the parameters of the oscillators (ε_∞, ε_0, ω_1, $\Gamma_a$etc.) may be deduced.

Reference - see CCC NAG library manual on routine FO4FAF.

```
0001        LIST
0002        LIBRARY(ED,L(1))
0003        LIBRARY(ED,L(2))
0004        MAP
0005        PROGRAM(GENF)
0006        EXTENDED
0007        INPUT5,20=CRO
0008        OUTPUT6,30=LP0
0009        TRACE2
0010        END

0011        MASTER FIDDLE
0012        DIMENSION R(150),Y(150),THETA(10),W(20,000),V(10)
0013        DIMENSION Z(150)
0014        COMMON Y,Z
0015        EXTERNAL FUNCT,MONIT
0016        N=10
0017        M=141
0018        IP=N+3+N/3
0019        IW=2*M+4*N+M*N+(N**2+N)/2+IP*(M+2*N+2)
0020        I FAIL=1
0021        THETA(1)=10
0022        THETA(2)=5
0023        THETA(3)=9
0024        THETA(4)=50
0025        THETA(5)=4
0026        THETA(6)=19
0027        THETA(7)=125
0028        THETA(8)=4
0029        THETA(9)=22
0030        THETA(10)=140
0031        V(1)=5
0032        V(2)=2
0033        V(3)=2
0034        V(4)=15
0035        V(5)=2
0036        V(6)=9
0037        V( 7)=20
0038        V(8)=2
0039        V(9)=2
```

```
0040          V(10)=20
0041          ALF=1.0E-5
0042          EPS=1.0E-6
0043          I PRINT=1
0044          MAXIT=1000
0045          READ(5,200) ZN,STEP
0046    200   FORMAT(F6,3,F5,3)
0047          DO 250 I=1,141
0048    250   Z(I)=(ZN+(I-1)*STEP)/10
0049          READ(5,500) (Y(I),I=1,141)
0050    500   FORMAT(141F0.0)
0051          WRITE(6,900)
0052    900   FORMAT(1H1)
0053          CALL E04FAF(M,N,THETA,R,S,EPS,ALF,V,W,IW,FUNCT,MONIT,
0054         1 I PRINT,MAXIT,I FAIL)
0055    300   FORMAT(44H0 FINAL LEAST SQUARES ESTIMATES OF THETA ARE,7E1
0056          WRITE(6,400) I FAIL                                      4.6)
0057    400   FORMAT(9H I FAIL=,I1)
0058          WRITE(6,800) EPS
0059    800   FORMAT(7H EPS=,F4.0)
0060          STOP
0061          END


END OF SEGMENT, LENGTH  334, NAME FIDDLE


0062          SUBROUTINE FUNCT(M,N,THETA,R)
0063          DIMENSION  THETA(N),R(M),Y(150),Z(150)
0064          DIMENSION ALPHA(150),BETA(150)
0065          DIMENSION COMPA(150,10),COMPB(150,10)
0066          DIMENSION DENOM(150,10)
0067          COMMON Y,Z
0068          DO 10 I=1,140
0069          DO 20 J=2,5,8
0070          DENOM(I,J)=(1-(Z(I)/THETA(J+1))**2)**2
0071         1 +(1.0E-6)*(THETA(J+2)**2)*((Z(I)/THETA(J+1))**2)
0072          COMPA(I,J)=THETA(J)*(1-Z(I)/THETA(J+1))**2/DENOM(I,J)
0073          COMPB(I,J)=(1.0E-3)*Z(I)*THETA(J)/(THETA(J+2)*DENOM(I,J))
0074          ALPHA(I)=THETA(1)*COMPA(I,2)+COMPA(I,5)+COMPA(I,8)
0075          BETA(I)=COMPB(I,2)+COMPB(I,5)+COMPB(I,8)
0076    20    CONTINUE
0077    10    R(I)=(SQRT(ALPHA(I)**2+BETA(I)**2)+1-1.414214*SQRT(SQRT
0078         1 (ALPHA(I)**2+BETA(I)**2)+ALPHA(I)))/
```

```
0079          2(SQRT(ALPHA(I)**2+BETA(I)**2)+1+1.414214*SQRT(SQRT(ALPHA(I)
0080          3**2+BETA(I)**2)+ALPHA(I)))-Y(I)
0081          RETURN
0082          END

END OF SEGMENT, LENGTH 358, NAME FUNCT

0083          SUBROUTINE MONIT(M,N,THETA,S,I TERC,SING,LIM)
0084          LOGICAL SING, LIM
0085          DIMENSION THETA(N)
0086          WRITE(6,100) I TERC
0087          WRITE(6,200) S
0088          WRITE(6,300) (THETA(I), I=1,N)
0089          IF(SING) WRITE(6,400)
0090          IF(LIM) WRITE(6,500)
0091          RETURN
0092    100   FORMAT(11HO ITERATION ,I2)
0093    200   FORMAT(16H SUM OF SQUARES ,E14.6)
0094    300   FORMAT(21H VALUES OF THETA ARE ,3F14.6)
0095    400   FORMAT(9H SINGULAR)
0096    500   FORMAT(8H LIMITED)
0097          END

END OF SEGMENT , LENGTH 111, NAME  MONIT
```

APPENDIX C

OPTICAL STUDIES ON MARMATITE

Introduction

   Marmatite (Zn,Fe)S crystallizes predominately in the
tetrahedral structure (Fig. C1) which is often developed
into forms resembling octahedra. It seldom appears with
sharp or smooth faces, but is usually curved, twinned,
striated, etc. (Fig. C2) [p.294,Sinkankas 1964,Minerology].
Simple and repeated twinning is very common on O(111) as
manifested by narrow striations and bands of slightly
differing lustre on crystal surfaces and cleavage planes.

   Marmatite is a typical member of the sphalerite (ZnS)
group [Boussingault,1829]. The space group is $F\bar{4}3m$ and the
unit cell contains 8 atoms [Palache et al, 1966].

   Marmatite is formed containing Fe partially substituting
for Zn.The iron concentration is always less than 26 per
cent,and no 100% Fe member of the sphalerite group is known
[Palache et al, 1966, pp.210].

   The colour of Marmatite varies with the Fe content from
white-brown(in which the ratio of Zn:Fe$>$5:1)to brown-black
in which Fe content is more than 10 per cent.The range in
the latter case is 6:5$>$Zn:Fe$>$5:1 with a maximum of 26 per
cent Fe.

   Marmatite is brittle and has a perfect cleavage plane
developed parallel to the dodecahedron d(110); with care,
a large fragment can be cleaved in this form [Sinkankas,
1964,pp.294]

   The pale coloured specimens are transparent through 2″

o(001)

o(111)

125° ρ σ o ρ
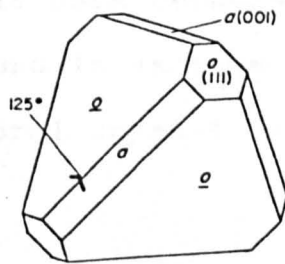
POSITIVE & NEGATIVE OCTA-
HEDRONS & CUBE

109½° n(112)

o(111) 160½°

n n n

146½°
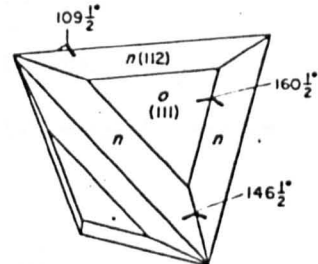
POSITIVE OCTAHEDRON &
TRISTETRAHEDRON n/112/

SPHALERITE

109½° o(111) ρ

SPINEL-TYPE TWIN

120° d d

m(311)

129½° d(110)
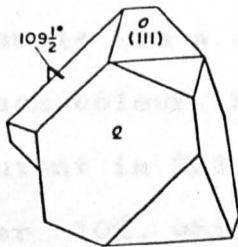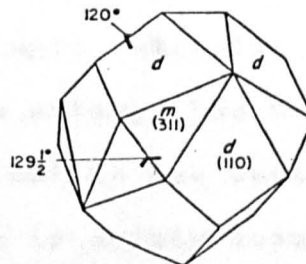
DODECAHEDRON & TRISTETRA-
HEDRON m/311/

Fig C1: Crystal Structure of Sphalerite.
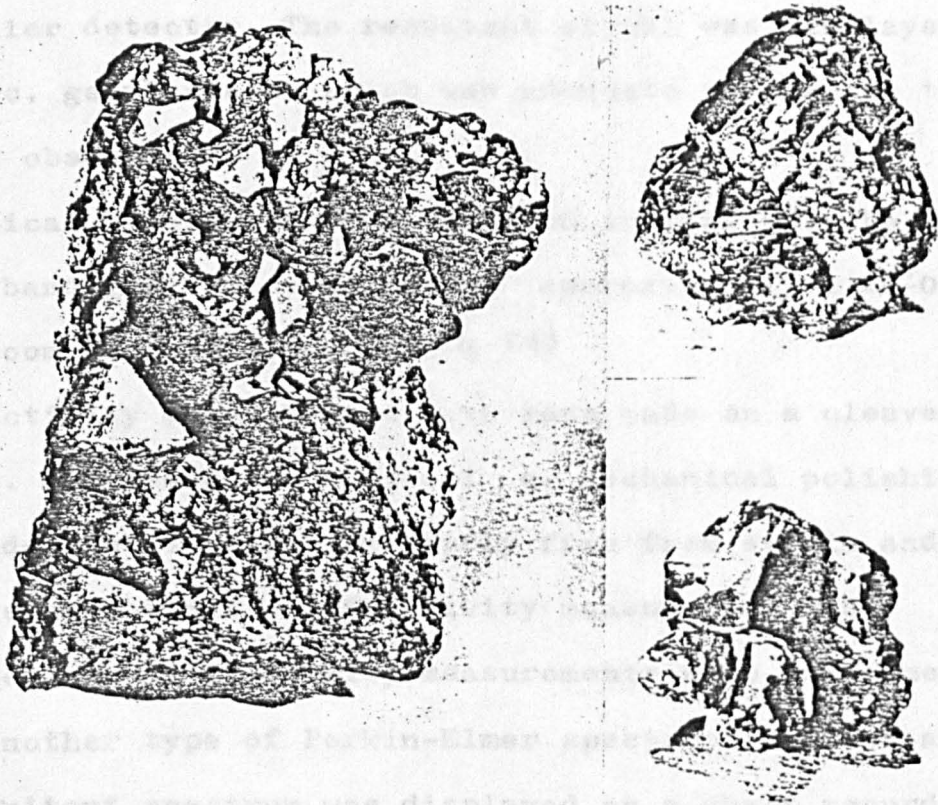
FIG. **C2:** Sphalerite. Left: Rude twinned black crystals on chert from southwest Missouri. Size
5½" by 3½". Top right: Transparent greenish-yellow curved and twinned crystals from Picos de
Europa, Santander, Spain. Size 1¾" by 1¾". Bottom right: pale green cluster of transparent
crystals from Franklin, Sussex County, New Jersey. Size 1½" by 1⅝".

of material, while dark coloured specimens are opeque.

It has been found in various colours with various Fe content as a natural crystal in different parts of the world.

Experimental Technique and Results.

The marmatite sample was a single naturally occurring crystal with a black colour. No attempt has been made to analyse the Fe content in ZnS, but it was certain that the Fe content was over 10%, which is safely assumed from its colour as discussed previously.

The sample for the tranmission experiment was of 400μ thickness stuck onto sellotape.The spectra were obtained using a Perkin-Elmer type spectrophotometer with a photomultiplier detector. The resultant signal was displayed on a d.c. galvanometer which was adequate to resolve the feature observed.

A typical specra obtained is shown in fig. C3. The indirect band gap is assumed to be approximately $1.28^{\pm}0.05$ eV at room temperature. (See, fig. C5)

Reflectivity measurements have been made on a cleaved surface. No attempt at chemical or mechanical polishing were made. The surface was fairly free from strain and striatae on which the reflectivity measurement was performed. The reflectivity measurements were performed using another type of Perkin-Elmer spectrophotometer and the resultant spectrum was displayed on a chart recorder. The spectrum was corrected for the apparatus characteristic by replacing the sample with a freshly aluminized mirror. A typical reflectivity curve is displayed in fig. C3 .
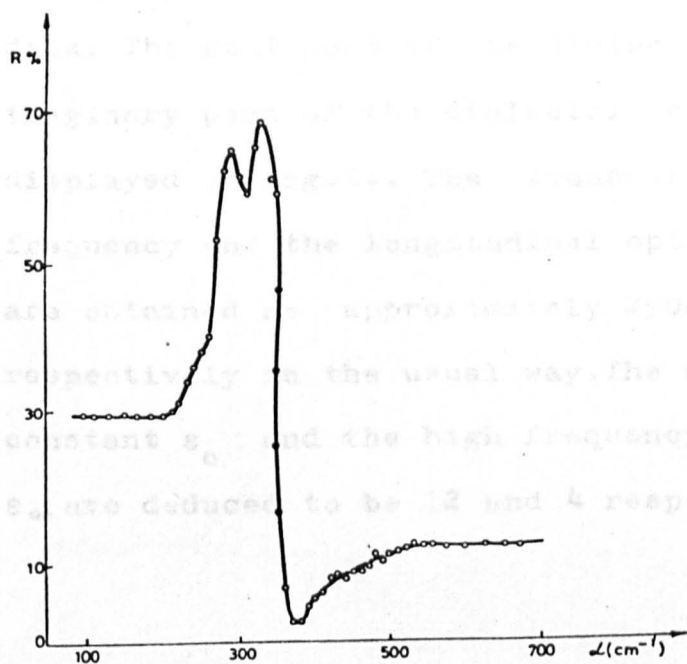
Fig. C3: Reflectivity Curve of Marmatite
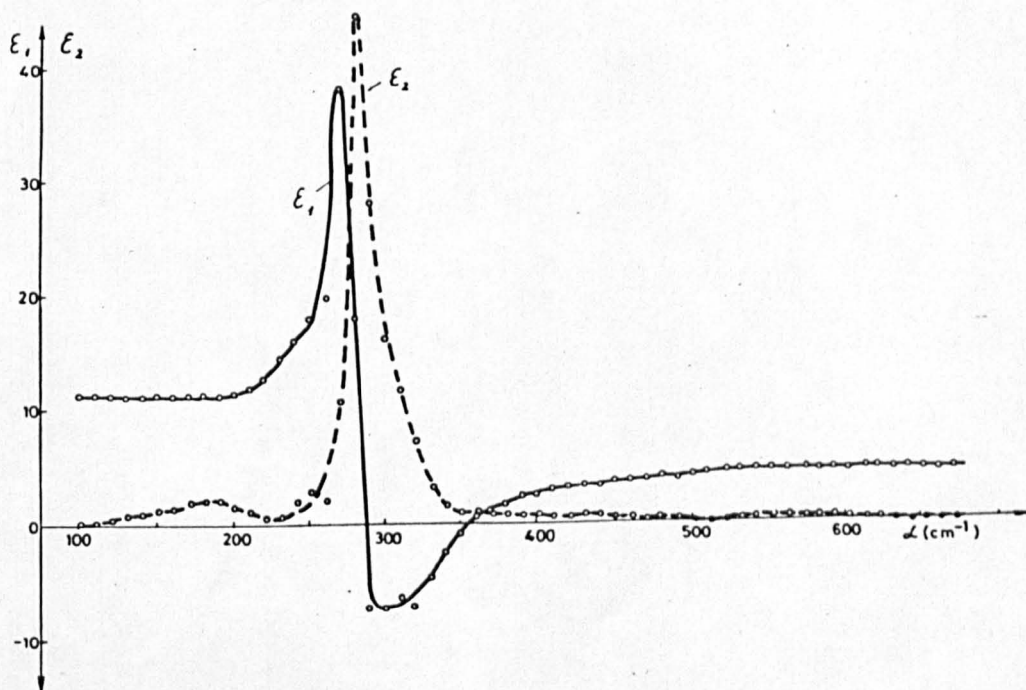
Fig. C4: Kramers-Kronig analysis of the reflectivity
spectra.

Optical constantswere obtained by performing Kramers-
Kronig analysis and oscillator fits on the reflectivity
data. The real part of the dielectric constant ε' and the
imaginary part of the dielectric constant ε'' spectrum are
displayed in fig.C4. The transverse optical phonon
frequency and the longitudinal optical phonon frequencies
are obtained as approximately $290cm^{-1}$ and 358 cm^{-1}
respectively in the usual way.The static dielectric
constant ε_o and the high frequency dielectric constant
ε_∞ are deduced to be 12 and 4 respectively.
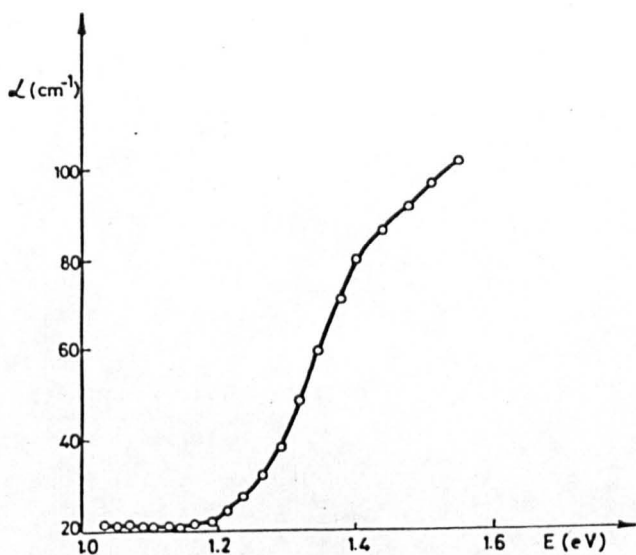
Fig. C5: Absorption of Marmatite
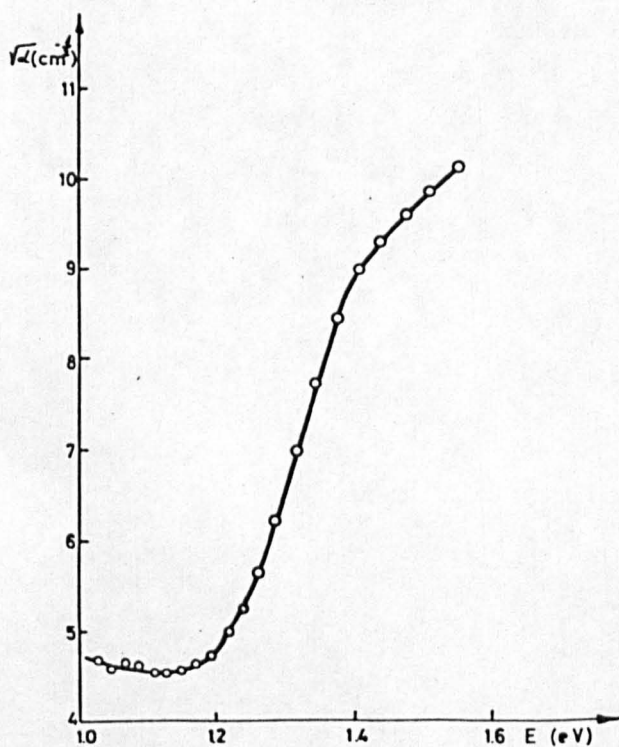
Fig. C6: √α versus Energy variations of Marmatite

ACKNOWLEDGEMENTS

R E F E R E N C E S

1. Abrikosov et al. 'Semiconducting II-VI, IV-VI and V-VI Compounds' Monographs in Semicond.Phys. Translated from Russian by Albin Tybulewicz, Plenum, New York, 1969.

2. Albers W. and Schol K., Philips Res.Repts.,16,329,1961,

3. Albers W.,Haas C.,Ober H.,Schodder G.R and Wasscher J.D.,J.Phys.Chem.Solids.,23,215,1962.

4. Albers W.,Haas C. and van der Maesen F.,J.Phys.Chem. Solids.,15,306,1960.

5. Albers W.,Haas C.,Vink H.J.and Wasscher J.D., J.Apply. Phys. Suppl. to 32,2220,1961.

6. Anderson J.S.and Clark M.C.,Nature, Lond. 152,75,1943.

7. Anderson J.S.and Morton M.C.,Proc.Roy.Soc.,(Lond.) A184,83,1945.

8. Anderson J.C. and Morton M.C.,Trans.Faraday Soc., 43,185,1947.

9. Anderson J.C.and Morton M.C.,Nature, Lond.155,112,1945.

10. Asanabe S.,J.Phys.Soc. Japan.,14,281,1959.

11. Asanabe S.and Okazaki A.,J.Phys.Soc. Japan.,15,989,1960.

12. Auton J.P.,Appl. Optics.,(USA).6,1023,1967.

13. Badachhape S.B.and Goswami A.,Indian J.Pure Appl. Phys., 2,250,1964.

14. Balkanski M.,'Optical Properties of Solids',1972. Ed. by Abeles F.,North-Holland,Amsterdam.

15. Barker A.S.,Phys.Rev.,136,A1290,1964.

16. Bhagavantam S.and Venkatarayudu T.,'Theory of Groups and its Application to Physical Problems'.Bangalore,

Bangalore City,India, 2 nd ed.1951.

17.   Bock E.,Ferguson J.,and Schneider W.G.,Can.J.Chem.
      36,507,1958.

18.   Bok L.D.C.and Boeyens J.C.A.,J.South African Chem.
      Inst.,10,49,1957.

19.   Born M.and Huang K.,'Dynamical Teory of crystal Lattices
      Oxford,U.P. Oxford,1954.

20.   Boussingault.,Ann.Phys. 17,399,1829.

21.   Boutin D.and Bourgon M.,Can. J. Chem.,39,915,1961.

22.   Bradley C.C.,Birch J.R.,Tech B.,and Stockton J.R.,
      (Private Comm.)

23.   Braitwaite J.G.M.,Proc.Phys.Soc. Lond.,B64,274,1951.

24.   Braun F.,Ann.Physik.Chem.,153,556,1874.

25.   Brixner L.H.,J.Electrochem.Soc.,110,289,1963.

26.   Bube R.H.,J.Chem.Phys.,21,1409,1953.

27.   Bube R.H.,'Photoconductivity of Solids'N.Y. John-
      Wiley,1960,Chap.5.

28.   Bube R.H.,'Photoconductivity of Solids'N.Y.John-
      Wiley, 1960.,Chap., 1-2.

29.   Bube R.H.and Thomsen S.M.,J.Chem.Phys.,23,15,1955.

30.   Chamberlain J.M.,Nikolic P.M.,Merdan M.and Mihajlovic
      P.,J.Phys. C:Solid State Phys.,9,L637,1976.

31.   Chandrasekhar H.R.and Zwick U.,Sol.Stat.Comm.
      18,1509,1976.

32.   Chantry G.W.,Evans H.M.,Chamberlain J. and Gebbie
      H.A.,Infrared Phys.,9,85,1969.

33.   Chantry G.W.,'Submillimeter Spectroscopy' Academic
      Press,1971 ,pp.81 and 90.

34. Clasen R.,Burkhard H.,Harbeke G.and Lang G. Verh.
    DPG(VI) 10,391,1975 .

35. Collins A.T. and Lightowlers E.C.,Phys.Rev.,171,843,1968

36. Davies G.J. and Haigh J.,Infrared Phys.,14,183,1974.

37. Doran C.J.,'Optical Studies on III-V and Related
    Semiconductors' Thesis.,Univ. Nott. 1974.

38. Dutta S.N. and Jeffrey G.A.,Inorg.Chem.,4,1363,1965.

39. Eymord R. and Otto A.,13th Int.Conf.Phys.Semiconductor
    Roma.1976.

40. Fataley W.G.,Dollish F.R.,McDevitt N.T.and Bentley
    F.F.,'Infrared and Raman Selection Rules for Molecular
    and Lattice Vibrations'.,Wiley-Interscience,N.Y.,1972.

41. Fataley W.G.,McDevitt.,Neil T.and Bentley F.F.,
    Appl. Spectroscopy.,25,155,1971.

42. Fellgett P.B.,Thesis.,Univ. Cambridge.,1951.

43. Fischer G.and Brebner J.L.,J.Phys. Chem. Solids.,
    23,1363,1962.

44. Fleming J.W.,Chantry G.W.,Turner P.A.,Nicol E.A.,
    Willis H.A.and Cudby M.E.A.,Chem. Phys. Letts.,17,
    84,1972.

45. Fletcher J.R.,Private Comm. Nott.Univ.

46. Fletcher R.,J.Phys.E:Sci.Instrum.,4,470,1971.

47. Frederikse H.P.R.and Blunt R.F.,Proc.Inst.Radio
    Engrs.N.Y.,43,1828,1955.

48. Gobrecht H.and Bartshat A.,Z.Physik 149,511,1957.

49. Gerasimov,,Kruglov.,and Rosenblum.,J.Gen.Chem.
    Moskow.,7,152,1937.

50. Gluyas M.,Hughes F.D.,and James B.W.,J.Phys.E:Sci.
    Instrum.,3,132,1970.

51. Gorlich P.,'Photoconductivity in Solids'Routledge and
    Kegan Paul Ltd.N.Y.,Dover P.,1967.

52. Gregore I.and Stetter W.,Phys.Stat.Sol.b.,71,K187,1975.

53. Gregore I.,Velicky B.and Zavetova M.,J.Phys.Chem.
    Solids.,37,785,1976.

54. Grisel A.and Schmid Ph.,Phys.Stat.Solid.b.,73,587,1976.

55. Guseinov G.D.and Rasulov A.I.,Phys. Stat. Solid.,18,
    911,1966.

56. Haas C. and Corbay M.M.G.,J.Phys. Chem.Solids.,20,197
    1961.

57. Handfield G.,D'amboise M.and Bourgon M.,Canad. J.Chem.,
    44,853,1966.

58. Henry N.F.M.and Lonsdale K.,'International Tables for
    X-ray Crystallography'.Vol.1.,Kynoch,Birmingham,2nd.
    Ed.1965.

59. Hofmann W.,Z.Krist.,92,161,1935.

60. Honig A.and Maxwell R., IX. Int. Conf.Phys. SemiCond.
    Nauka Publishing House Leningrade 1968.

61. Hornig D.F., J.Chem.Phys., 16,1063,1948.

62. Jacquinot P., J.Phys. Radium,Paris.,19,223,1958.

63. Jones J.N., Practical Electronics Dec. 1974 pp:1084.

64. Karakhanova M.I.et al., Izv.An.SSSR,Norganic materially
    2,991,1966.

65. Kogan,SH.M. and Lifshits T.M., Phys.Stat.Sol(a).,39,
    11,1977.

66. Kress W.,Frey A., Dorner B. and Kaiser W., 'Proc.
    Conf.Neutron Scattering' Gatlingburg, Tennesse,USA
    Ed. Moon R.M.,Vol.1, 1976.

67. Krimm S. and Bank M.I., J.Chem.Phys.,42,4059,1965.

68. Kurtin S.,McGill T.C. and Mead C.A. Phys.Rev.Lett. 22,1433,1969.

69. Kroger F.A.,Vink H.J. and Volger J., Philips Res. Rept.,10,39,1955.

70. Lambros A.P.,Geraleas D. and Economou N.A., J.Phys. Chem.Solids,35,537,1974.

71. Laugier A., J.Cryst.Growth., 21,234,1974.

72. Lawson W.D. and Nielson S 'Preparation of Single Crystals', Butterworth,London,Chapter 8 and 9.,1958.

73. Loewenstein E.V. 'Aspen International Conf. on Fourier Spect.' Ed. by Vanasse et al.,1970,pp.3.

74. Lucovsky G.,Mikkelson J.C.,Liang W.Y.,White R.M and Martin R.M. Phys.Rev.B.,14,1663,1976.

75. Lucovsky G., deNeufville J.P. and Galeener., Phys.Rev. B.,9,1591,1974.

76. Lucovsky G.,White R.M.,Liang W.Y, Zallen R and Schimid Ph., Sol.Stat.Comm.,18,811,1976.

77. Lukes F., Czech.J.Phys.B.,13,784,1968.

78. Lyden A., Phys.Rev.,134, A1106,1964.

79. Lyman T.,'Metals Hand Book' Amer.Soc.Metal,1948.

80. McGill T.C.,J.Vac.Sci.Technol.,11,935,1974.

81. Mead C.A.,Solid-State Electronics.,9,1023,1966.

82. Mead C.A.,'Ohmic Contacs to Semiconductors'.Ed.by. Schwartz B.,Electrochemical Soc.N.Y.,pp.3.,1969.

83. Mead C.A. and Spitzer W.G.,Phys.Rev.,A134,713,1964.

84. Mihajlovic P.,Nikolic P.M.and Hughes O.H.,J.Phys.C: Solid State Phys.,9,L599,1976.

85. Mootz D.and Kunzmann R.,Acta Cryst.,15,913,1962.

86. Morton G.A.,Hahn E.E.and Schultz M.L.'Photoconductivity Conf.'Ed.Breckenridge R.G.,Russell B.R.,Hahn E.E.,

N.Y.,John-Wiley.,1957.

87. Moss T.S.,Rep.Prog.Phys.,28,15,1965.

88. Nikolic P.M.,Thesis.,Univ. Nott.,1969.

89. Nikolic P.M.and Hughes O.H., To be Published

90. Nikolic P. M.,Merdan M.,Cvekic V and Vujatovic S.S.,
    Proc.20th Conf. Etan, Opatija.,1976.

91. Nikolic P.M.,Miljkovic Lj.,Mihajlovic P.and Lavrencic B.,
    J.Phys.C:Solid state Phys.,10,L289,1977.

92. Nikolic P.M.,Vujatovic S.S.,Hughes O.H.,Doran C.J.and
    Chamberlain J.M.,'Proc. 12th Int. Conf. Phys. Semicond.,
    Stutgart.,Teubner.,pp.331,1974.

93. Okazaki A.,J. Phys.Soc. Japan.,13,1151,1958.

94. Okazaki A.and Ueda I.,J.Phys. Soc. Japan.,11,470,1956.

95. Orr R.L.and Christensen A.U.,J.Phys.Chem.,62,124,1958.

96. Ota Y.and Rabii S.,'Physics of IV-VI Compounds and
    Alloys'.Ed.Rabii S.,Gordon and Breach.,Science P.
    London.,pp.113,1974.

97. Palache C.,Berman H.and Trondel C.,'Minerology'
    John-Wiley and Sons,Inc.,N.Y,.Vol:I,8th print.pp.222,
    1966.

98. Pauling L.,'The Nature of the Chemical Bond'.Conell.U.P.
    Ithaca,N.Y.,3rd pp.93,1960.

99. Perkowitz S and Thorland R.H.,Phys.Rev.,B9,545,1974.

100. Plesiewicz W.and Swierczwski J.,J.Phys.E:Scientific
     Instrum.,7,944,1974.

101. Pries R.W.and Moore B.K.,Rev. Sci. Instrum.,41,996,1970.

102. Rau H.,J.Phys. Chem. Solids.,27,761,1966.

103. Rideout V.L.,Solid state Electron(GB).,18,541,1975.

104. Rochlin G.I.,Rev. Sci. Instrum.,41,73,1970.

105. Rose A.,Proc.IRE.,43,1850,and phys. Rev.,97,322,1955.

106. Schafer H.,'Chemical Transport Reactions'.Academic
     Press,.1964.

107. Siapkas D.I.,Kyriakos D.S.and Economou N.A.,Sol.Stat.
     Comm.,19,765,1976.

108. Sinkaskas J.,'Minerology'.Van Nostrand Reinhold Comp.
     N.Y.,pp.294,1964.

109. Slater J.C.,'Quantum Theory of Molecules and Solids'.
     McGraw-Hill,N.Y.,Vols.I,II,and III,

110. Smith A.J.,Meek T.E.and Liang W.Y.,J.Phys.C:Solid
     State Phys.,10,1321,1977.

111. Smithells C.J.,'Metals Reference Book'.Butterworth.,
     London.,1955.

112. Spitzer W.G.and Mead C.A.,J.Appl.Phys.,34,3061,1961.

113. Takahashi K.,Arai T, and Kudo K.,Science of Light.,
     21,131,1972.

114. Valk H.J.L.,and Haas C.,Phys.Stat. Sol(b).,80,321,1977.

115. Verble J.L.and Wietng T.J.,Phys.Rev.Letts.,25,362,1970.

116. Vlachos S.V.,Lambros A.P.,Thanailakis A.and Economou
     N.A.,Phys.Stat. Sol(b).,76,727,1976.

117. Vujatovic S.S.,(Private Comm.)

118. Vujatovic S.S.and Nikolic P.M.,(UNpublished).

119. Wheeler R.G.and Hill J.C., J.O.S.A.,56,657,1966.

120. Wieting T.J.and Verble J.L.,Phys.Rev.,B3,4286,1971.

121. Wiley J.D.,Breitschwerdt A.and Schonherr E.,Sol.Stat.
     Comm.,17,355,1975.

122. Wiley J.D.,Buckel W.J.,Schmidt R.L.,Phys. Rev.B13,
     2489,1976.

123. Williamson D.E.,J.O.S.A.,42,712,1952.

124. Wilson A.and Yoffe.A.D.,Adv. Phys.,18,193,1969.

125. Winston H.and Halford R.S.,J.Chem. Phys.,17,607,1949.

126. Wood E.A.,Bell Syst. Tech. J.,43,541,1964.

127. Wyckoff R.W.G.,'Crstal Structures'.Wiley.,N.Y.,Vol. I-II,1963-1964.

128. Yabumoto T.,J.Phys. Soc. Japan.,13,559,1958.

129. Zallen R.,Proc.12th Int.Conf. Phys.Semicond.(Teubner, Stutgart).pp.62,1974.

130. Zallen R. and Slade M.,Phys.Rev. B9,1627,1974.

131. Zallen R.,Slade M.L.and Ward A.T.,Phys.Rev.B3,4257,1971.

132. Zeyher R.,Kress W.and Frey A.,To be Published.